Soil Moisture-Atmosphere Feedbacks on Atmospheric Tracers: The Effects of Soil Moisture on Precipitation and Near-Surface Chemistry

by

Ahmed B. Tawfik

A dissertation submitted in partial fulfillment
of the requirements for the degree of
Doctor of Philosophy
(Atmospheric and Space Sciences)
in The University of Michigan
2012

Doctoral Committee:

Assistant Professor Allison L. Steiner, Chair
Professor Joyce E. Penner
Associate Professor Christopher J. Poulsen
Research Professor Sanford Sillman

For my incredibly supportive and loving wife and family

ACKNOWLEDGMENTS

I would first like to express my tremendous gratitude to all those that have helped and guided me through the uncharted academic graduate school world. I was lucky enough to be Professor Allison Steiner's first graduating student and I could not have asked for a better advisor, mentor, and role model. Allison has treated me as a peer from day one and valued my opinion, even when it was ridiculously incorrect. She always had a way of making me question my own premise without squashing my enthusiasm. She allowed me to learn by mistake, but never let my error propagate too long. I really have to thank her for those nudges to get me back on course. I have felt very empowered and in command of my research throughout graduate school and that is a true testament to her guidance. Beyond her academic guidance, she has been a proactive mentor making sure I balance life and academics. It made the stressful times a lot easier knowing that when the workload got heavy, Allison was right there working hard with me and, at the very least, ready to offer words of encouragement. She has taught me so many lessons and for that I am thankful. I've been lucky to have an advisor like her. I would also like to acknowledge the members of my dissertation committee, Sandy Sillman, Joyce Penner, and Chris Poulsen. Their input and comments have definitely made for stronger work that I can be proud of. I'd especially like to thank Sandy for his insight and detailed comments regarding atmospheric chemistry and its treatment in models.

Outside of my committee there have been many other faculty members that at some point have provided me with inspiration, assistance, opportunity, or just good conversation, Frank Marsik, Derek Posselt, Ricky Rood, Natasha Andronova, Mark Flanner, and Christiane Jablonowski. A special thank you to the excellent administrative support staff. Without Sandee, Margaret, Mary, Kristi, Barb, Faye, Sandra, Melissa, Darren, and Bryan I would have been a poor, computerless, moneyless, wandering zombie incapable of meeting basic academic requirements and reduced to yelling at my computer with these people in my life.

Of course my time in Michigan would have been much more difficult had it not been for the many adventures and friends (e.g. friend ships) in my life. One of the motivating reasons why I even ended up in Michigan was because of Tami McDunn. I thank her for encouraging me to visit UofM before I was accepted into the University. She is a large reason why I chose to come to Michigan and has been a good friend from the start. I do not know many people that can tolerate my random acts of headbutting like Tami and laugh about it. There are so many people to thank for making my life better I think it is only right to at least give a nod to each them (in quasi-chronological order of course). To Corinne for still being my friend even after the spilled beverage fiasco. To Pookie Bywater for allowing me to eat all of her food. To Heckathorn for being the only person around that enjoyed basketball as much as me the first year here. To Hector, Azarias, Robinson, David, and the rest of the Rackham Merit Summer Institute fellows for carrying me through my first summer. To Illisa and Catalina for letting me counsel them even though they didn't want me to. To Star for the wonderful conversations reminding me why I do research. To Jen for being a strong soprano and Soyee for her alto. To Adam for being a brilliant mind and a good sport when I would try to imitate his voice. To Coach Puckett the mastermind behind the wildcat offense and Groskopf for the execution as QB and team captain for all AOSS athletics. To Applbaum for always having the hook-up and the delicious humus. To SXT for developing the voweless language and inspiring the next generation of entrepreneurs. To Brecht for her post presence and tolerating my frequent office visits. To Catherine for always laughing at my jokes even when they are not funny. To Shannon for not laughing at my jokes even when they are hilarious. To Sidbiscuit and Sidarth Vader for knowing where free food is like it was his job and for forming a united front of brown. To Fang and Weiya for teaching me "necessary" Chinese words. To Gruesbeckistan for his steak appreciation and vast knowledge of music, even the obscure. To Tranthsylvania, Tranthtula, and Tranthafest Destiny for being on Solar Car. To Paullrich who always knows how to have pun. To Kevin Reed for looking good in suits and making me Go Blue. To DiBraccio for be shoppin'. To my current officemates Alex and Melissa for the good heart-to-heart conversations and ability to lift each other up when we are down or hitting roadblocks. The mutual support has been great and I hope to have that in the

nice place I end up. To Chengs, who although she has only been here in at Michigan for a little bit, has had an incredibly strong impact on my life. Her wisdom and willingness to disagree and buttheads with me has made me better and she will always haz smartz. To Dan "the Dan" Gershman who has been my partner in crime from the beginning. I could not have done grad school without Dan setting me straight, raising my standards for being a student, and willingness to look like a fool with me. He is the founder of the Great Ideas list that has revolutionized the way we brainstorm and dances the finest of lines between genius and utter indecipherable nonsense.

Just as my dedication says I have to give a special thank you to my amazing wife, Kristen. I have so much gratitude for her gentleness, support, kindness, love, generosity, and fun spirit. She has the unique ability to lift my spirits when I feel beaten even when she herself isn't feeling so great. Most importantly she knows my flaws and does not beat me up for them. As my defense date approached and my stress level rose she selflessly, and gracefully took care of me and didn't give me a single ounce of guilt for being negligent. Her strength was inspirational and let me know I always had someone to support me, for PhD and beyond. If it wasn't for her love, I wouldn't have eaten and would have been living in a uninhabitable sty of a home. She deserves more than an acknowledgment or dedication.

My loving family has brought me the necessary grounding I need to remind me what life is really about. To my mother and father who would call me every day to see how I was doing and just to hear my voice. Although it was bothersome on occasion that kind of care let me know I was loved and always on their minds. I hope I can make them proud to at least repay a fraction of the opportunities they gave me. To my brothers who never let me get a big head and keep my mind fresh with constant debt, even when I'm not looking for it. Finally I recognize that all blessings and praise are due to Allah. All my achievements are due to Allah's mercy upon me and there is none like Allah, the Creator and Sustainer.

TABLE OF CONTENTS

LIST OF FIGURES

LIST OF TABLES

Chapter 1

INTRODUCTION

1.1 Land-Atmosphere Interactions

The land surface is the lower boundary condition for the atmosphere, providing a source of energy, momentum, and mass of important tropospheric constituents. The transfer of these exchange variables is referred to as fluxes, or the quantity of energy, momentum or mass per unit area per time. Similarly, the atmosphere communicates these quantities back to the land surface. As the atmosphere transfers energy, momentum, and mass to the land surface, land surface fluxes change and respond. This constant communication and modification of fluxes between the atmosphere and land is defined as land-atmosphere coupling. When the coupling between the land and atmosphere is amplified (or dampened) by perturbations in either component, this is referred to as a land-atmosphere feedback.

Soil moisture is one quantity that plays a crucial role in the strength of land-atmosphere coupling and is the focus of subsequent chapters. In the remainder of the introduction, soil moisture is defined and its role in several land-atmosphere interactions is described within the climate system (Section 1.2). There are three paradigms by which

land-atmosphere interactions will be discussed, including soil water cycling (soil moisture-precipitation coupling; Section 1.3), the surface energy budget (soil moisture-temperature coupling; Section 1.4), and biogenic emissions and tropospheric ozone (Section 1.5). Section 1.6 describes the use of regional climate modeling in simulating these interactions and Section 1.7 outlines the remainder of the thesis.

1.2 The land surface and its role in the climate system

1.2.1 Soil Moisture Definition

Soil moisture is a critical component of land-atmosphere interactions. The definition of soil moisture may vary depending on the research field and context, and common definitions are absolute, volumetric, and soil moisture index. Absolute soil moisture content refers to the total mass of water within a specific soil layer (Equation 1.1) and is generally used when assessing the total water budget within a particular system

$$S = \Psi_{H2O} \bullet dz \qquad (1.1)$$

Here dz is the thickness of the soil layer and Ψ_{H2O} is the soil mass per unit volume.

Volumetric soil moisture is the total volume of water contained within the total soil volume (Equation 1.2) and is widely used for calculating soil moisture from measured soils.

$$\theta = \frac{\Psi_{H2O}}{\Psi} \qquad (1.2)$$

Ψ is the total mass of soil plus water per volume of soil. Finally, because soil moisture is necessary for vegetation, the soil moisture index can be used. The soil moisture index (*SMI*) defines the amount of soil water available for use by plants, where

$$SMI = \frac{\theta - \theta_w}{\theta_{fc} - \theta_w} \qquad (1.3)$$

where θ_{fc} is the field capacity, θ_w is the wilting point, and θ is the volumetric soil moisture. Wilting point is the point at which plants can no longer extract water from the soil matrix, and field capacity is the maximum amount of soil water that can be held by the soil matrix. SMI is often used to compare soil moisture across multiple soil and land cover types because field capacity and wilting point are functions of the soil texture and type. For the remainder of this introduction, the use of the term soil moisture refers to absolute soil moisture (Equation 1.1).

1.2.2 Importance of Soil Moisture in the Climate System

The land surface and atmosphere have very different responses times with respect to the climate system. The atmospheric component is described by rapid fluctuations in typical state variables, such as temperature and water vapor, on timescales of hours to days. Therefore the atmosphere may be regarded as a fast evolving reservoir with a "short memory" of prior events. This is largely due to the specific heat capacity and density of gases that make up the atmosphere and the fast coupling between temperature

and water vapor. The land component has a longer "memory" of past atmospheric events. For example, when rain falls over land, the water is retained by the soil. This retained moisture can then transfer information via surface fluxes back to the atmosphere well after the precipitation event has passed. This makes the land surface a slowly evolving moisture source changing on daily to yearly timescales. Timescales of change are largely determined by soil properties, vegetation/land cover type, and the proximity of a soil layer to the rapidly changing atmosphere. Due to the slowly evolving nature of the land surface, an understanding of the soil moisture reservoir and influence on land surface fluxes is necessary to understand and predict the evolution of climate.

1.3 Soil Water Cycling

1.3.1 Historical Context and Background

The ability for evaporated surface moisture to return as precipitation locally with minimal horizontal transport was first suggested late in the 19th century (Aughey, 1880). This local recycling of moisture gained further credence during the large-scale droughts of the 1930's over the Great Plains, causing some policy makers to recommend installing open-water ponds and large plantations throughout the United States. Although there were attempts to refute the local recycling claim (Holzman, 1937), it remained for over half a century. McDonald (1962) addressed this claim directly and referred to it as the "evaporation-precipitation fallacy" pointing out that weather patterns operated on daily-to-weekly time scales making the average residence time of water vapor far too long to be driven by local non-advected moisture recycling. By the mid 20th century, it was well

understood within the scientific community that precipitation was driven by a lifting mechanism, whether instigated by moist convection or frontal passage (Manabe and Strickler, 1964; Arnason et al., 1968). This encouraged a more mechanistic approach to understanding surface evaporation.

At this time, new theoretical and numerical models were developed for evaporation. Budyko (1956, 1974) described two separate regimes controlling evaporation, one controlled by soil moisture and the other by atmospheric factors. Conceptually, when soil moisture is sufficiently wet (greater than some critical soil moisture value), evaporation rate is independent of the soil moisture content or limited by atmospheric variables. Once soil moisture falls below this critical soil moisture threshold, the soil is sufficiently dry and begins to limit the evaporation rate (e.g. soil moisture limited). This construct has proven to be very useful and is still applied in describing evaporation regimes today (Koster et al., 2004; Seneviratne et al., 2006; Teuling et al., 2006).

Expanding this conceptual framework to numerical models, Manabe (1969) described surface evaporation in terms of a theoretical "bucket model." A bucket model is based on the basic surface water balance

$$\frac{dS}{dt} = P - E; S < S_{crit} \qquad (1.4)$$

where P is precipitation, E is evaporation, S is absolute soil moisture, and S_{crit} is soil moisture saturation. In the bucket model, the sub-surface represents a reservoir with a finite amount of water that can change over time (dS/dt). Using precipitation as the input

and evaporation as the output, the amount of water in the "bucket" reservoir is equal to precipitation minus evaporation ($P - E$). When the reservoir is fully saturated ($S>S_{crit}$), residual rainfall is converted to surface runoff. The application of the bucket model was widely used by first-generation land surface models (Sellers et al., 1997) due to its ease of implementation and simple theoretical framework.

As described by Sellers et al., (1997), first generation models often used time-constant values for important surface parameters. Two such parameters were soil properties and vegetation interactions. Soil properties control the porosity, wilting point, and drainage (Equation 1.4). More specifically, different soil types (e.g. clay, silt, and sand) have unique structures (matrices) that bind soil water to the soil matrix with varying strengths (Mccuen et al., 1981; Rawls et al., 1991). Soil water is most strongly bound to clayey soils and loosely bound in sandier soils. Soils types exist across a continuum. Recognizing this continuum, McCuen et al., (1981) showed that a majority of soil types can be captured as percentages of the three mentioned classes. These soil properties are inherent characteristics of the soil at a location and largely do not change over decadal timescales.

Another important determinant of soil water cycling is the presence and type of vegetation. During photosynthesis, as plants take in ambient CO_2 through small pores found on the leaf's surface (stomata) some water is lost to the atmosphere. This water loss is referred to as transpiration. The root structure of vegetation allows plants to access soil water that is not in direct contact with the atmosphere and bring moisture from the subsurface to the atmosphere to compensate for transpired water loss. This can reduce the amount of soil water at deeper soil layers dramatically that otherwise would not have been directly influenced by rapidly evolving atmospheric phenomenon (Dirmeyer, 1994).

Early work on this topic demonstrated that modeled evapotranspiration was underestimated by a factor of two when neglecting vegetation (Deardorff, 1978). Deardorff (1978) also showed that vegetated canopies can shade the underlying soil modifying the amount of available energy at the soil surface. Canopy shading was later found to be overstated in first-generation models because the vegetation layer was essentially nonresponsive and did not transpire (Sellers et al., 1997).

With the concept of including an active biosphere, second-generation land surface models were developed in which vegetation had the ability to interact with subsurface soil moisture (Sellers et al., 1986; Henderson-Sellers et al., 1993). This transpiration interaction is modeled by describing the leaf area and stomatal resistance of vegetation (Jarvis, 1976). Jarvis (1976) demonstrates that transpiration can be considered a function of water vapor gradients and stomatal openness. Although this approach was developed for leaf-level measurements, it was scaled to land surface model grid resolutions by assuming that the individual resistance of all leaves act in series (Dickinson, 1984). In order to achieve this scalability stomatal resistance is divided by the leaf area index to achieve a canopy scale resistance factor applicable for model grid resolutions.

1.3.2 Current Understanding of Soil Moisture-Precipitation Interactions

The advent of more realistic representations of soil moisture and evapotranspiration spurred investigation into the coupling between soil moisture and precipitation. Since the early work of Holzman, Budyko, and McDonald, the concept of soil moisture-precipitation coupling has been refined and extensive work has been devoted to quantifying the pathways promoting precipitation (Atlas et al., 1993; Beljaars

et al., 1996; Betts et al., 1996; Findell and Eltahir, 1997; Eltahir, 1998; Fennessy and Shukla, 1999; Schar et al., 1999; Douville and Chauvin, 2000; Pal and Eltahir, 2003; Dirmeyer, 2006; Dominguez et al., 2006; Bisselink and Dolman, 2008; Zhang et al., 2008b). Current research suggests that there are two prominent pathways whereby soil moisture can affect precipitation: the direct and indirect pathways (Schar et al., 1999). For the direct pathway, local evapotranspiration provides the moisture for precipitation within the same evaporative basin. This direct pathway is often referred to as moisture recycling (Schar et al., 1999). Precipitation in the indirect pathway is derived from nonlocal evapotranspiration, that is, water vapor is advected to a region where soil moisture conditions favor rainfall. Providing a quantitative basis for early theoretical rejection of local moisture recycling, several studies have shown that the indirect pathway is the dominant recycling mechanism (Schar et al., 1999; Zhang and Frederiksen, 2003).

More recent investigations of soil moisture-precipitation coupling focus on identifying regions where the land and atmosphere are strongly coupled (Koster et al., 2004; Seneviratne et al., 2006; Zhang et al., 2008b; Koster et al., 2010) and attempt to describe the underlying physical mechanisms (Teuling et al., 2006; Fischer et al., 2007b; Hirschi et al., 2011; Santanello et al., 2011). There has been widespread consensus that regions lying between arid and wet areas, often called transition regions, tend to have the strongest feedbacks between soil moisture and precipitation (Koster et al., 2002; Koster et al., 2004; Seneviratne et al., 2006). These regions follow the conceptual framework of Budyko (1956, 1974), where local evaporation is limited by soil moisture. Examples of strongly coupled regions in wet-to-dry transition zones include the Great Plains and the Sahel in Africa (Koster et al., 2004). The complexity of understanding soil moisture-precipitation coupling lies in how evapotranspiration and sensible heat flux interact with

the boundary layer (Santanello et al., 2011). Anomalously dry conditions may not necessarily correspond to less favorable convective conditions (Findell and Eltahir, 2003a, b).

Past studies have focused on these soil moisture and atmosphere interactions in the summer, when surface evaporation and convection are greatest. Chapter 2 explores and introduces the concept of soil phase-precipitation coupling in colder climates, where freezing and thawing of subsurface soil moisture can also feedback to atmospheric variables such as temperature and precipitation.

1.4 Surface Energy Budget

1.4.1 Historical Context and Background

In addition to the surface water budget (Section 1.3 and Equation 1.4), the surface energy budget is another important aspect of land-atmosphere interactions. Broadly, the surface energy budget describes the way energy interacts with the land surface in direct contact with the atmosphere and is described as:

$$R_n = H + \lambda E + G + \Delta S \qquad (1.5)$$

where R_n is the net radiation at the surface, λE is the latent heat flux, H is the sensible heat flux, G is the ground heat flux, and ΔS is the surface heat storage term. The sign convention is positive for fluxes entering the atmosphere (emitted from the surface) and negative for fluxes from atmosphere to land. Net radiation is the primary input of energy to the system and can be regarded as an external forcing.

Early developments of a prognostic land surface energy budget were needed to improve forecasts of surface temperatures and evaporation for agricultural purposes

(Penman, 1948; Carlslaw and Jaeger, 1959; Geiger, 1965; Monteith, 1965; Blackadar, 1966; Corby et al., 1972; Deardorff, 1978). Penman (1948) first considered evaporation over bare and vegetated surfaces as requiring two conditions: 1) enough incoming energy to evaporate water and 2) a process for transferring the evaporated liquid away from the surface (turbulent fluxes). Combining the concepts of radiant energy evaporation and eddy diffusion, Penman derived a surface energy balance that used measurable quantities, temperature, dew point temperature, and near surface wind.

$$E = \frac{\lambda_e R_n \Delta + E_a \gamma}{\Delta + \gamma} \qquad (1.6)$$

Here E is evaporation (kg m^{-2} s^{-1}), E_a is the evaporation rate for an open water surface using the saturation vapor pressure for air temperature (kg m^{-2} s^{-1}), Δ is saturation vapor pressure-temperature dependency curve (Pa K^{-1}), R_n is net surface radiation (W m^{-2}), λ_e is one over the latent heat of vaporization (kg J^{-1}), and γ is an empirical constant (=0.27 Pa K^{-1}). This surface energy balance unified the concepts of energy and turbulent evaporation providing a useful model and measurement comparison framework. Priestley and Taylor (1972) later improved the Penman formulation to only require the direct measurement of radiation. One shortcoming of this calculation is its lack of time dependence.

As forecasting temperature became necessary for numerical weather prediction (Corby et al., 1972), the surface energy balance required a prognostic component by which temperature could change with time. Using the Penman (1948) surface energy construct, temperature increases over time when input energy (e.g. radiation) rises at a faster rate than could be removed via surface fluxes (e.g. evaporation or sensible heating).

The change in temperature would therefore correspond to a simple partial derivative formulation of the Penman equation. To simplify the time-dependent calculations, heat transfer through the soil column was typically neglected in early models (Manabe et al., 1974; Gates and Imbrie, 1975). However, it was found that neglecting soil heat flux in prognostic temperature calculations produced high amplitude diurnal cycles (Deardorff, 1978). Deardorff (1978) found the force-restore method to be the best (Bhumralkar, 1975) because it avoided large diurnal temperature changes. The force-restore method uses two soil layers where the top layer is "forced" by incoming solar radiation and the lower soil layer acts as a heat reservoir and can "restore" the surface layer temperature. The deep soil layer temperature is generally prescribed by a climatological value, although studies have noted that the partitioning of surface energy was quite sensitive to the prescribed deep soil temperature in the force-restore method (Mihailovic et al., 1999). The force-restore technique was widely used in climate models for several decades until high performance computing allowed for more explicit calculations of multiple-layer soil structures that calculate soil heat conduction (Oleson et al., 2008). A description of current model parameterizations is provided in the next section.

1.4.2 Current Understanding of Soil Moisture-Temperature Coupling

In current versions of climate models, surface fluxes (H and λE) are calculated using gradients of temperature and humidity between the surface and atmosphere (typically at a 2 m or equivalent observation height). These gradients are then scaled by the ability of heat and water vapor to be transferred across a particular flux boundary where the ease of transfer is called the aerodynamic resistance. For example, the transfer

of heat from the surface to the boundary layer is proportional to turbulent fluxes with surface fluxes increasing with increasing wind speeds and surface-to-atmosphere gradients. Considering a dry, bare soil surface, the water vapor gradient under these conditions would favor higher λE; however, as the soil dries, evaporation becomes limited by the amount of soil water. This drying over time reduces the amount of latent heat flux and increases the amount of energy partitioned towards sensible heat. The increase in sensible heat flux consequently causes a rise in near-surface temperatures. This process is known as soil moisture-temperature coupling and has been the focus of an increasing number of studies (Fischer et al., 2007b; Fischer and Schar, 2009; Lorenz et al., 2010; Hirschi et al., 2011; Jaeger and Seneviratne, 2011; Zhang and Wu, 2011) due to its role in extreme events, such as heat waves and droughts.

Near surface air temperature plays a key role in regional climate, as explored in Chapter 2. The influence of soil moisture on climate scales may be present in long-term tropospheric ozone records through 1) its role in modifying near-surface temperatures thereby controlling chemical reaction rates, 2) its ability to influence precipitation, which can remove ozone precursor species through wet deposition/scavenging, 3) its control on emission rates of ozone precursor species emitted from vegetation, and 4) its effects on near-surface water vapor concentrations. Chapters 3-5 explore the potential contribution of soil moisture-atmosphere interactions on naturally occurring (biogenic) ozone precursor emissions and tropospheric ozone.

1.5 Biogenic Emissions, Air Quality and Climate

1.5.1 Historical Context

Early work examining chemical emissions and near-surface atmospheric composition was motivated by its effects on human health and agriculture (Dallwigk and Briner, 1950; Rasmussen, 1970). For humans, high concentrations of certain gas-phase pollutants, in particular ozone (O_3), were found to cause eye irritation and respiratory issues. From the perspective of crops, high ozone concentrations can damage the leaf cellular structure reducing crop yields.

Haagen-Smit (1952) was the first to propose that the production of ozone requires nitrogen oxides ($NO_x = NO + NO_2$), fast reacting hydrocarbons (referred to below as RH representing a non-methane hydrocarbon (NMHC)), and sunlight through the following set of gas-phase chemical reactions:

$$NO_2 + h\nu \rightarrow NO + O \qquad (1.7)$$

$$O + O_2 \rightarrow O_3 \qquad (1.8)$$

$$O_3 + NO \rightarrow NO_2 + O_2 \qquad (1.9)$$

$$RH + OH \xrightarrow{O_2} RO_2 + H_2O \qquad (1.10)$$

$$CO + OH \xrightarrow{O_2} HO_2 + H_2O \qquad (1.11)$$

$$RO_2 + NO \rightarrow NO_2 + RO \qquad (1.12)$$

$$HO_2 + NO \rightarrow OH + NO_2 \qquad (1.13)$$

The reaction sequence is initiated by sunlight that photodisassociates NO_2 producing atomic oxygen, O, which quickly reacts with molecular oxygen yielding O_3 that can then react with NO to reproduce NO_2. These first three equations describe a null cycle, where ozone is not created or destroyed. The inclusion of hydrocarbon species, RH, and carbon monoxide, CO, allows for the conversion of NO to NO_2 (reaction 1.12 and 1.13) without

destroying ozone (reaction 1.9), allowing for net ozone production (e.g. reactions 1.12 and 1.13 can outcompete reaction 1.9).

While this reaction is frequently triggered by the presence of anthropogenic hydrocarbons, natural or biogenic sources of hydrocarbons can be important as well. An important biogenic source of hydrocarbons to the atmosphere is isoprene (1-methyl 2,3-butadiene; C_5H_8). This was first identified existing within plant tissue, (Rhoades, 1960; Radtke et al., 1963) and later directly observed as an emissions source with a significant source (Rasmussen (1970)). Rasmussen (1970) further demonstrated that isoprene was dependent on sunlight and suggested that it would behave chemically similar to tailpipe-emitted olefins in the atmosphere. Currently, isoprene is widely recognized as an ozone precursor in the presence of NO_x (Chameides et al., 1988; Atkinson, 2000; Fiore et al., 2005; Carlton and Baker, 2011) and has been measured across many regions (Lamb et al., 1986; Baldocchi et al., 1995; Goldstein et al., 1998; Guenther and Hills, 1998; Greenberg et al., 1999; Graus et al., 2006; Calfapietra et al., 2008a; Gantt et al., 2010). Over the past two decades, many other biogenic NMHCs have also been identified, including monoterpenes (Arnts et al., 1982; Rinne et al., 2002), sesquiterpenes (Helmig et al., 1994; Helmig et al., 2006; Helmig et al., 2007), and a broad suite of oxygenated species (Konig et al., 1995; Kirstine et al., 1998; Warneke et al., 1999; Tie et al., 2003; McKinney et al., 2011; Stavrakou et al., 2011). While these other species are important for tropospheric gas and particulate phase chemistry, isoprene remains the dominant biogenic VOC emission and accounts for ~40% of the total annual mass of biogenic NMHCs globally (Guenther et al., 1995; Arneth et al., 2008). Further, an overwhelming majority (>90%) of isoprene is emitted from terrestrial vegetation (Guenther et al., 1995).

1.5.2 Current Understanding

Because isoprene is emitted from vegetation and can influence tropospheric ozone formation, it is of particular relevance in the climate system. In general, broadleaf trees and shrubs in temperate and tropical climates are among the highest emitters (Guenther et al., 2006). Some particular species that tend to have high isoprene emissions include *Quercus* (oak), *Populus* (poplars), and *Salix* (willows) (Benjamin et al., 1996; Geron et al., 2001). Isoprene emission rates are known to depend primarily on instantaneous temperature (Guenther et al., 1993) and light (Sharkey et al., 1996) in the short term following exponential response curves. Longer-term responses include prior day-to-week temperature and light (Petron et al., 2001), ambient CO_2 (Heald et al., 2009; Wilkinson et al., 2009) and O_3 (Velikova et al., 2005; Calfapietra et al., 2008b), leaf phenology (Kuhn et al., 2004), and soil moisture stress (Pegoraro et al., 2007; Llusia et al., 2008; Centritto et al., 2011). Emissions increase under warm, sunny conditions and tend to increase (decrease) with higher O_3 (CO_2) concentrations.

Of the environmental factors controlling isoprene emissions, soil moisture stress is least understood. Observational studies of the response of isoprene emissions to drought and soil water stress have yielded inconsistent results. Several leaf and ecosystem level measurements indicate that isoprene emissions decrease under severe soil water stress (Fall and Monson, 1992; Sharkey and Loreto, 1993; Brilli et al., 2007; Pegoraro et al., 2007), however this decrease only occurs under prolonged severe soil water stress when photosynthesis is severely restricted. Because isoprene is not a stored reservoir compound within the plant, carbon assimilation must almost completely stop before isoprene emissions are appreciably reduced (Brilli et al., 2007; Centritto et al., 2011). In agreement with the previous studies, Warneke et al., (2010) observed a factor of two

reduction in isoprene emissions in Texas between a drought and non-drought year and attributed these changes to either soil moisture stress or lower leaf biomass (leaf area index; LAI). However, Pegoraro et al., (2005) demonstrated that ecosystem level isoprene emissions increased during the early stages of drought followed by an emissions decline as drought continued, thus confounding prior studies.

There have been large-scale efforts to model isoprene flux to the atmosphere due to its effects on ground-level ozone. The two most popular models are the Model of Emissions of Gases and Aerosols from Nature (MEGAN) and the Biogenic Emission Inventory System (BEIS) (Pierce and Waldruff, 1991; Guenther et al., 1993; Guenther et al., 1995; Guenther et al., 1999; Guenther et al., 2006). Both of these models rely on empirical relationships and use standard emissions factors, which are based on vegetation type and define the magnitude of standard emissions at constant atmospheric conditions. Standard emission factors can then be modified by meteorological or climatological data to develop a time series of isoprene emissions. The main differences between these two models are (1) the spatial distribution and magnitude of the standard emissions factor and (2) the data used to derive the empirical environmental relationships. Current studies show that MEGAN overestimates isoprene flux and BEIS underestimates isoprene flux as compared to against eddy covariance measurements of isoprene flux (Warneke et al., 2010; Carlton and Baker, 2011). When including a soil moisture stress term to the empirical relationship of MEGAN, MEGAN is shown to underestimate surface fluxes compared to observations (Muller et al., 2008). Chapter 3 examines the sensitivity of the soil water stress parameter to MEGAN in a regional climate model and highlights its importance in controlling isoprene flux interannual variability (Tawfik et al., 2012).

1.6 Regional Climate Modeling

To better examine each of land-atmosphere feedbacks described above, systematic and significant model development was undertaken to upgrade a regional climate, RegCM, in this thesis. Each upgrade served to expand the ability to investigate the particular interactions outlined above. The improved model is compared against a suite of ground-base, gridded, and data assimilated products to ensure confidence in the model. This section provides a brief history and description of regional climate models followed by a summary of model updates.

1.6.1 Brief History

Early general circulation models (GCMs) focused on synoptic scale systems typically at very coarse global grids (than 4° by 4° grid areas) (Charney and Stone, 1976). These grids were not capable of capturing regional patterns in climate, making it difficult to highlight features and patterns more relevant to the regional or local scale information (Grotch, 1988; Rind et al., 1989). At that time, computational limitations made increasing the resolution of these models impractical. To work around this computational issue, Dickinson et al., (1989) and Giorgi and Bates (1989) recommended developing techniques to simulate climate for smaller domains focused on regions. This technique is known as regional climate modeling or dynamical downscaling and uses GCM output as initial and lateral boundary conditions to simulate climate at a finer resolution for a smaller domain. The GCM is providing the large-scale forcing and the regional model would be of sufficient resolution as to reproduce finer-scale features, such as orographic lifting for precipitation (Giorgi, 1990). The technique of dynamical downscaling is still in use today, with models typically covering continental scale regions

and simulating climate at resolutions of 20-60 km (Gutowski et al., 2010; Giorgi et al., 2012)

1.6.2 Model Development for use in Land-Atmosphere Interactions

The regional climate model used throughout this dissertation is the Abdus Salam International Centre for Theoretical Physics (ICTP) Regional Climate Model (RegCM; (Giorgi et al., 2012)). This model is a primitive equation, hydrostatic model and was originally developed with the broader research community in mind, especially those with limited computing resources and in developing countries. RegCM has gone through several upgrades since it was first introduced by Dickinson et al., (1989). To develop the model for the scientific questions presented here, several model updates were made to customize RegCM4.

Following the work of Steiner et al., (2005), the land surface model component was updated and included the coupling of the Community Land Model (CLM) version 3.5 (Oleson et al., 2008) to RegCM3 (Pal et al., 2007; Tawfik and Steiner, 2011). The CLM is a third-generation land surface model that replaces the Biosphere-Atmosphere Transfer Model (BATS), a second-generation land surface model. A list of differences between BATS and CLM is summarized in Table 1.1, including the following components relevant to the questions of land-atmosphere interactions: 1) CLM explicitly solves for soil temperature whereas BATS uses the older force-restore method (see Section 1.6.1), 2) distinguishes between sunlit and shaded components of the forest canopy, which is important for the calculation of isoprene emissions, and 3) CLM uses sub-grid tiling that allows for more than one land cover type per model grid cell. Further modifications

to CLM3.5 were required for high resolution RegCM simulations, including (1) the weighted averaging of grid cells containing ocean and land were modified, and (2) a set of high-resolution time-invariant land surface input fields were included to improve the representation of regional heterogeneity (Lawrence and Chase, 2007). A comparison of RegCM-CLM with observations is provided in Chapter 2 and direct comparison of CLM version 3 against BATS can be found in Steiner et al., (2009).

Table 1.1 Comparison between Biosphere-Atmosphere Transfer Model (BATS) and the Community Land Model version 3.5 (CLM3.5)

BATS	CLM3.5
3 soil layers	10 soil layers
Force-restore method	Explicit soil temperature solution
1 snow layer	5 snow layers including tracer layer
1 vegetation layer	1 vegetation layer
Pre-defined soil textures derived from landcover type	Soil texture divided in percent sand, silt, and clay
Non-adjusted Monin-Obukhov	Monin-Obukhov adjusted for free convection
Vegetation receives same radiation	Canopy divided in sunlit and shaded fraction
Stomatal conductance depends on minimum stomatal resistance adjustment using light, moisture, and vapor pressure	Stomatal conductance depends on photosynthetic rates, leaf area, and vapor pressure
----------	Gridcells divided in sub-grid landcover types (tile Mosaic method)
----------	Land/Ocean gridcells perform weighted average on prognostic variables

Additionally, improvements to the RegCM-CLM biogenic emissions model (MEGAN in the CLM version) were added, including 1) the use of a high-resolution 30

second standard emission factor map, 2) the influence of prior day to week temperature and light on isoprene emissions, and 3) a soil moisture stress factor (Guenther et al., 2006). The coupled RegCM-CLM with MEGAN is used in Chapter 3 to evaluate the influence of all modeled environmental factors on isoprene flux interannual variability and in Chapter 4 to explore the role of land-atmosphere coupling on isoprene and regional ozone formation.

To evaluate the effects of soil moisture-atmosphere interactions on ozone air quality, a gas-phase chemical mechanism, the Carbon Bond Mechanism (CBM-Z) adapted by Zaveri and Peters (1999), is coupled to RegCM-CLM-MEGAN. The coupling of CBM-Z and RegCM-CLM-MEGAN was part of a large-scale multi-institute collaborative effort. Some particular improvements include 1) direct interaction between MEGAN and CBM-Z allowing for direct coupling between biogenic emissions and chemistry, 2) addition of a new interannually varying anthropogenic emissions inventory (MACCity; (Lamarque et al., 2010)), 3) improved treatment of chemical tracers producing smoother time evolution and time step insensitivity, 4) an updated dry deposition scheme from CLM4 compatible with CLM3.5 (Wesely, 1989), and 4) inclusion of a widely-used wet deposition scheme (Horowitz et al., 2003; Emmons et al., 2010). A complete description of the fully coupled regional model (RegCM-CHEM) can be found in Shalaby et al., (2012) and further elaboration on RegCM-CHEM components are presented in Chapter 5.

1.7 Thesis Overview

The goal of this work is to explore several unexamined feedbacks between soil moisture and the climate system bridging the gap between regional climate analysis and atmospheric chemistry. The second chapter focuses on land-atmosphere coupling in the United States and highlights the importance of the land surface throughout the entire seasonal cycle. The third chapter determines the primary environmental variables driving biogenic isoprene flux interannual variability as soil moisture and temperature, and present a novel methodology for quantifying isoprene flux variability within models. Chapter four shows the effect of soil moisture and land-atmosphere coupling on ozone air quality using ground-based chemical observations and data assimilated environmental variables. The physical processes dictating commonly observed features between ozone and atmospheric variables such as temperature and relative humidity are then described. Finally, Chapter five evaluates the capacity of coupled climate-chemistry models to reproduce the observed relationships between ozone and its control variables described in Chapter four, and identifies the inability of coupled models to reproduce the ozone sensitivity to temperature due to the balance between isoprene and its primary oxidant. The broad implications of this work for air quality managers and policy makers is detailed in Chapter 6 with recommendations for future work related to land-atmosphere interactions.

Chapter 2

The role of soil ice in land-atmosphere coupling over the United States

2.1 Abstract

We perform two 23-year simulations using a regional climate model coupled with the NCAR Community Land Model version 3.5 (RegCM-CLM) to investigate land-atmosphere coupling in the continental United States during the cold season (October-April) and the role of soil water phase. One simulation allows the land surface to interact freely (RunI) while the other simulation uses monthly climatological soil moisture (soil liquid plus soil ice) to represent an uncoupled land surface (RunC). A winter land-atmosphere coupling signal occurs slightly south of the freezing line, indicating that the freezing line could be regarded as temporally varying transition zone similar to the dry-to-wet transition zone identified in prior studies during boreal summer. Warmer soil temperatures in RunI translate into additional available surface energy (sum of latent and sensible heat) producing locally elevated moist static energy in the atmosphere. Additionally, warmer temperatures and greater moist static energy increase both large-scale (6-30% increase; March) and convective precipitation (>100% increase; April). As a

result of the increased liquid precipitation during transition months, soil liquid water increases thereby warming winter ground and air temperatures in the interactive run and enhancing the potential for subsequent liquid precipitation. While RunC includes more persistent soil ice than is likely present in the real land-atmosphere system, this precipitation-soil moisture feedback underscores the role of soil moisture phase and variability as an important surface parameter in the winter months.

2.2 Introduction

The land surface can be considered the lower boundary condition to the atmosphere, and represents a key source of energy input to the atmosphere through the release of sensible and latent heat fluxes. Many variables can affect this release of energy, including the amount of incoming solar radiation, landcover type, soil properties, and soil water phase. Across many regions, soil moisture is an important determinant in both the partitioning of surface energy and the magnitude of these fluxes to the atmosphere (Betts, 2004; Dirmeyer, 2006). This interaction between the land and atmosphere is well documented during summer months (Schar et al., 1999; Pal and Eltahir, 2001; Findell and Eltahir, 2003b), but is often regarded as too weak to be important during winter (Zhang et al., 2008a). This study focuses on the impact of soil moisture and its phase on the seasonal evolution of the land-atmosphere feedback, with particular emphasis on the winter months. We find that the presence of soil ice can trigger land-atmosphere feedbacks through modifications of available surface energy, moist static energy, and convective and large-scale precipitation.

Soil moisture can interact with the atmosphere on a broad range of spatial scales. At the local scale, evaporation can directly produce local precipitation (Schar et al., 1999). Additionally, moisture from remote locations can be advected into a region and amplified by local soil moisture, creating precipitation and an indirect interaction between the land surface and precipitation. The relative importance of the direct and indirect pathways can be quantified using the recycling ratio, b (Schar et al., 1999):

$$\beta = \frac{ET}{ET + IN} \qquad 2.1$$

where ET is evapotranspiration, and IN is the moisture transported into a defined region. Previous studies have shown that the indirect mechanism tends to dominate over local precipitation recycling in most basins (Schar et al., 1999; Zhang and Frederiksen, 2003).

In addition to spatial influences, soil moisture can affect the atmosphere through a continuum of temporal scales (Betts and Ball, 1995; Betts et al., 1996). Typically, the concept of soil moisture "memory" on the seasonal time scale refers to the ability of soil moisture to provide some residual information of past atmospheric events. This memory occurs because soil moisture evolves at relatively longer timescales than the overlying atmosphere. For example, an increase in soil moisture can produce anomalously high latent heat fluxes long after a precipitation event has occurred. Several modeling studies have found that springtime dry soil moisture anomalies tend to decrease summer rainfall (Fennessy and Shukla, 1999; Pal and Eltahir, 2001; Kim and Wang, 2007; Wu et al., 2007b), and field measurements in the Central US confirm a similar soil moisture-precipitation feedback (Findell and Eltahir, 1997; Eltahir, 1998).

The relationship between land surface conditions such as soil moisture and atmospheric variables are often described with a parameter known as "coupling strength"

(Dirmeyer, 2001; Koster et al., 2002). The coupling strength quantifies impacts of soil moisture anomalies on atmospheric variables (e.g., precipitation and surface air temperature) and describes the extent of communication between the land and the atmosphere. Koster *et al.*, (2002) examined the inter-model variability and found marked differences in coupling strength between four Atmospheric General Circulation Models (AGCMs) during boreal summer. The Global Land-Atmosphere Coupling Experiment (GLACE) expanded upon this work using 12 AGCMs and identified common "hot spots" across models, generally located between dry and wet regions (Koster et al., 2004; Guo et al., 2006; Koster et al., 2006). Observations have further emphasized the role of soil moisture transition zones as regions with greater land-atmosphere coupling (Zhang et al., 2008b). Recent studies have explored land-atmosphere coupling using regional climate models to determine if similar coupling regimes are present with higher spatial resolution models. Using the Weather Research and Forecasting (WRF), Zhang *et al.*, (2008a) could not confirm the presence of a land-atmosphere "hot spot" as identified by GLACE over the Southern Great Plains, and found coupled regions to be within a specific surface air temperature range (23°C -29°C).

To date, the literature regarding land-atmosphere coupling has been focused on the feedbacks between soil moisture and atmospheric variables during boreal summer. This is under the presumption that soil moisture and local evaporative feedbacks would be less significant than synoptic scale processes in modifying temperature and precipitation in the winter mid-latitudes. While synoptic systems dominate mid-latitude winter climates due to strong meridional temperature gradients (Sickmoller et al., 2000; de la Torre et al., 2008), the potential coupling between land and atmosphere could occur in seasons outside of boreal summer. For example, soil water phase may have strong

impacts on the surface energy budget (Viterbo et al., 1999; Boone et al., 2000). Limited observational studies suggest a connection between soil water phase and atmospheric processes, where reduced winter precipitation is found to promote soil freezing throughout the season when snow cover is thin (Isard and Schaetzl, 1998; Henry, 2008).

Similar to reduced spring rainfall triggering summer drought, reduced winter precipitation could support more soil water freezing, cooler temperatures, and decreased surface fluxes. These modifications to surface conditions could then feedback to additional reductions in precipitation. Observational studies suggest this relationship between reduced winter precipitation and soil freezing is most pronounced for locations near the freezing line (Isard and Schaetzl, 1998; Henry, 2008), which could allow the surface freezing line to act as a transition zone analogous to the wet-dry transition zone normally associated with land-atmosphere "hotspots". This study examines the seasonal evolution of land-atmosphere coupling and the role of soil water phase, and suggests a likely mechanism for winter land-atmosphere coupling. Section 2.3 describes the model and experiment design used in the analysis, Section 2.4 evaluates model sensitivity of coupling strength, Section 2.5 discusses model evaluation and present results of the experiment, and a discussion of the winter feedback mechanism is presented in Section 2.6.

2.3 Methods

2.3.1 Description of climate-land surface model (RegCM-CLM)

To evaluate land-atmosphere feedbacks, high resolution regional climate model simulations are conducted using the Abdus Salaam International Centre for Theoretical Physics (ICTP) Regional Climate Model (RegCM), coupled with the NCAR Community Land Model version 3.5 (CLM; (Oleson et al., 2008). RegCM is a community-based, compressible, hydrostatic, primitive-equation model (Giorgi and Mearns, 1999; Pal et al., 2007).

Large-scale precipitation is parameterized in RegCM-CLM using the subgrid explicit moisture scheme (SUBEX), which utilizes the grid cell averaged relative humidity and cloud fraction to represent subsaturated and saturated fractions within a model grid cell (Pal et al., 2000). A temperature dependent autoconversion threshold, Q_c^{th}, is compared to cloud liquid water, Q_c, to determine if precipitation occurs. As temperatures increase, Q_c^{th} increases and affects the precipitation rate (P):

$$Q_C^{th} = C_{acs} 10^{-0.49+0.013T} \qquad 2.2$$

$$P = C_{ppt}(Q_c - Q_c^{th} FC) \qquad 2.3$$

where T is temperature, FC is fractional cloud cover, and C_{ppt} is an empirically derived autoconversion rate (C_{ppt} = 5x10^{-4} 1/s). When cloud liquid water (Q_c) exceeds the weighted autoconversion threshold ($Q_c^{th} FC$), precipitation occurs and falls instantaneously. The difference between cloud liquid water and weighted autoconversion threshold (ΔQ) physically represents the available precipitable cloud water. Therefore, the formation of large-scale precipitation ultimately depends on temperature, cloud liquid water, and fractional cloud cover. Cumulus precipitation is described by the Grell

convection scheme with Arakawa-Schubert closure (Grell, 1993), shown to produce the most realistic precipitation in RegCM over North America compared to gridded precipitation products (Pal et al., 2000; Walker and Diffenbaugh, 2009).

CLM is the land surface model developed as part of the Community Climate System Model (CCSM), described in detail in Collins *et al.,* (2006) and Oleson *et al.,* (2008). CLM contains five possible snow layers with an additional representation of trace snow and ten unevenly spaced soil layers with explicit solutions of temperature, liquid water and ice water in each layer. Because we extend our analysis to the winter months, soil moisture includes water in both the ice and liquid phase and subsequent discussion refers to "soil moisture" as the sum of soil liquid and soil ice. To account for land surface complexity within a climate model grid cell, CLM uses a tile or "mosaic" approach to capture surface heterogeneity. Each CLM gridcell contains up to four different land cover types (glacier, wetland, lake, and vegetated), where the vegetated fraction is divided into 17 different plant functional types. Hydrological and energy balance equations are solved for each land cover type and aggregated back to the gridcell level. A detailed discussion of CLM version 3 implemented in RegCM3 and comparative analysis of land surface parameterization options is presented in Steiner *et al.* (2009).

In this version of RegCM-CLM several input files and processes were modified, including (1) the use of high resolution input data, (2) soil moisture initialization, and (3) and an improved treatment of grid cells along coastlines. For the model input data, CLM requires several time-invariant surface input parameters, including soil color, soil texture, percent cover of each land surface type, leaf and stem area indices, maximum saturation fraction, and land fraction (Lawrence and Chase, 2007). The resolution was increased for several input parameters to capture surface heterogeneity when interpolating to the

regional climate grid. Soil color, soil texture, glacier, lake, wetland, and land fraction have been improved to 0.05° by 0.05° horizontal spacing, while plant functional types, leaf area index, stem area index and maximum saturation fraction remain at 0.5° by 0.5° grid spacing. Similar to Lawrence and Chase (2007), the number of soil colors was extended from 8 to 20 classes to resolve regional variations. The second modification was to update the soil moisture initialization based on a climatological soil moisture average (Giorgi and Bates, 1989) over the use of constant soil moisture content throughout the grid. By using a climatological average for soil moisture, model spin-up time is reduced with regards to deeper soil layers. This is especially true in semi-arid conditions, where soil moisture can often take years to equilibrate (Cosgrove et al., 2003). The third modification to the RegCM-CLM coupling is the inclusion of a mosaic approach for gridcells that contain both land and ocean surface types. With this approach, a weighted average of necessary surface variables was calculated for land/ocean gridcells using the land fraction input dataset. This method provides a better representation of coastlines using the high-resolution land fraction data.

2.3.2 Experiment design

Model simulations for this study focus on the contiguous United States, with a Lambert conformal projected grid centered at 100°W and 39°N spanning 3625 km by 5600 km at 25 km grid spacing. There are 18 vertical atmospheric model layers in sigma coordinates from the surface to 100 mb. Initial and lateral atmospheric boundary conditions are provided by NCEP reanalysis 1 at 2.5° by 2.5° horizontal spacing and 17 pressure levels (only 8 levels for humidity) every 6 hours (Kalnay et al., 1996). Weekly

updated sea surface temperatures are prescribed using the NOAA Optimum Interpolation SST V2 dataset (Reynolds et al., 2002).

Two 23-year simulations from 1982-2004 (inclusive) were performed. The first 2 years are removed in order to allow the model to spin-up and reach equilibrium. The first simulation allows the atmosphere and land surface to interact freely (the interactive run, or RunI) and the land surface model is called every sixth atmospheric model timestep, allowing exchange of all variables between the land surface and the atmosphere. The second simulation (the climatological run, or RunC) replaces soil liquid and soil ice with monthly climatological averages from RunI at every land surface time step. Because RunC utilizes prescribed monthly soil moisture, it represents an uncoupled land surface as the lower boundary condition. By comparing the two simulations, we can attribute changes in atmospheric variables to the effects of soil moisture content and phase change. Additionally, if strong land-atmosphere feedbacks are present, we expect to see changes in the mean atmospheric state between the two simulations (further discussion in Section 2.4).

Because prior studies have noted the impact of soil freezing on the climate (Viterbo et al., 1999; Boone et al., 2000; Niu and Yang, 2006), soil liquid and soil ice were both held to climatological averages for RunC, capturing the seasonality of soil moisture. Sensitivity of this experiment design is discussed in Section 2.4. As shown in Figure 1 for the North Great Plains (NGP; see box in Figure 3), inter-annual variability is captured by RunI, while RunC shows a constant seasonal cycle throughout the full simulation because it is forced with constant climatological soil moisture. We focus on the NGP throughout the analysis because of the strong coupling and clear seasonal transition. Other regions were examined and demonstrated a similar coupling mechanism, therefore NGP is

highlighted in subsequent discussion for illustrative purposes of the winter feedback mechanism.

Land-atmosphere coupling strength is evaluated using two methods, the standard deviation difference method, $\Delta\sigma_T$ (Seneviratne et al., 2006; Zhang et al., 2008a) and the GLACE coupling parameter, $\Delta\Omega$ (Koster et al., 2006). The standard deviation method is defined as:

$$\Delta\sigma_T = \sigma_{RunI} - \sigma_{RunC} \qquad 2.4$$

where σ_{RunI} and σ_{RunC} are the standard deviations of 2-m air temperature for RunI and RunC, respectively. Because the only difference between the RunI and RunC simulations is the treatment of soil moisture, the difference between the standard deviations of RunI and RunC should describe the degree to which surface air temperature variations are caused by changes in soil moisture magnitude and soil moisture phase.

The GLACE coupling parameter has generally been used during the summer by dividing JJA into 16 pentads (neglecting the first 10 days of the summer) for a specific atmospheric variable (Koster et al., 2004; Koster et al., 2006; Seneviratne et al., 2006; Zhang et al., 2008a). Here we focus on the spring transition months (March-May) when employing $\Delta\Omega$, neglecting the first 12 days to maintain a 16 pentad season. $\Delta\Omega$ is defined as Ω_X(RunI) - Ω_X(RunC) where Ω_X is:

$$\Omega_X = \frac{N\sigma^2_{\langle X\rangle} - \sigma^2_X}{(N-1)\sigma^2_X} \qquad 2.5$$

N is the number of simulation years (=21), $\sigma^2_{\langle X \rangle}$ is the variance across average pentads, and σ^2_X is the variance of every pentad for all year (e.g. 21 years by 16 pentads).

Zhang *et al.,* (2008a) demonstrated that standard deviation differencing method yields similar results over the contiguous United States to coupling strength parameter (Koster et al., 2006) and the variance method (Seneviratne et al., 2006). For this analysis, D_{ST} is used to identify regions where coupling between the land surface and air temperatures exists (Sections 2.5.2-2.5.4), whereas $\Delta\Omega$ is used to described similarity of liquid precipitation between pentads for March through May (Section 2.5.5.3).

Our assessment of the coupling strength is similar to GLACE with several notable exceptions: (1) a single model is used for multiple years, unlike the GLACE which performed ensemble simulations with 12 different AGCMs for one season, (2) the model simulations are at a higher spatial resolution of 25km, (3) simulations are continuous (e.g., simulations are run continuously for 23 years, while the GLACE performed 16 member ensembles per model for only JJA) and, (4) analysis is extended to all seasons.

2.4 Coupling Strength Sensitivity

In order to assess the sensitivity of coupling strength to the treatment of soil ice, two additional 7-year simulations were performed from 1982-1988 with the first two years discarded for model spin-up. Similar to RunC, one simulation prescribes 50% of the climatological soil ice and 100% soil liquid water from RunC (ICE50). By comparing the RunC and ICE50 simulations to the RunI simulation, we can assess the influence of the amount of soil ice on coupling strength and inter-annual variability. The second

simulation holds the total soil water mass (liquid + ice) constant and allows ground temperatures to determine the phase of water in the soil (MASS). The MASS simulation helps identify regions where inter-annual variability of total soil moisture (liquid + ice) has the greatest impact on the atmosphere.

The standard deviation coupling strength method for 2-m air temperature is calculated for each of the three climatological simulations (RunC, ICE50, and MASS) relative to RunI (e.g. $\Delta\sigma_T^{\text{climatological}} = \sigma_{\text{RunI}} - \sigma_{\text{climatological}}$; Figure 2). When comparing the $\Delta\sigma_T$ values across the three sensitivity tests, the spatial distribution of coupling strength is similar for RunC and ICE50. Notably, RunC and ICE50 have similar coupling strength magnitudes in March and April over the central and northern Plains (> 0.8 K), suggesting the magnitude of ice prescribed does not have a strong influence on the magnitude of land-atmosphere coupling parameter.

The coupling strength is markedly weaker in the MASS simulation than the other two climatological simulations with fixed amounts of soil ice (RunC and ICE50). Further, MASS demonstrates no distinct spatial coupling pattern with weak to no coupling over much of the U.S. (< 0.4K), indicating that the inter-annual variability of 2-m air temperature is similar for MASS and RunI. Unlike traditional land-atmosphere coupling studies performed for summer, soil water phase transitions provide additional complexity. By introducing phase change in MASS, soil moisture is no longer constant inter-annually for soil liquid and ice individually. Soil water freezing (melting) can then be regarded as an energy and moisture sink (source). As a consequence, soil liquid water available for evaporation changes from year to year, dampening the response in the land-atmosphere coupling parameter. Because the goal of our study is to evaluate the role of soil water

phase on land-atmosphere coupling, the inter-annual variability of soil liquid/ice partitioning in MASS complicates the assessment of the role of soil water phase on land-atmosphere coupling. Therefore, subsequent discussion regarding the feedback mechanism compares RunI and RunC to highlight the role of soil moisture phase in land-atmosphere coupling.

Although by design there is no inter-annual variability in soil liquid and ice for the climatological simulations (RunC and ICE50), the climatological method has specific behaviors that merit discussion. Because soil ice is prescribed in these simulations, the atmosphere could continue to transfer energy into the soil column attempting to melt a persistent soil ice mass during conditions when the atmosphere is warmer than the land surface. When soil ice is present, energy that would have warmed the land surface is now transferred into the ground to melt the soil ice. Therefore in the climatological simulations, the mean climate may become colder than RunI. However, this cold bias does not affect the magnitude or spatial pattern of coupling, because the standard deviation method (Equation 2.4) effectively removes mean bias and represents inter-annual variability about the mean condition. As noted above, the magnitude of ice did not have a strong effect on the coupling strength (RunC and ICE50 have similar coupling strengths; Figure 2.2), suggesting that the presence of ice phase is key to the land-atmosphere coupling.

2.5 Results

2.5.1 Model Evaluation of Climate Variables

To evaluate the ability of RegCM-CLM to reproduce the mean climate state, we compare modeled temperature and precipitation results against the monthly 0.5° gridded observational dataset developed by the Climate Research Unit at East Anglia (CRU)(Mitchell et. al. 2004). Because CRU data are only available through the end of 2002, we compare the model versus measurements for the time period 1984-2002. The RegCM-CLM produces a warm bias over the Great Plains that is prevalent during each season (Figure 2.3). During March-April-May (MAM) and September-October-November (SON), the model is on average 1-2 K warmer from northern Texas through central Canada, with some localized biases exceeding 3 K. Summertime (June-July-August, JJA) has a warm bias of similar magnitude, but the bias extends further east over the Great Lakes region. Winter (December-January-February, DJF) demonstrates the largest deviation from observed temperatures in the Northern Great Plains and Canada (1-4 K warmer than CRU), a feature common to most regional climate models (Walker and Diffenbaugh, 2009). In addition to the warm bias over the Great Plains, there is a consistent 1-3 K cool bias over western Mexico. Despite these biases in surface temperature, the model reproduces the seasonal cycle of temperatures on a regional basis in the South, Northeast, and our NGP analysis region. The modeled inter-annual variability of temperature can also be compared to the observed temperature inter-annual variability through the relative model bias of inter-annual variability (defined as $1 - \sigma_{RunI}/\sigma_{OBS}$; Figure 2.3). For temperature, the model shows less inter-annual variability over much of the Central U.S. and Mountain West for winter, spring, and fall. During summer in the Southeast, the model has more inter-annual temperature variability than observed, suggesting that land-atmosphere coupling may be overestimated by the model in these regions in the summer (Figure 2.3).

Precipitation in RegCM-CLM tends to be greater than observed in the western US throughout the year. Areas with complex topography yield the greatest discrepancies between modeled and observed precipitation. Specifically, western Mexico and the Pacific Northwest show the greatest wet bias in the model throughout the year (>60 mm/month; Figure 2.4), correlated with locations that have the greatest annual precipitation amounts. This overestimation of precipitation over complex terrain is common to many regional climate models (Leung et al., 2003; Duffy et al., 2006; Wang et al., 2009). The northern Plains are wetter by 10-35 mm/month than observed for DJF and MAM, with improved agreement in SON. The southeastern U.S. tends to be drier than observed (20-50 mm/month) for SON and DJF and wetter during JJA (15-35 mm/month), with maxima along the eastern seaboard north of the 35th parallel. The model shows similar difficulty capturing inter-annual variability over complex terrain, generally overestimating inter-annual precipitation variability over much of the US domain. However, the best performance in capturing inter-annual variability occurs during the fall and spring east of the Rocky Mountains (Figure 2.4). A discussion of the coupling strength results will be described with respect to these model biases (Section 2.7).

2.5.2 *Seasonal Evolution of Coupling Strength*

Based on $\Delta\sigma_T$ definition of coupling strength (Equation 2.4), we note a strong coupling region over the southern and central Great Plains during the warmer months (June-September) (Figure 2.5). More specifically, temperatures vary 0.5-1 K more with interactive soil moisture (RunI) for May through September over Texas and Oklahoma. While there is general agreement regarding the southern Plains "hotspot" found by the

GLACE (Koster et al., 2004; Koster et al., 2006), the strong coupling region extends eastward into the Tennessee and Ohio River Valleys in August indicating a broader spatial coverage than prior studies (results not shown).

When extending our analysis to the colder months (October-April), we find a more pronounced coupling strength compared to summer. The magnitude of temperature variability attributable to variations in soil moisture content and phase increases during the fall to winter transition. The soil-moisture driven variability peaks in February at 0.75-1.5 K, then gradually decreases in strength in the spring (March-May) (Figure 2.5). In addition to having stronger coupling, the coupled region covers a broader spatial extent, present from the foothills of the Rocky Mountains eastward to the Atlantic coast (Figure 2.2). The broad winter coupling pattern first appears in October primarily over central Canada (Figure 2.5). The region then migrates towards the southeastern U.S. by January and northward once again into Canada during spring, eventually disappearing by June. This migration of coupling strength appears to follow the freezing line as it migrates with season. In the following sections, we examine the cold-regime land-atmosphere feedback mechanism that produces this pattern (Section 2.5.3-2.5.5) and summarize the winter land-atmosphere feedback mechanism in Section 2.6.

2.5.3 Coupling Strength Relation to Soil Liquid Water and Surface Energy

Surface energy fluxes are a primary mechanism of energy transfer between the land surface and the atmosphere. Here, we define the available surface energy as the sum of sensible and latent heat from the surface and the available surface energy deficit as difference in available surface energy between RunI and RunC. During the transition

months over the NGP region, latent and sensible heat contribute approximately the same amount to available surface energy (e.g. the Bowen ratio is not substantially different between the two runs; figure not shown). The sign of available surface energy flux varies with both time and space. Positive values indicate that the land surface is a source of energy to the atmosphere, while negative values suggest that the ground temperatures are cooler than the overlaying atmosphere thereby drawing down heat from the atmosphere and acting as a heat sink.

We focus on March to isolate the winter-to-spring transition of the coupling strength, and evaluate a meridional cross-section from 23°N to 55°N (averaged from 100°W to 90°W) of available surface energy, coupling strength, ground temperature, and net surface longwave radiation inter-annually and climatologically (Figure 2.6). In March, available surface energy differences between RunI and RunC occur around the 40th parallel with differences of 30-75 W m^{-2} (Figure 2.6a). Additionally, Figure 2.6d illustrates that areas with increased available surface energy are co-located with more intense coupling. Along the transect, RunI has approximately 30 W m^{-2} more available surface energy than RunC for December and January and approximately 50 W m^{-2} for February through April.

Because available surface energy and ground temperature are strongly correlated, the ground temperature is a key component of the land-atmosphere feedback mechanism. In the coupled region, RunC is 1-7 K colder than RunI (Figure 2.6b and 2.6e). In March, the surface soil temperature is often below the freezing point at latitudes 4-8° farther south in RunC compared to RunI (Figure 2.6b). This indicates that climatological soil moisture simulations are colder throughout the simulation period, leading to less available surface energy in RunC. Additionally, the coupling strength tends to peak

slightly south of the freezing line in RunI. Once both simulations have reached the freezing line, the available surface energy deficit and ground temperatures are nearly identical with increasing latitude. The sharp changes in the north-south temperature gradient in RunC indicate that temperatures reach freezing more rapidly than the fully interactive run (RunI). For 1996 and 2002, the coldest March years, the freezing line in RunI approaches the RunC freezing line, corresponding to weaker temperature differences.

As ground temperatures change, we could also expect a change in the surface snow cover. A common land-atmosphere feedback in cold climates is the temperature-snow albedo feedback, where colder temperatures lead to the presence of more snow on the ground, increasing the albedo and reducing absorbed solar radiation, thereby enhancing the colder temperatures (Yang et al., 2001; Bony et al., 2006). We evaluate this feedback in our two simulations, and find that absorbed solar radiation at the surface is not substantially different between RunI and RunC (less than 5% difference; figure not shown). This indicates that albedo modifications induced by variable snow or cloud cover are likely not the driver for the observed differences in available surface energy and ground temperature between the two simulations. However, there are noticeable changes in net surface longwave radiation (Figures 2.6c and 2.6f). Longwave radiation shows similar behavior to ground temperature and available surface radiation, with maximum differences in March occurring around 40°N and migrating seasonal behavior. Further, March years with the greatest longwave radiation differences (1986 and 1991) correspond to years containing the greatest ground temperature differences. This implies much of the difference in longwave energy is likely due to warmer ground temperatures in RunI.

In March, the inter-annual variability of ground temperature differences between RunI and RunC follow the differences in surface percent soil liquid water (Figure 2.7; surface soil layer defined as ~10cm depth). This relationship is particularly clear during March 2002 where there is a large difference in percent soil liquid (RunI 14% less percent soil liquid as water) and a corresponding decrease in ground temperature differences (RunI colder by 0.5 K). This indicates that the percent of soil moisture in the liquid phase is important in controlling ground temperature variability over coupled regions.

2.5.4 Soil Temperature and Moist Static Energy

As described above, the percentage of soil moisture that is liquid water appears to be a driving variable that affects ground temperature and the amount of surface energy that can propagate into the atmosphere. The soil column temperature can act as a slowly varying heat reservoir and explain changes in the available surface energy on a seasonal scale. Figure 8 displays the difference (RunI minus RunC) in soil temperature profile and moist static energy (MSE) atmospheric profile for the same meridional cross-section and time period as Figure 2.6. Throughout the column, the soil temperature for RunI is 2-5 K warmer than RunC during March (similar to surface ground temperature). Additionally, the peak soil temperature differences occur between 0-20 cm (Figure 2.8a). From January-May, there is a clear northward migration of the soil temperature maximum (Figure 2.8b). By May, the temperature differences have weakened, implying conduction by the soil column towards the surface and a release of this energy to the atmosphere in RunI. Again, we note that the deviation in RunC soil temperatures from the climatological mean is due to the persistent presences of ice. While this likely

overestimates the persistence of ice compared to true conditions, it highlights the role of soil ice in land-atmosphere coupling.

Moist static energy is defined by the equation

$$MSE = c_p T + L_v q + gz \qquad 2.6$$

where c_p is specific heat capacity at constant pressure, T is temperature, L_v is the latent heat of vaporization, q is water vapor mixing ratio, g is acceleration from gravity, and z is the height. MSE is used as an indicator of instability within the troposphere (Emanuel, 1995; Pal and Eltahir, 2001). In March, the MSE profile model differences are tightly co-located with the soil temperature differences. MSE for RunI is 1-8 kJ/kg greater, with changes reaching as high as 700mb (Figure 2.8a). This suggests that the soil temperature changes have the ability to affect the vertical profile of MSE, thereby creating a land-atmosphere feedback during the months in the transition from winter to spring.

2.5.5 Effects on Precipitation

During the colder months (October-April) in the northern mid-latitudes, precipitation typically occurs as a result of large-scale frontal features rather than local convective precipitation. Our simulations show a distinct soil moisture-precipitation feedback occurring during these winter months, and we evaluate contributions from convective and large-scale precipitation as well as the phase of precipitation. In the NGP, the greatest precipitation changes occur in the transition seasons, with total precipitation in RunI increasing 21% in April and 22% in November compared to RunC (Figures 2.9a and 2.9b). When examining the relative contributions of large-scale and convective

precipitation to the total winter precipitation, two distinct signatures arise: (1) changes in convective precipitation and large-scale precipitation contribute roughly equally to the increase in total precipitation (April and October; Figure 2.9b) and (2) large-scale precipitation contributes >80% to the increase in total precipitation (November and March; Figure 2.9b). Section 2.5.5.1 focuses on the first signature and mechanism controlling the increase in convective precipitation, and the second signature dominated by large-scale precipitation is discussed in Section 2.5.5.2. The phase of precipitation is analyzed and discussed in Section 2.5.5.3.

2.5.5.1 Convective Precipitation

The recycling ratio (b; Equation 2.1) is an indicator of local moisture recycling efficiency, and the degree of local moisture influence is illustrated in the monthly climatology of b over NGP (Figure 2.9c). The peak difference in recycling between simulations occurs in April (RunI is greater by 0.07) and to lesser extent in October (RunI greater by 0.02). In April, evaporation is greater for RunI by 25mm month^{-1}, which is about two times the magnitude of change in moisture flux into the region (Figure 2.9d). During peak evaporation (April and October) we find a corresponding increase in convective precipitation, implying a local feedback between evaporation and convective precipitation consistent with a higher b.

The convective precipitation mechanism is linked to the amount of evaporated surface moisture in the region. Specifically, surface evaporation is incorporated into the available surface energy calculation as latent heat flux, therefore increases in evaporation are reflected as increases in available surface energy. As ground temperature increases

(Figure 2.6b), available surface energy also increases (Figure 2.6a) providing additional energy flux into the atmosphere. This energy transfer from the surface to the atmosphere translates into elevated MSE (Figure 2.8a) that in turn promotes convective precipitation. Because differences in these surface and atmospheric variables have nearly identical seasonal cycles, this strongly suggests the presence of a positive land-atmosphere feedback cycle. This type of feedback cycle is the one that drives the summertime feedbacks of most land-atmosphere coupling studies (e.g., Koster *et al.,* 2004), yet we note its presence in a relatively colder region and also outside of boreal summer.

2.5.5.2 Large-scale Precipitation

Although convective precipitation contributes to roughly half of the precipitation increases seen in October and April (Figure 2.9b), large-scale precipitation dominates the change in precipitation in the colder transition months (November and March). The ΔQ_{Tot} profile (Figure 2.10a) describes the difference in large-scale precipitation occurring at each level in the atmosphere, as precipitation is merely ΔQ multiplied by the autoconversion rate, C_{ppt} (Equation 2.3). The March-April and October-November time periods have a greater amount of large-scale precipitation in RunI. Further, there are two clear levels in the atmosphere where large-scale precipitation is noticeably elevated, at 500mb and 950mb. The atmospheric temperature profile (Figure 2.10b) indicates that RunI is warmer by 2-3.5 K during the coupled months and the warm anomaly extends to approximately 700mb. The temperature profile also indicates that there is less warming occurring in March and November relative to April and October, months when convection contributes more to total precipitation. Warmer temperatures increase the

autoconversion threshold and inhibit large-scale precipitation. However, we find there is an increase in large-scale precipitation below 700mb coincident with increasing temperatures for RunI. Large-scale precipitation differences below 700mb can only then be attributed to reduced fractional cloud cover (Figure 2.10c) in RunI through decreasing the weighted autoconversion threshold ($Q_c^{th}FC$). As the weighted autoconversion threshold increases (decreases), it takes more (less) cloud liquid water to reach saturation and produce precipitation. Therefore, less low-level cloudiness in RunI allows for more large-scale precipitation by lowering the autconversion threshold.

Since temperature differences are primarily restricted to below 700mb, temperature differences cannot account for the changes in large-scale precipitation seen at 500mb. Figure 2.10d shows the vertical profile of cloud liquid water differences between the two simulations where warmer (cooler) colors imply more cloud liquid water for RunI (RunC). March and November have the greatest increases in cloud liquid water above 700mb. The increase in cloud liquid water and relatively similar values of temperature and cloud fraction between simulations demonstrate that elevated cloud liquid water causes the increase in large-scale precipitation higher in the atmosphere.

To summarize, large-scale precipitation-soil moisture feedback is dictated by two factors. The first factor is greater low-level (< 700mb) cloud fraction in RunC increases the autoconversion threshold, thereby inhibiting large-scale precipitation. Since cloud fraction is calculated using relative humidity (Pal et al., 2000), the colder air temperatures in RunC tend to produce higher cloud fraction with less available moisture. This results in persistent non-precipitating clouds for RunC (Figure 2.10a and 2.10c). The second factor is greater cloud liquid water at higher levels in the atmosphere (> 700mb). With greater cloud liquid water, RunI is likely to exceed the autoconversion threshold and

produce precipitation. The two factors are not independent in that with greater low-level cloud cover, evaporated surface moisture is less likely to extend higher into the atmosphere. To that effect there is less moisture aloft (> 700mb) in RunC and less large-scale precipitation throughout the column.

2.5.5.3 Precipitation Phase

In addition to differences in total precipitation (convective and large-scale), the phase of precipitation also differs in the NGP region. During the winter and transition months RunC has 3-14% more total precipitation falling as snow (Figure 2.11b). The maximum differences in percent precipitation as snow coincide with the greatest differences in total precipitation (Figure 2.9b). This implies that RunI not only has more total precipitation during the transition months, but also a greater percent of precipitation falling in the liquid phase. While this change in phase does not make a substantial difference in the amount of snow cover on the ground, it does appear to influence amount of liquid water in the soil. Using the GLACE coupling parameter to examine liquid precipitation similarity across pentads for March through May, we find a clear region of soil moisture-liquid precipitation coupling over the northern and central Great Plains (Figure 2.11a). This indicates that liquid precipitation falling in one pentad coincides with subsequent liquid precipitation in other pentads over the coupled region. This identifies the northern and central Great Plains as regions with an intra-seasonal soil moisture-precipitation feedback during the March transition season.

2.6. Discussion of Winter Feedback Mechanism

The feedback diagram presented in Figure 2.12 broadly describes the proposed winter feedback mechanism with associated correlation coefficients between variables involved in the convective precipitation feedback for NGP (April and October). Correlations for the large-scale precipitation portion of the feedback were not included due to the complex processes occurring at multiple layers in the atmosphere to produce large-scale precipitation. During colder months, our results indicate that soil water phase plays a role in moderating soil temperatures as shown by strong correlation between percent soil moisture as liquid and subsurface temperatures (R=0.626; Figure 2.12). For years with warmer winters, the amount of available surface energy increases (R=0.397 for ground temperature and available surface energy), leading to an increase in liquid phase precipitation (Figure 2.9 and 2.11). This causes more water to enter the soil column resulting in warmer surface temperatures during the cold season in RunI. This tendency of precipitation-soil moisture feedbacks to moderate especially cold temperatures in RunI prevents ground and air temperatures from reaching the freezing point during the transition into and out of winter (Figure 2.6). As such, subsequent precipitation events are more likely to produce liquid phase precipitation (Figure 2.11) that can further contribute to the feedback cycle. In contrast, RunC has a fixed amount of soil liquid water and ice, resulting in colder climatological temperatures due to the lack of land-atmosphere feedbacks and persistent soil ice. While this feedback is likely amplified by the persistent soil ice in the experiment construct, it highlights the role of soil ice in cold season land-atmosphere coupling.

The land-atmosphere feedbacks can affect two precipitation pathways, convective and large-scale precipitation. For convective precipitation, MSE increases due to increased atmospheric moisture and warmer air temperatures in RunI (Equation 6 and

R=0.224). This is evident in Figure 2.8 where there is a direct relationship between MSE anomalies and surface soil temperature differences (a difference of 1 K in soil temperature at the surface corresponds to a 1 kJ/kg change in MSE). This soil moisture-convective precipitation feedback cycle is most important during the fringe winter months (April and October for the NGP region) within the coupled region. The winter land-atmosphere feedback also affects large-scale precipitation through warmer temperatures and increased evapotranspiration in the interactive run (RunI). Warmer temperatures decrease relative humidity at lower levels in the atmosphere (< 700mb), corresponding to a decrease in fractional cloud cover. Due to the reduction in cloud cover, the autoconversion threshold decreases requiring less in-cloud water to produce large-scale precipitation (Figure 2.10). Additionally, increased evapotranspiration provides more moisture to the atmosphere. The higher moisture flux into the atmosphere further promotes large-scale precipitation higher in the atmosphere (> 700mb). The large-scale soil moisture-precipitation feedback occurs during transition months that are colder and have more large-scale precipitation (March and November for the NGP region).

Regions where this feedback is valid are determined by the frequency and persistence of cold air masses. As a region transitions further into winter, the heat reservoir from the near-surface soil column (e.g., shallower than 50cm) is drawn down and eventually extinguished. This terminates the land-atmosphere feedback, as seen at higher latitudes during DJF (Figure 2.6 and 2.8). This behavior is also reflected in the migrating behavior of the coupling region, which tends to be located slightly south of the surface freezing line. Therefore, the freezing line represents a time-evolving transition zone.

2.7 Conclusions

This study outlines a winter land-atmosphere feedback mechanism that highlights the importance of the soil water phase and soil moisture-precipitation feedbacks throughout the seasonal cycle. We find that there are two distinct land-atmosphere coupling regimes present. The first coupling regime is the feedback traditionally observed during the summer, where an increase in soil moisture increases latent heat release, MSE in the atmosphere and convective precipitation (e.g., Pal *et al.*, (2001) and references therein). The RegCM-CLM reproduces this type of coupling regime as noted in the GLACE over the Southern Plains during JJA. However, here we highlight a second, previously undiscussed land-atmosphere coupling regime during the winter mid-latitudes that is a function of soil water phase. This winter coupling regime is driven by the ability of soil moisture phase to control surface fluxes, which can create a set of feedbacks that influence convective and large-scale precipitation (Figure 2.9 and 2.11). As a result of this winter feedback, the land-atmosphere winter coupling regimes are located slightly south of the freezing line. In this respect, the freezing line may be regarded as a temporally varying transition zone similar to the semi-arid to moist transition zone discussed in Guo *et al.*, (2006) for boreal summer.

The results are discussed from the perspective of simulations performed by one regional climate model, RegCM-CLM. Prior land-atmosphere coupling studies with multiple models indicate that coupling strength can vary substantially between models (Dirmeyer et al., 2006), therefore studies with other high-resolution models would further elucidate this mechanism and identify any inherent model biases that could affect the winter coupling strength and mechanism. Additionally, there are known biases in our simulation of temperature and precipitation (Section 2.5.1), yet the model biases do not

appear to track the coupling pattern. Therefore the proposed mechanism and the winter coupling is likely not an artifact of those specific model biases. However, the temperature and precipitation biases may enhance or dampen the coupling strength and affect the timing of the land-atmosphere feedbacks.

The nature of the climate model experiment and fixed climatological soil water phase can lead to a deviation from the mean climate state where RunC develops atmospheric temperatures that are on average colder than the RunI simulations (e.g., Figures 2.6 and 2.7). Although this experiment design may represent a case that is not observed in the atmosphere, comparing RunC to RunI demonstrates the ability of the presence of soil ice to guide the atmosphere to a colder mean state and illustrates the winter land-atmosphere feedback. These limitations not withstanding, the results in this paper present a seasonal perspective on land-atmosphere coupling and suggest a winter feedback triggered by the presence of soil ice.

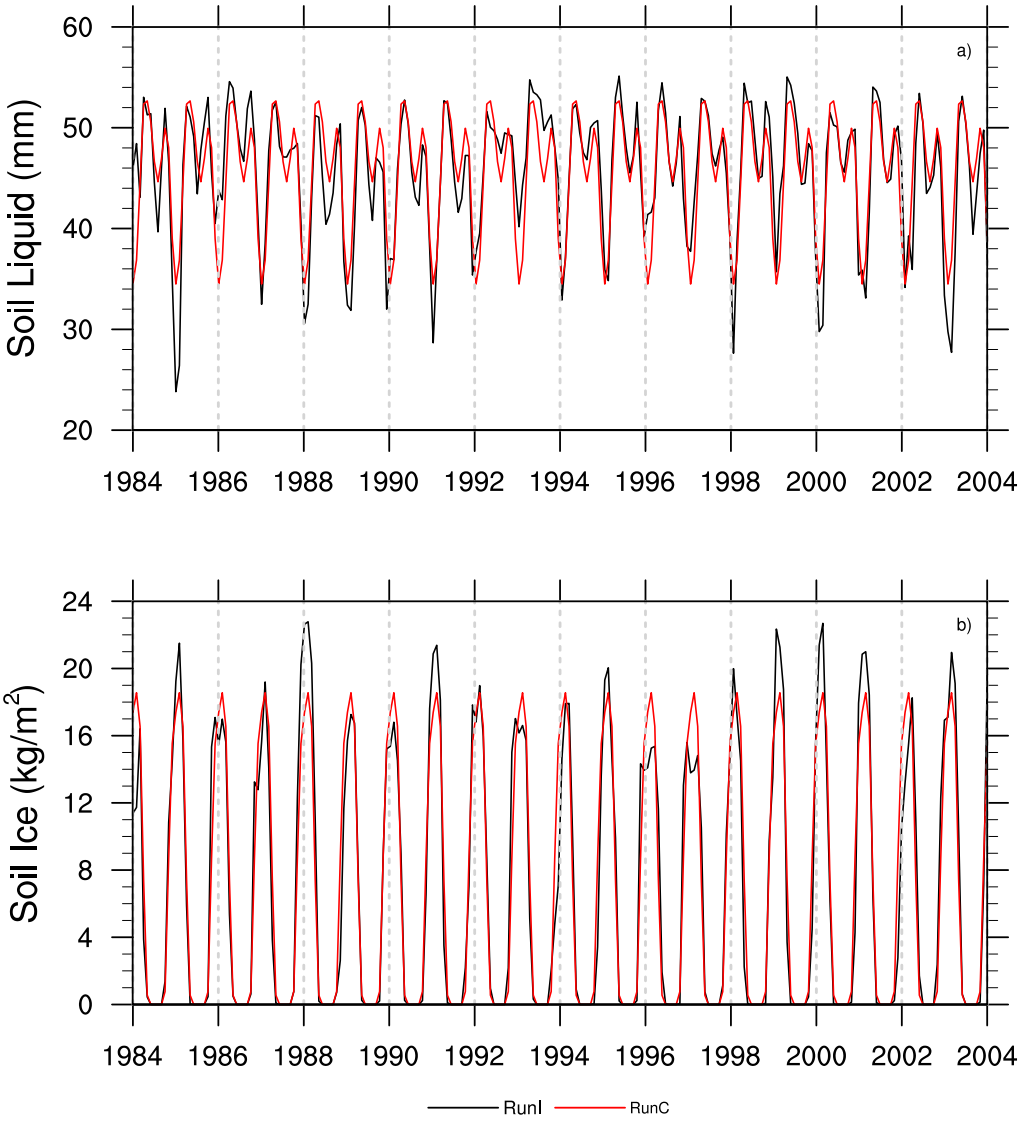

Figure 2.1 Inter-annual variability of the surface soil layer (top 10cm) of (a) soil liquid (mm H2O) and (b) soil ice (kg m^{-2}) for RunI (black) and RunC (red) over Northern Great Plains region (NGP; see box in Figure 2.3).

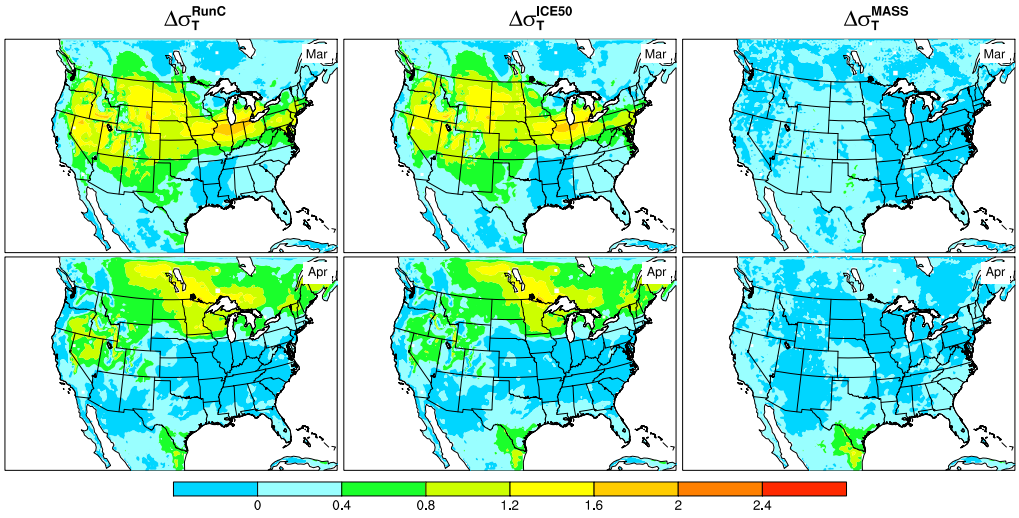

Figure 2.2 March and April coupling strength, $\Delta\sigma_T = \sigma_{RunI} - \sigma_{climatological}$, where warmer colors signify stronger land-atmosphere coupling.

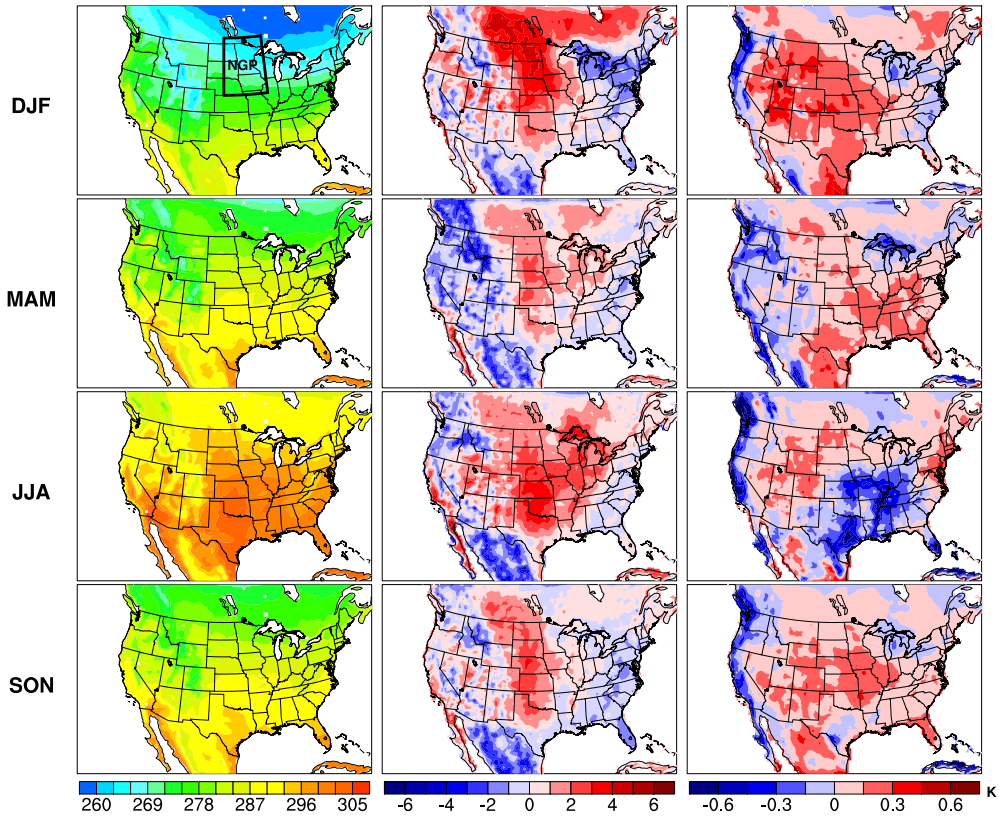

Figure 2.3 Seasonal temperatures (K; left column), absolute biases compared to CRU (center column), and relative bias of inter-annual variability ($1 - \sigma_{RunI}/\sigma_{CRU}$; right column). Red (blue) colors imply the model is warmer (colder) than CRU observations for absolute bias figure. For relative bias of inter-annual variability, red (blue) colors imply the model has less (more) inter-annual variability than CRU observations. The black box identifies the Northern Great Plains (NGP; 40-50°N and 100-90°W) averaging region used in subsequent analysis

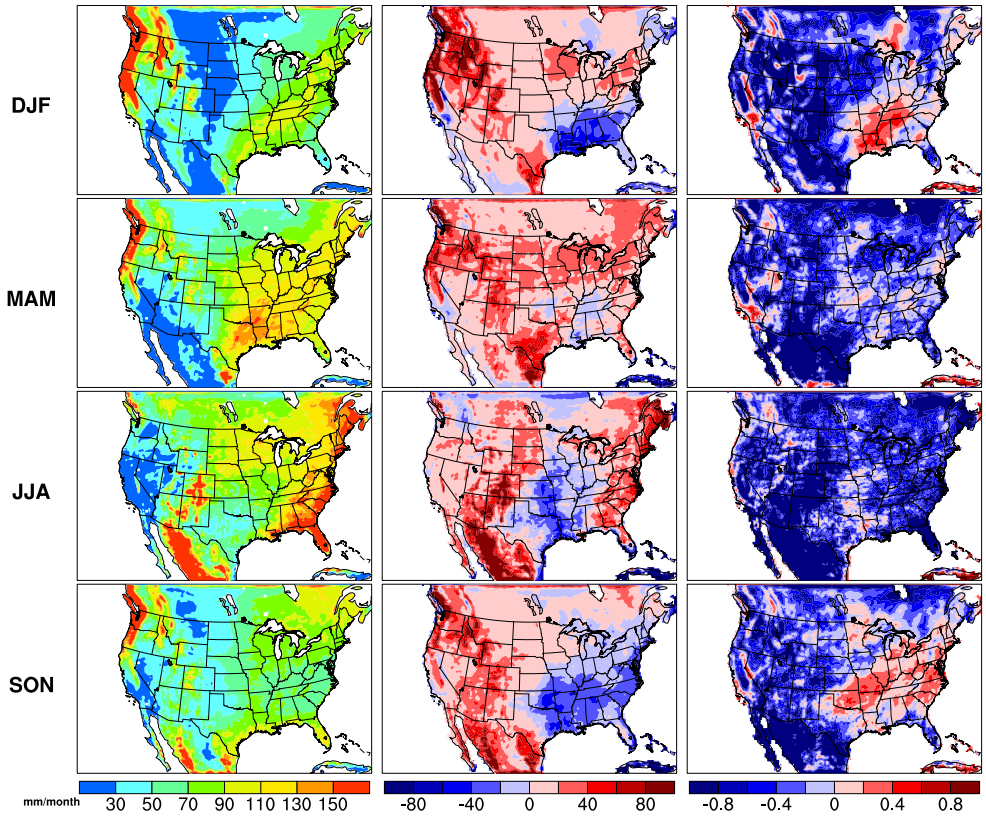

Figure 2.4 Seasonal precipitation (mm month^{-1}; left column), absolute biases compared to CRU (center column), and relative bias of inter-annual variability ($1 - \sigma_{RunI}/\sigma_{CRU}$; right column). In the center column, redder (blue) colors imply the model is wetter (drier) than CRU observations. In the right column, redder (blue) colors imply the model has less (more) inter-annual variability than CRU observations.

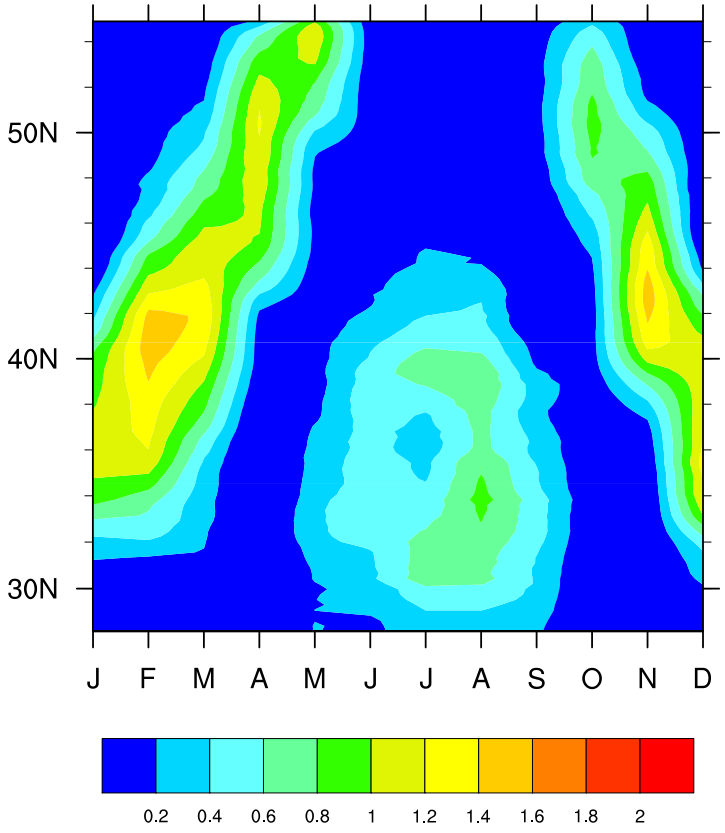

Figure 2.5 Seasonal meridional coupling strength, $\Delta\sigma_T = \sigma_{RunI} - \sigma_{RunC}$, averaged over 100-90°W.

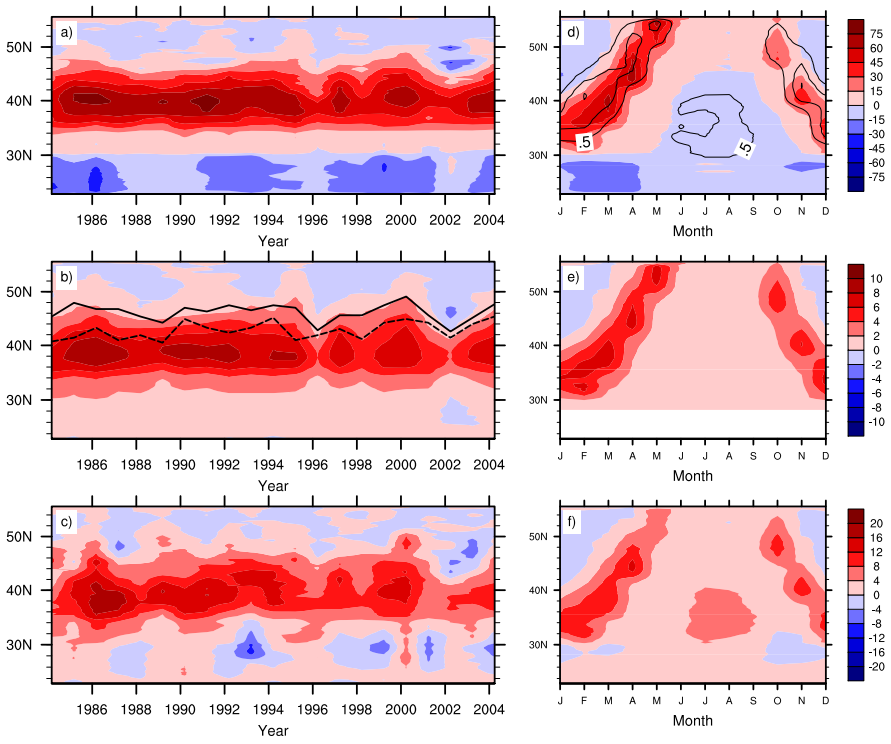

Figure 2.6 (Left) Meridional averages (100-90°W) of March interannual variability for differences between RunI and RunC (RunI-RunC) for (a) available surface energy (W m^{-2}), (b) ground temperature (K), and (c) surface net longwave radiation (W m^{-2}). (Right) Meridional (100-90°W) climatolological averages of (d) available surface energy, (e) ground temperature, and (f) surface net longwave radiation (W m^{-2}). Solid and dashed lines in (b) represents RunI and RunC freezing lines, respectively. Contour lines in (d) represent coupling strength ($\Delta\sigma_T$).

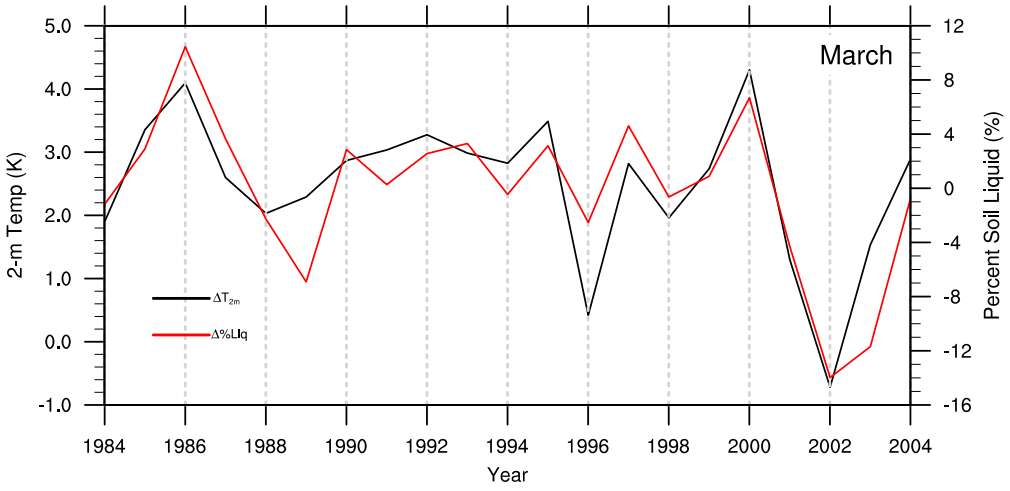

Figure 2.7 Inter-annual variability of the difference of ground temperature (RunI minus Run C; black) and the difference in percent soil water as liquid (RunI minus RunC; red) during March averaged over the NGP region.

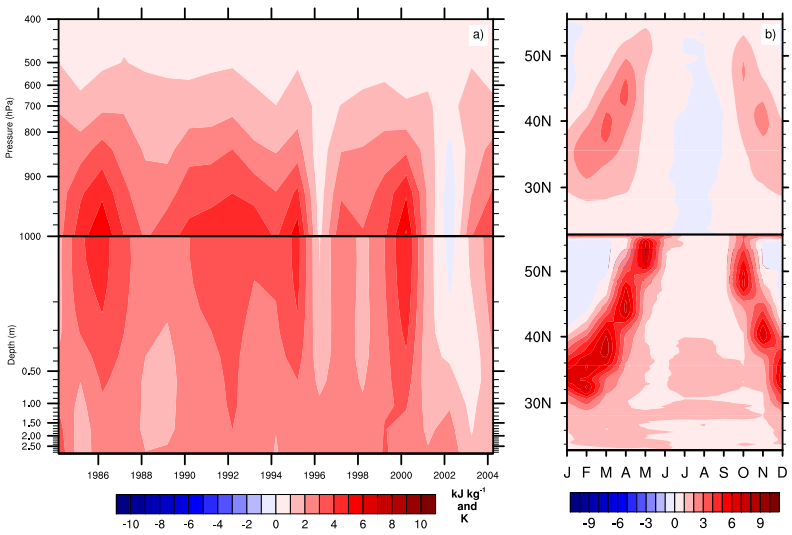

Figure 2.8 Meridional averages (100-90°W) of Mar ch interannual variability (a) and annual climatologically averaged (b) differences between RunI and RunC (RunI-RunC) for vertical profiles of moist static energy (kg/kJ; top) and soil temperature (K; bottom). Red (blue) colors mean RunI is warmer (colder) or has more (less) MSE than RunC.

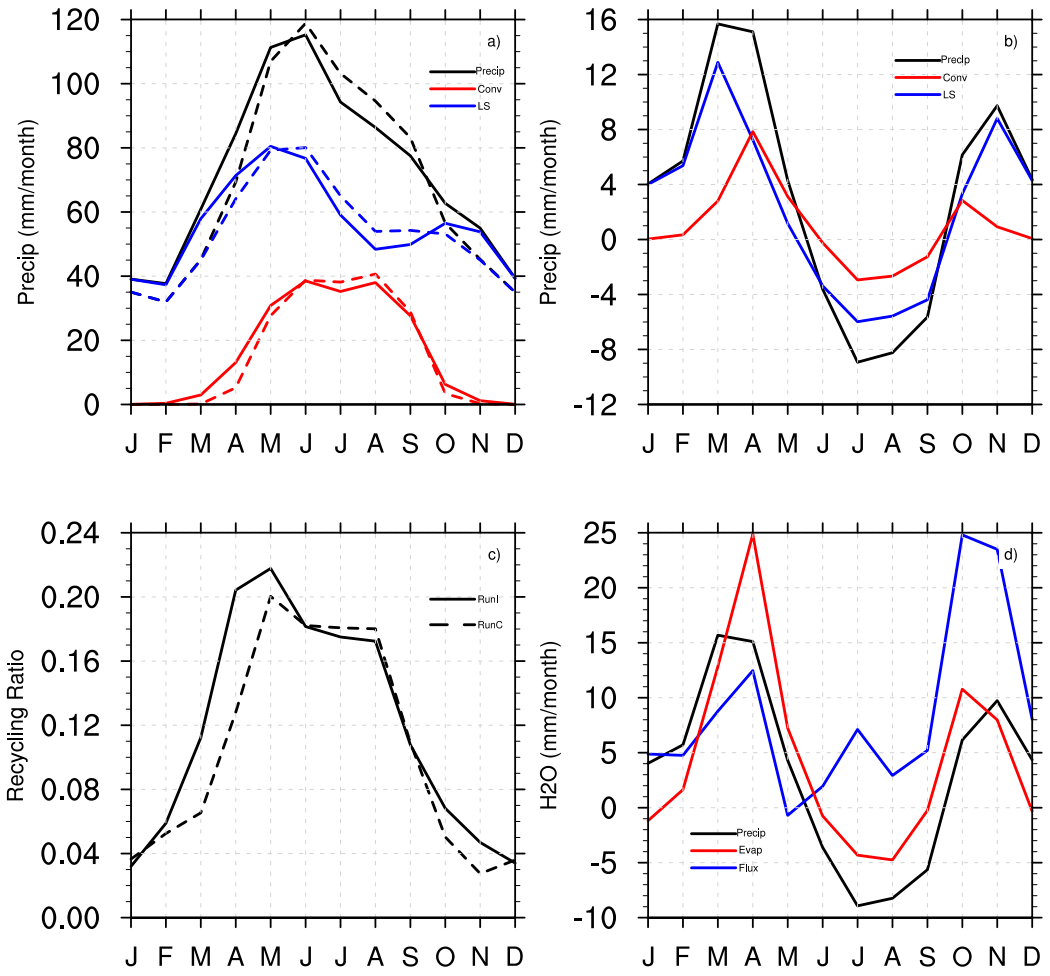

Figure 2.9(a) Monthly climatologies of large-scale, convective, and total precipitation for RunI (solid) and RunC (dashed). (b) Monthly climatological differences (RunI – RunC) for contributions of large-scale (blue) and convective (red) precipitation to the total (black). (c) Monthly climatologies of recycling ratio (β) for RunI (solid) and RunC (dashed). (d) The difference (RunI - RunC) in atmospheric moisture sources for total precipitation (black), moisture flux into the region (blue; IN from equation 1), and evapotranspiration within the region (red; ET from equation 1). All are averaged over the NGP region shown in Figure 2.

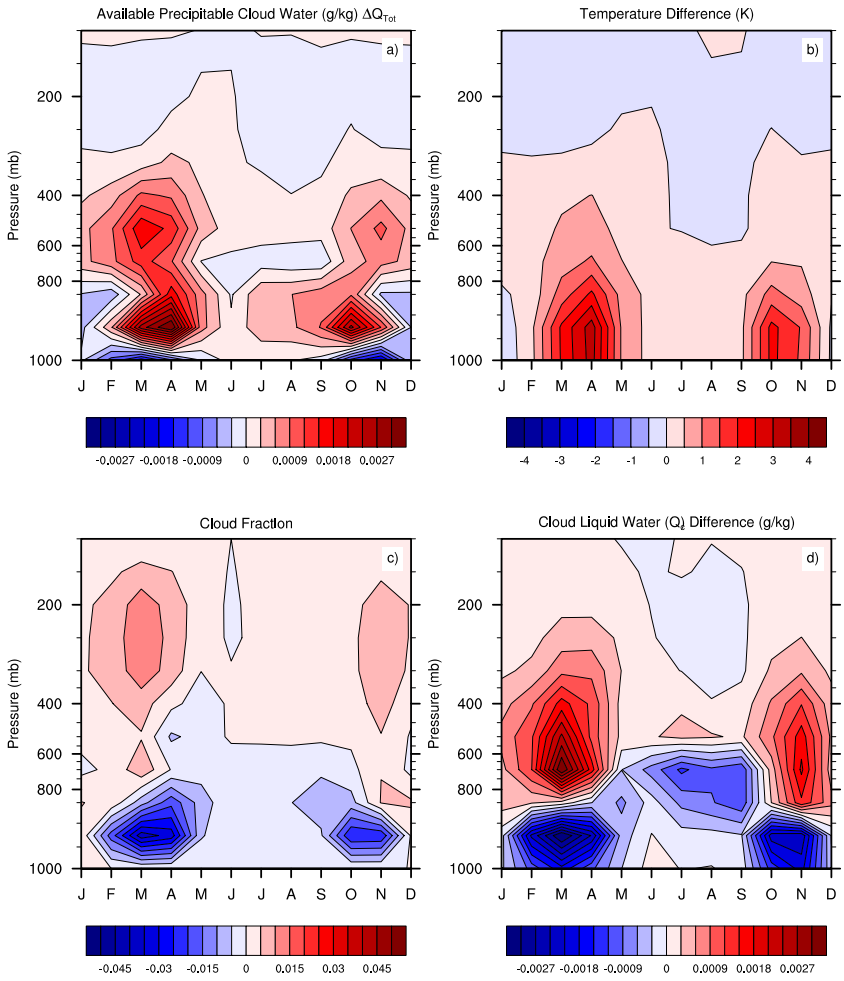

Figure 2.10 Monthly climatological difference between RunI and RunC over NGP for (a) available precipitable cloud liquid water (ΔQ_{tot}), (b) temperature (K), (c) cloud fraction and (d) cloud liquid water. Warmer (cooler) colors indicate that RunI (RunC) values are greater than RunC (RunI).

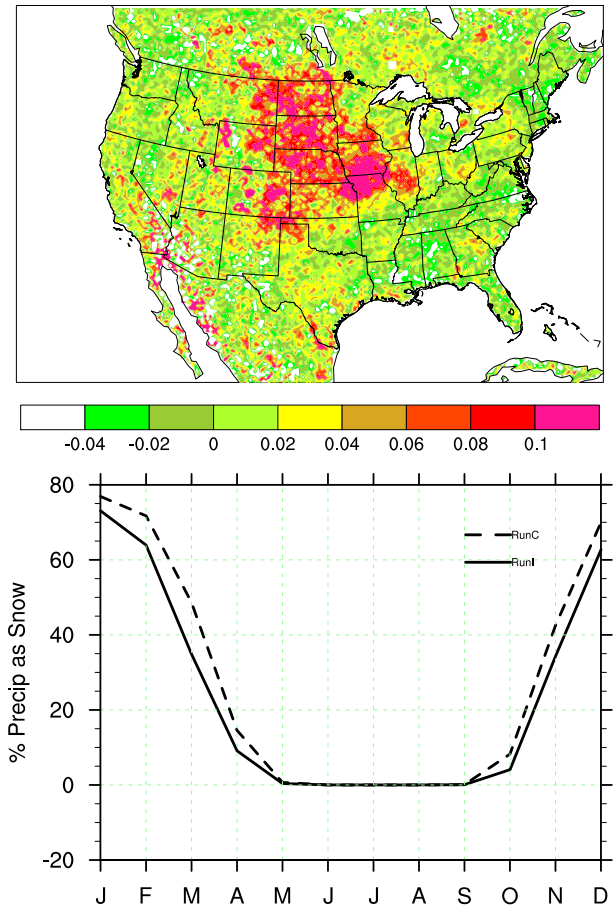

Figure 2.11 GLACE coupling parameter, $\Delta\Omega$, of liquid precipitation for MAM (top) and monthly mean climatology of percent precipitation as snow for RunI (solid) and RunC (dash).

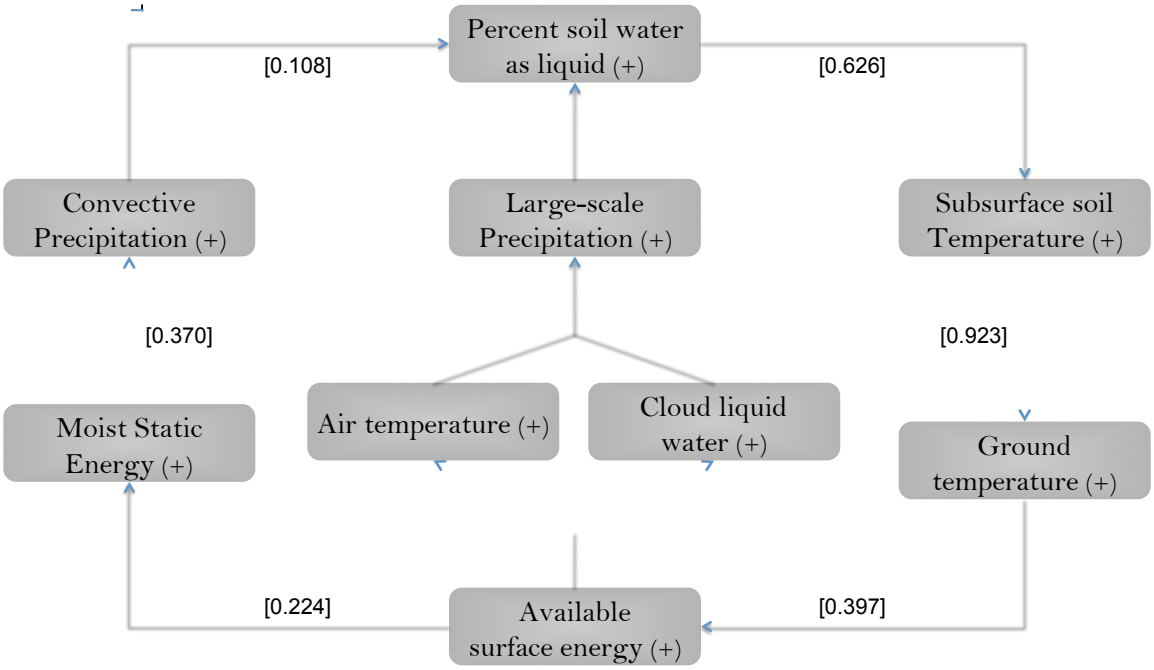

Figure 2.12 Winter land-atmosphere feedback mechanism with cross-variable correlations for $\Delta\sigma_T > 1K$ East of Rocky Mountains during April for RunI.

Chapter 3

Quantifying the contribution of environmental factors to isoprene flux interannual variability

3.1 Abstract

Terrestrial isoprene emissions directly respond to leaf temperature, photosynthetically active radiation (PAR), soil moisture, and plant characteristics such as leaf area index (LAI). Prior work has estimated isoprene interannual variability at 5-25%, however the relative contributions of individual environmental factors have not been delineated. A biogenic isoprene emissions model (MEGAN) is coupled to a regional climate model (RegCM4-CLM) to evaluate variations in monthly isoprene emissions. We use a novel approach to estimate the contribution of environmental factors to monthly averaged isoprene flux variability and analyze regional differences over the contiguous U.S. for summers spanning 1994-2008. Consistent with earlier studies, isoprene flux varies 8-18% interannually with the greatest variability occurring in July. Yearly changes in isoprene flux are poorly described by any single environmental factor, yet temperature and soil moisture together account for at least 80% of the total isoprene flux variations for

all regions during the summer. Soil moisture plays the most significant role in controlling variability over the Northeast and Southeast, but only exceeds temperature in importance during August in the Northeast and July in the Southeast. PAR and LAI are nearly negligible contributors to summer interannual variability. Uncertainty in climate model soil moisture parameterizations can drive large variability in isoprene fluxes when including the isoprene soil moisture dependency factor, suggesting a need for further validation.

3.2 Introduction

Isoprene (C_5H_8) is an important ozone precursor in the presence of nitrogen oxides (NO_x) (Chameides et al., 1988) and its oxidation products can condense to produce secondary organic aerosols (Dentener et al., 2009). Both tropospheric ozone and atmospheric aerosols can lead to poor air quality and also influence the Earth's radiative budget either directly or indirectly (Andreae and Rosenfeld, 2008; Zhao et al., 2011). The primary source of isoprene to the atmosphere is emissions from terrestrial vegetation, with global estimates between 400-700 Tg yr^{-1} (Guenther et al., 2006; Arneth et al., 2008; Muller et al., 2008; Ashworth et al., 2010). Isoprene emissions are known to be controlled by several environmental factors, including temperature (Petron et al., 2001), light (Sharkey et al., 1996), soil moisture (Llusia et al., 2008), ambient carbon dioxide (CO_2) concentrations (Wilkinson et al., 2009), and phenology (Kuhn et al., 2004). As coupled climate-chemistry models move towards long-term simulations of tropospheric chemical environments (Fu et al., 2011), it is necessary to understand how individual environmental factors contribute to interannual isoprene flux variability.

Past studies have used observed isoprene concentrations and fluxes to estimate isoprene flux variability. In a hardwood forest site in Michigan, four years of canopy-level isoprene flux measurements showed low (~10%) inter-annual variability during the summer (Pressley et al., 2005). Although year-to-year variability at this site was strongly correlated to light and temperature, other unnamed environmental variables were implicated in controlling emissions variations. In Texas, two studies have investigated isoprene flux interannual variability (Gulden et al., 2007; Warneke et al., 2010). Gulden et al., (2007) concluded that modeled summer emissions yielded greater interannual variability when leaf area index (LAI) was allowed to respond to atmospheric forcing data (25%) as opposed to the typical LAI annual climatology (12%). In the second study, aircraft measurements of isoprene concentrations were used to infer isoprene emissions over northeastern Texas in 2000 and 2006 (Warneke et al., 2010) and found a factor of two difference in isoprene flux estimates between the two years. This difference was attributed to the unusually warm and dry conditions recorded in the summer of 2000, however the factor of two uncertainty in the inferred isoprene emissions is comparable to inter-annual variability. Comparing these inferred isoprene fluxes to several emissions inventories, Warneke et al., (2010) further demonstrated that models had difficulty capturing the observed interannual variation and was likely due to the lack of a direct soil moisture suppression of emissions during drought stress and/or lack of yearly varying LAI. However, neither of the two Texas studies account for direct emission suppression under decreasing soil moisture, which has been found to reduce global emissions by 20% (Muller et al., 2008).

At the regional scale, satellite-derived observations of formaldehyde column concentrations have been used to infer top-down isoprene emission fluxes and quantify

isoprene flux interannual variability (Abbot et al., 2003; Palmer et al., 2006; Duncan et al., 2009). Abbot et al., (2003) used this technique with the Global Ozone Monitoring Experiment (GOME) satellite to estimate August interannual variability of 30% over the southeastern United States. They found that flux variations followed surface air temperature but interannual changes in temperature alone could not explain the variations in isoprene emissions. Palmer et al., (2006) also used GOME formaldehyde measurements to quantify interannual variability and estimated a range between 22-35% during the summer and suggested that 75% of variations are controlled by surface temperatures. In Palmer et al., (2006), the temperature-driven variation was estimated from the temperature dependency algorithm of an empirically-based isoprene emissions model (Guenther et al., 1995). A subsequent study focusing on the southeastern U.S. and utilizing higher resolution formaldehyde measurements (Ozone Monitoring Instrument; OMI) were in agreement with earlier estimates of variability (22% for the summer) and also implicated temperature as the primary driver (Duncan et al., 2009).

A global study using an interactive vegetation model supports the importance of land use in emissions calculations and estimates lower interannual variability (10%) for North America (Lathiere et al., 2006), yet we note that this study also does not account for emissions reductions due to soil water limitations (Guenther et al., 1995). Arneth et al., (2011) found that different isoprene emissions algorithms using the same climate forcing data estimated similar isoprene flux interannual variability. This suggests that climate variables (e.g. temperature, radiation, LAI, and soil moisture) play a strong role in controlling year-to-year emissions changes. Further, Arneth et al., (2011) found that interannual variability over the mid-latitudes was relatively small (5-10%) and attributed this to conflicting climate variable interactions. For example, warmer temperatures that

increase emissions are well correlated with drier soils, which decrease emissions. This further emphasizes the need to quantify the role each control variable has on emissions variations.

Several of these studies (Pressley et al., 2005; Duncan et al., 2009; Warneke et al., 2010) cited are for specific locations where differences in observed isoprene flux variability may reflect regional differences. This highlights the need for a multi-region analysis of isoprene variability. As noted by Duncan et al. (2009), evaluating the influence of an individual climate variable on observed isoprene flux variability is difficult due to the strong correlations between climate variables. Although prior studies have provided estimates of the isoprene flux variability, there is little attribution of each environmental factor to flux variability that accounts for the direct effect of soil water limitations on emissions. Studies that include the soil moisture dependency can reduce global emissions up to 7-20% (Guenther et al., 2006; Muller et al., 2008) and can improve regional agreement with observations (Muller et al., 2008). Additionally, most studies operate on global domains and use land models forced with half-hourly or longer atmospheric data, resulting in coarse temporal and/or spatial resolution. Due to the heterogeneous nature of isoprene source strength and the sensitivity to temporal resolution of climate data (Ashworth et al., 2010), using a coupled, high-resolution regional model is likely to improve understanding of the influence of environmental factors on isoprene flux variability. The primary objectives of this study are to quantify the relative contributions of temperature, light, LAI, and soil moisture on isoprene emissions variability and to assess regional differences in the environmental variables controlling emissions over the contiguous U.S. A secondary goal is to introduce a simple methodology for calculating

percent contributions of the environmental dependency factors that could be applied to other environmental control variables not considered in this study.

3.3 Methods

A biogenic emissions model (the Model of Emissions of Gases and Aerosols from Nature; MEGAN) (Guenther et al., 2006), described in Section 3.3.1, is coupled to the International Centre for Theoretical Physics (ICTP) Regional Climate Model version 4 (RegCM4; (Giorgi et al., 2012)) to examine the relative contributions of leaf temperature, soil moisture, photosynthetically active radiation (PAR), and LAI to biogenic isoprene emissions. RegCM4 is a compressible, hydrostatic, primitive-equation model with a land surface described by the Community Land Model version 3.5 (Oleson et al., 2008), which determines the canopy-scale environment variables for input into MEGAN (Section 3.3.2). Based on RegCM4-CLM-MEGAN model output, the contribution of individual environmental factors is calculated as described in Section 3.3.3.

3.3.1 Biogenic isoprene emissions model: MEGAN

MEGAN is a biogenic emissions model (Guenther et al., 2006) that parameterizes observed relationships to estimate emissions. The canopy environment version of MEGAN determines isoprene emissions for each model grid cell as:

$$E = \varepsilon \rho C_{CE} \gamma_{PT} \gamma_{SM} \gamma_{age} LAI \qquad 3.1$$

$$\gamma_{PT} = \gamma_T (\gamma_{Psun} + \gamma_{Pshade}) \qquad 3.2$$

where E is the isoprene emission flux (μg h^{-1} m^{-2}), ε is a standard emission factor taken at standard conditions described in Guenther et. al., (2006) (μg h^{-1} m^{-2}), ρ is the in-canopy loss or production factor (=0.96), C_{ce} is an empirical adjustment factor for the canopy environment (=0.4), and γ_T, γ_P, γ_{SM}, and γ_{age} describe the influence of leaf temperature, PAR, soil moisture, and leaf age on isoprene emissions, respectively. The canopy description is based on that of the RegCM4 land model, the CLM version 3.5. CLM contains a single layer canopy model that is divided into sunlit and shaded fractions, which allows the calculation of γ_P and emissions based on the fraction of sunlit and shaded leaves (Equation 3.2). A high-resolution 30" emission factor map, ε, is used (http://cdp.ucar.edu) and bi-linearly interpolated to the model gridcell-level and is not linked to the CLM land cover type. The effects of past temperature and light conditions on time scales of 24 hours and 10 days are included in the current implementation.

The response of isoprene emissions to soil moisture is defined as (Guenther et al., 2006)

$$\gamma_{SM} = \sum_j f_{root}^j \max(0, \min(1, (\theta^j - \theta_{wilt})/0.06)) \qquad 3.4$$

where f_{root}^j is the fraction of root in a given model soil layer (j), θ_{wilt} is the wilting point, and θ^j is the volumetric soil moisture (m^3 m^{-3}) at a given layer. The current parameterization only captures the effects of long-term drought conditions and can only reduce emissions (Pegoraro et al., 2004); short-term drought responses are not included. Inclusion of γ_{SM} in isoprene emissions models indicates improved measured-modeled agreement for isoprene fluxes (Muller et al., 2008). The CLM method for calculating γ_{SM}

includes ten unevenly spaced soil layers and determines f_{root}^{j} for each soil layer using plant functional types (PFT). Up to four different PFTs can exist in a single grid cell providing a more detailed land surface description in regions with heterogeneous vegetation types. All gamma dependency factors are calculated at the PFT-level and then aggregated to the gridcell-level.

3.3.2 RegCM4-CLM Experiment Design and Input data

RegCM4-CLM has been shown to reproduce mean climatological conditions over the contiguous United States (Tawfik and Steiner, 2011). The horizontal grid spacing is 60 km centered at 96W and 38N over the continental US (Figure 3.1) and the atmosphere contains 18 vertical layers in hybrid-sigma coordinates. The time resolution is 200 seconds for the dynamical core, and the land surface (CLM) and biogenic emissions model (MEGAN) are called every 600 seconds within the coupled model framework. Because RegCM4 is a limited area model, we use 6-hourly European Centre for Medium-Range Weather Forecasts Interim Reanalysis (ERA-Interim) boundary conditions for the atmosphere and weekly-prescribed ERA sea surface temperatures to drive the RegCM4-CLM (Dee et al., 2011). Simulations are performed from 1992-2008, and the model is initialized in June 1992 using average soil moisture from the Global Land Data Assimilation System (GLDAS) CLM model realization (Rodell et al., 2004) and run for 1.5 years to achieve model equilibrium. Model output is analyzed for the last 15 simulation years (1994-2008).

As prior studies have demonstrated, accurate biomass density information can play a key role estimating regional isoprene emission rates (Lathiere et al., 2006; Gulden

et al., 2007). Therefore, a half-degree daily satellite-derived LAI product (Stockli et al., 2011) is used to represent seasonal and interannual variations in LAI. The LAI data are spatially bi-linearly interpolated to the model grid and 1994 LAI is used for the model spin-up years. The summer (June-July-August; JJA) is the focus of analysis due to the high isoprene emission rates and its corresponding relevance to air quality.

3.3.3 Variability Attribution Calculation

To assess each variable's relative contribution to emissions, a first order Taylor series approximation is performed on isoprene emissions (E). E can be written in two ways, as a Taylor series (Equation 4) and as a variation about a mean (Equation 3.5):

$$E = \overline{E} + \frac{\partial E}{\partial \gamma_T}\Delta\gamma_T + \frac{\partial E}{\partial \gamma_{SM}}\Delta\gamma_{SM} + \frac{\partial E}{\partial \gamma_P}\Delta\gamma_P + \frac{\partial E}{\partial LAI}\Delta LAI + O^2 \quad 3.4$$

$$E = \overline{E} + dE \quad 3.5$$

Setting these equations equal to one another and dropping higher order terms (O^2), the equation becomes

$$dE = \frac{\partial E}{\partial \gamma_T}\Delta\gamma_T + \frac{\partial E}{\partial \gamma_{SM}}\Delta\gamma_{SM} + \frac{\partial E}{\partial \gamma_P}\Delta\gamma_P + \frac{\partial E}{\partial LAI}\Delta LAI \quad 3.6$$

where dE is the total variability about the mean and each term on the right hand side is a single dependency factor's contribution to the total variability. The Δ term on the right-hand side of the equation is the deviation from the mean for a particular year and month of a given dependency factor. Hereinafter, we refer to each γ term as a dependency factor (e.g., γ_T is the "temperature dependency factor"). To retrieve a percent

contribution to the total variation, *dE*, each term on the right hand side is correlated with *dE*. The R^2 correlation coefficient measures the percent to which a dependency factor can explain variations in *dE* using a linear relationship. The influence of higher order, non-linear terms on reconstructing *dE* was found to contribute less than 10% to the total calculated flux, suggesting that 1st order linear terms represent a majority of *dE* and gamma dependency factors are largely independent of one another. This simple Taylor series approach could be applied to other environmental factors not considered in this study such as CO_2 (Heald et al., 2009).

3.4. Results

3.4.1 Comparison with Observed Flux Measurements

The highest absolute modeled isoprene emissions occur over the southern Plains and southeastern U.S. during JJA (> 5 mg m^{-2} h^{-1}; Figure 3.1a) due to the underlying vegetation cover and high isoprene-emitting vegetation located in this region. Figure 2 compares the average diurnal isoprene emissions from RegCM4-CLM against two mid-latitude measurement sites, Harvard Forest for July 1995 (Goldstein et al., 1998) and the University of Michigan Biological Station (UMBS) for July 2000 (Pressley et al., 2005). RegCM4-CLM generally underestimates emissions at both locations with the largest underestimate occurring at UMBS by a factor of 4 during the daily maximum. Model evaluation improves when compared to Harvard Forest emissions, where the model underestimates the midday peak by only 2 mg m^{-2} h^{-1}. These emissions are consistent with other modeling studies comparing MEGAN versus Harvard forest measurements, with the model underestimating emissions by a factor of 1.35 (Muller et al., 2008). For the

north- and southeastern U.S., other modeling studies find MEGAN overestimates emissions by a factor of 2 (Stavrakou et al., 2009; Warneke et al., 2010). Because absolute isoprene flux emissions depend heavily on the e map (Arneth et al., 2008), the large biases found at UMBS may be due to underestimated ε at that particular model gridcell.

3.4.2 Normalized Isoprene Emissions and Interannual Variability

To remove the isoprene emissions bias related to vegetation information contained within e found in Section 3.3.1, we calculate a normalized isoprene flux ($E_N=E/\varepsilon$). Using E_N isolates the effects of the dependency factors on emissions (Equation 1) because the canopy chemical production/loss factor, ρ, and empirical coefficient, C_{ce}, do not vary spatially. Normalized isoprene emissions are greatest East of the Rockies with the highest fluxes over the eastern half of Texas into Arkansas and Louisiana (Figure 3.1b). Additionally, the locations with the greatest E_N generally correspond to regions with the greatest absolute emissions (E) (Figure 3.1a). This implies that areas containing the highest base ε also have the strongest contributions from environmental controls. Because the temperature and light dependency factors vary non-linearly, a 1 K temperature decrease (10%) and 15 W/m^2 decrease in radiation (11%) corresponds to a 0.45 mg m^{-2} h^{-1} (or 22%) reduction in E. Both LAI and soil moisture modify emissions linearly in the current parameterization and are unlikely to be important intra-seasonally when changes in temperature and light vary most.

Interannual variability (IAV) of isoprene emissions for each month and region is calculated using E_N (Table 3.1). Here we define IAV as the average absolute percent departure from the mean for a particular month:

$$IAV = \frac{1}{n}\sum_{y=1}^{n}\left|\frac{x_{y,m} - \bar{x}_m}{\bar{x}_m}\right| x100 \qquad 2.7$$

where $x_{y,m}$ is isoprene flux for a particular year (y) and month (m), $\bar{x}_m$ is the average isoprene flux for month m over all years of the simulation (1994-2008) and n is the total number of simulation years.

In the Southeast, IAV ranges from 13% in July to 7.8% in August. The northeast demonstrates similar behavior with greatest variability in July (13.7%) but comparably weaker variability in June and August. Year-to-year variations in isoprene emissions over the Plains peak in early summer (10.4%) and gradually decrease as the summer progresses. IAV for the West is greatest relative to the other regions with up to 18.4% variability on average for July. The consistently high IAV in summer emissions in the West can be attributed to high single-year departures from the mean, such as in August and July of 1998. This was a known strong El Niño year where percent departure from mean reached 60% (Figure 3) and is consistent with prior studies demonstrating global isoprene emissions are higher during strong El Niño events (Naik et al., 2004; Lathiere et al., 2006). When excluding these single year extremes, yearly departures from the mean more closely resemble variability seen in other regions. It should also be noted that the West has weaker emissions (Figure 3.1), therefore a 40% departure from the mean in the aggregate dependency factors results in only a 0.016 mg m^{-2} h^{-1} change in absolute emissions. Other regions occasionally show large departures, such as the Southeast in June 1998 and the Northeast in July for 2005 and 2007 (Figure 3.3). The large deviations from the mean found in the Southeast for July occur in 2000 and 2007, corresponding with strong drought years (Lawrimore et al., 2001; Luo and Wood, 2007).

3.4.3 Variability of Dependency Factors and Relationship with Isoprene Emissions

Two metrics are used to assess the sensitivity of emissions to each dependency factor. The first is linear correlation, where strong correlations indicate the specific dependency factor has a large effect on emissions. Figure 3.4 shows the relationships between a dependency factor (γ_T, γ_P, γ_{SM}, and LAI) and E_N for each region. The second metric is the IAV of the individual dependency factors (Figure 3.5). The behavior of these metrics and implications on controlling variability are discussed for each region below.

For the Southeast, γ_T is well correlated with E_N for June (R=0.64) and August (R=0.65), but decreases for July (R=0.3). IAV of γ_T peaks in August (16%) and has minimum variations in July (11.5%; Figure 3.5). Variations in γ_P are weak for the Southeast (< 4.5 %), but exhibit good correlation with E_N for July (R=0.59) and August (R=0.58). In July, the soil moisture dependency factor, γ_{SM}, and LAI are also well correlated to E_N (R=0.56 and R=0.66, respectively); however, LAI varies by less than 2% from year to year (Figure 3.5) and is further highlighted by the tight clustering pattern around a single LAI value in Figure 3.4. γ_{SM} and γ_T are the only dependency factors to exhibit strong correlation with E_N as well as IAV greater than a few percent (11.5% for γ_{SM}; Figure 3.5). We note that γ_{SM} and γ_T are strongly negatively correlated (R=-0.69, -0.59, and -0.85 for JJA) and correlations between γ_{SM} and E_N are weak outside of July (R=0.08 for June and R=-0.27 for August). The implications of the strong correlation between γ_{SM} and γ_T are discussed in Section 3.5.

The Northeast consistently demonstrates the strongest relationship between temperature and E_N with correlations of 0.81, 0.83, and 0.53 for June, July, August, respectively. Throughout the summer, IAV in γ_T is also large relative to other dependency factors (11-18% for JJA). For light dependence, July is the only month that γ_P shows good correlation with E_N (R=0.55). The soil moisture dependency factor, γ_{SM}, exhibits weak correlation with E_N throughout the summer. IAV of γ_{SM} for a given month increases as summer drying deepens from June (3.8%) to August (10.5%). Similar to the Southeast, γ_T and γ_{SM} are negatively correlated for JJA (see Section 3.4). Finally, LAI is not well correlated with normalized emissions and year-to-year variability is low (< 1.5%) throughout the summer, making it an unlikely driver of emissions in the Northeast.

The Plains exhibit the highest average temperatures of all the regions especially in August of 2000 (γ_T = 2.05 and a corresponding average temperature of 303 K), a drought year (Warneke et al., 2010). Despite the relatively warm temperatures and large IAV of γ_T (19, 13, and 21% for JJA), γ_T correlates well with E_N only in early summer (R=0.69 in June; Figure 3.4). The influence of γ_T on E_N is dampened later in the summer for July (R=0.1) and August (R=0.38) due to the negatively correlated relationship between γ_T and γ_{SM}. The light dependency factor, γ_P, is the only dependency factor to remain well correlated for all months in this region (R=0.5-0.58), although IAV of γ_P is small (e.g. less than 4.5% variability). LAI and γ_{SM} do not show any strong correlation with E_N over the Plains throughout the summer. The soil dependency factor, γ_{SM}, varies between 11-17% interannually which is much greater than γ_P variability (Figure 3.5). The possible consequence is that although γ_{SM} has a weaker correlation with E_N, higher variability may

still influence E_N IAV to a greater degree than γ_P. LAI has the lowest interannual variations of all the dependency factors at less than 3%.

E_N for the West are the lowest and do not vary by more than 0.38, or 0.1 mg m^{-2} h^{-1} in absolute emissions. Low emissions notwithstanding, γ_T is identified as the dependency factor with the strongest influence on E_N for the West in June (R=0.51) and comparable to γ_{SM} in August (R=0.56). Light dependency is poorly correlated (R=0.03-0.31) with E_N throughout the summer, as is LAI. The response of E_N to changes in soil moisture is important for July and August with correlations of 0.57 and 0.58, respectively. Unlike other regions, the temperature-soil moisture relationship found in the West is not as pronounced for July and August with correlation coefficients of -0.36 and -0.14, respectively. June is the only month that is well correlated for the West (R=-0.65). This indicates that soil moisture and temperature are largely decoupled for this region and can be considered independent of one another outside of June.

In summary, the response of E_N to environmental factors can vary from region to region due to differences in regional climate. One similarity is that LAI and γ_P exhibit weak IAV across all regions (Figure 3.5) and, in the case of LAI, rarely correlates well with normalized and absolute emissions. This lack of variability limits the importance of LAI and γ_T as drivers of year-to-year emissions changes. γ_T and γ_{SM} generally have the largest IAV coinciding with strong correlations with E_N, although correlations with E_N are often dampened by the negative correlation between γ_T and γ_{SM}. Additionally, γ_{SM} has the best correlation with E_N where deeper root structures are collocated with summer root soil drying.

It should be noted that γ_{SM} values from this study are generally 0.2 lower than values quoted by other studies (Guenther et al., 2006; Muller et al., 2008). This reduced γ_{SM} is attributed to the higher wilting point in RegCM4-CLM. More specifically, wilting point ranges from 0.204-0.222 m^3 m^{-3} for this study over all U.S. regions, which is considerably higher than values used by Muller et al., (2008) (0.171 m^3 m^{-3} constant for all locations) and Guenther et. al., (2006) (0.01 m^3 m^{-3} for sand and 0.138 m^3 m^{-3} for clay). This highlights the wilting point as an important model parameter affecting the magnitude of γ_{SM}. Furthermore, lower γ_{SM} in this study reduces the total U.S. summer monthly emissions by 5-8 Tg C $month^{-1}$ as compared to Palmer et al., (2006), a study that did not account for soil moisture effects on isoprene emissions (e.g. $\gamma_{SM} = 1$).

3.4.4 Attribution of Dependency Factors to Interannual Variability

Using the first-order Taylor series approximation (Equation 3.6; Section 3.3.3), each dependency factor component is correlated with *dE*. This correlation, R^2, quantifies the degree to which variations in *dE* can be explained by the linear relationship between *dE* and a specific dependency factor (Figure 3.6). The light dependency factor, γ_P, shows poor correlation with *dE* ($R^2 < 0.3$) for all regions throughout JJA, with the exception of June and July over the Northeast and all of JJA for the Plains (Figure 3.6). Although absolute emissions are sensitive to changes in γ_P on daily to hourly timescales, low year-to-year variability (Figure 3.5) and poor correlation for most regions indicate that γ_P is likely not the primary driver of interannual changes in isoprene emissions. Variations in LAI exhibit an even weaker control on isoprene flux variability with R^2 less than 0.2 (Figure 3.6). This is contrary to prior studies suggesting that variations in LAI play a comparable

role to temperature and light over the eastern half of Texas (Gulden et al., 2007). However, we note that Gulden et al., (2007) used an observationally constrained phenology model to estimate LAI and did not include the influence of soil water limitations on emissions. The indirect influence of soil moisture on LAI variability may be the reason for this difference in attribution and is discussed further in Section 3.5.

The soil moisture dependency factor, γ_{SM}, consistently shows good correlation with *dE* for the West ($R^2 > 0.5$) and can account for at least 50% of *dE* variations for the West. It should be noted that this was the only region where γ_T and γ_{SM} were not well correlated (e.g. the dependency factors were decoupled). Similarly, the Northeast in June and July has an R^2 between *dE* and γ_T greater than 0.4. Aside from the West and early summer in the Northeast, no dependency factor is well correlated with *dE* suggesting that no single dependency factor is a good predictor of emissions variability despite the clear linear dependence of the parameterization (Equation 3.1). This lack of correlation between any particular dependency factor and *dE* (Figure 3.6) likely arises from the opposite effects between the dependency factors, such as with γ_T and γ_{SM}. When the negative correlation is strong between γ_{SM} and γ_T, the terms on the right hand side of Equation 3.6 are opposite in sign and can weaken the influence each variable has on emissions variability (*dE*) (e.g., weak correlations in Figure 3.6). Summing the γ_{SM} and γ_T terms in Equation 6 and calculating an R^2 correlation with *dE*, we find that over 80% of the variations in isoprene emissions can be explained by the net contribution of soil moisture and temperature (Figure 3.6).

3.5 Discussion and Conclusions

Temperature (Palmer et al., 2006; Duncan et al., 2009), land use (Lathiere et al., 2005), and LAI (Gulden et al., 2007) have all been implicated as important drivers of isoprene interannual variability over the U.S. Here we evaluate isoprene flux IAV and compare the relative importance of each dependency factor using a regional climate model coupled with MEGAN, a widely used biogenic emissions model. Average interannual variations of isoprene emission fluxes are between 8-18%, similar to earlier work.

Past studies have suggested that emissions variability is largely driven by the choice of climate forcing data (Arneth et al. 2011), and in this study, MEGAN was contained within the RegCM4-CLM model framework and isoprene fluxes were calculated every 10 minutes. Model biases in the underlying climate variables relevant to MEGAN may serve to either amplify or dampen the percent contribution of environmental factor presented in this study. As Tawfik and Steiner (2011) have shown, RegCM4-CLM overestimates summer temperatures over the Plains by an average of 2-4 K. This warm model bias in the Plains region may result in overestimates of absolute emissions, but likely does not influence the contribution analysis because deviations about mean conditions are used. RegCM4 overestimates temperature IAV in the Southeast and underestimates the variability in the Plains, which overestimate (underestimate) the total isoprene IAV (Table 3.1) for the Southeast (Plains). Additionally, recent land surface model development has shown that CLM3.5 tends to be too wet (Oleson et al., 2008; Decker and Zeng, 2009), which would underestimate the soil moisture contribution to variability especially in regions with highly variable summer soil drying.

One of the primary differences between this study and prior modeling work (Lathiere et al., 2006; Gulden et al., 2007) is the implementation of the soil moisture

dependency factor. The exclusion of the soil moisture dependency factor neglects the direct suppression of isoprene emissions and could lead to an overestimate of isoprene emissions in these models. Gulden et al., (2007) and Lathiere et al., (2006) utilize dynamic vegetation models that constrain LAI using remotely sensed vegetation products, which indirectly account for soil moisture effects on emissions through modification of LAI. Therefore, a portion of the attribution to LAI as a significant driver in Gulden et al., (2007) may include the indirect response of soil moisture. In this work, LAI is a diagnostic model state prescribed from a daily satellite-based reanalysis dataset, which is not responsive to modeled soil moisture; the indirect influence of realistic soil moisture is captured, however, and LAI can modify atmospheric conditions. As a result, any feedback related to model biases in temperature, incident radiation, or soil moisture are not amplified by modifications to LAI, which likely decreases the control LAI may have on isoprene emissions. A simulation was performed using the 1994 daily LAI map for each year (e.g. removing LAI interannual variations; not shown), and percent contributions and interannual variations presented in Section 3.4 were not significantly affected. This is consistent with Muller et al., (2008) who also found that interannual variations in LAI play a small role in determining yearly changes in isoprene flux globally.

Although estimates of isoprene interannual variability appear to be consistent across studies and different versions of the Guenther algorithms (Guenther et al., 1995; Guenther et al., 1999; Guenther et al., 2006), attribution to a single environmental variable is difficult. The results presented in this study highlight the importance of using the soil moisture dependency factor and quantify the relative contributions of temperature, soil moisture, PAR, and LAI to yearly changes in isoprene flux. We demonstrate that no single environmental factor serves as a good predictor or driver of

isoprene flux and that the combined first-order contributions of the soil moisture and temperature dependency factors account for at least 80% of modeled isoprene flux variations. Because the soil moisture-temperature relationship controls yearly variations in isoprene emissions, greater attention should be given to improving soil moisture isoprene flux parameterizations and soil moisture representations in models.

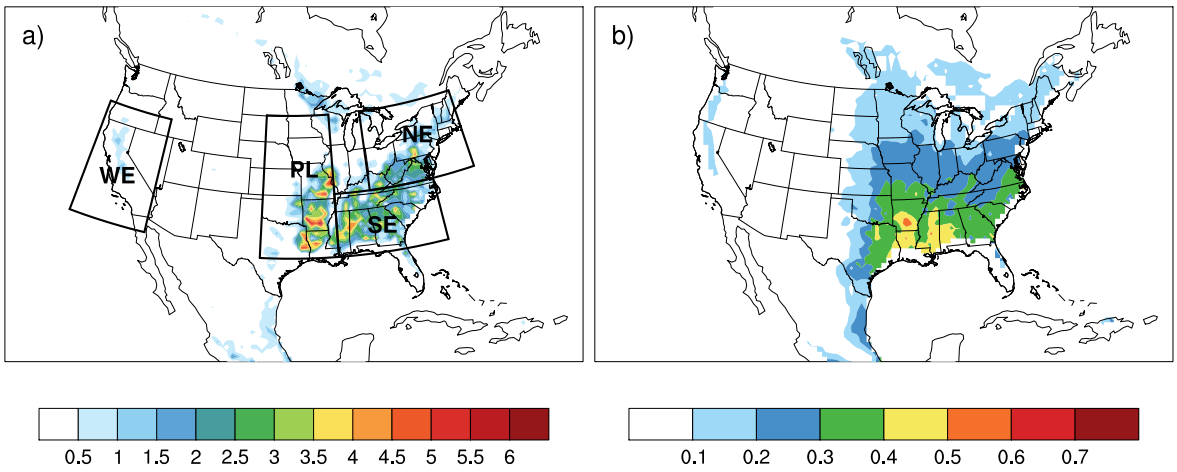

Figure 3.1 Summer (June-July-August) average of (a) absolute isoprene emissions (mg m^{-2} h^{-1}) and (b) normalized isoprene flux, E_N, for 1994-2008 with averaging regions for the Southeast (SE), Northeast (NE), Plains (PL), and West (WE).

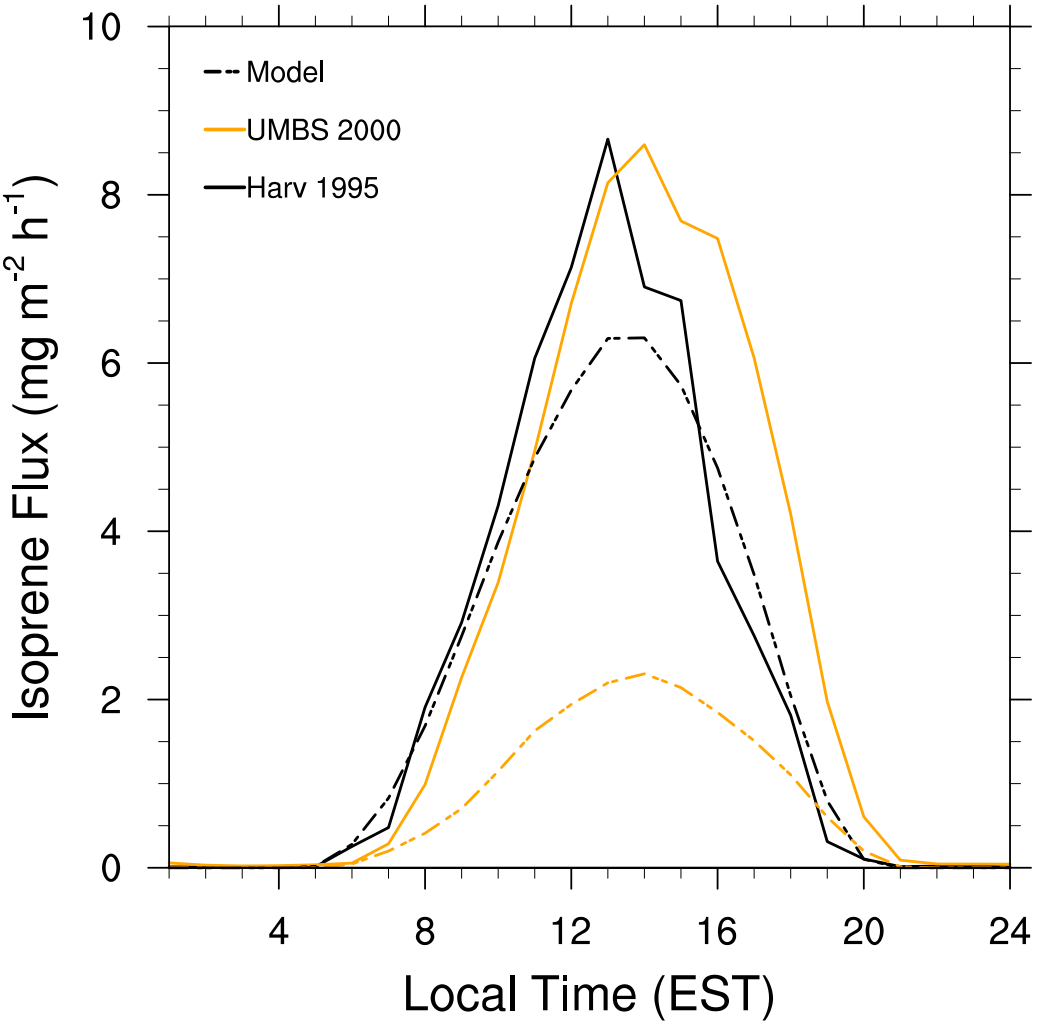

Figure 3.2 Average diurnal cycle of absolute isoprene emissions (mg m^{-2} h^{-1}) at two mid-latitude stations: July 1995 at Harvard Forest (black) and July 2000 at the University of Michigan Biological Station (orange). Dashed lines are from modeled RegCM4-CLM-MEGAN output.

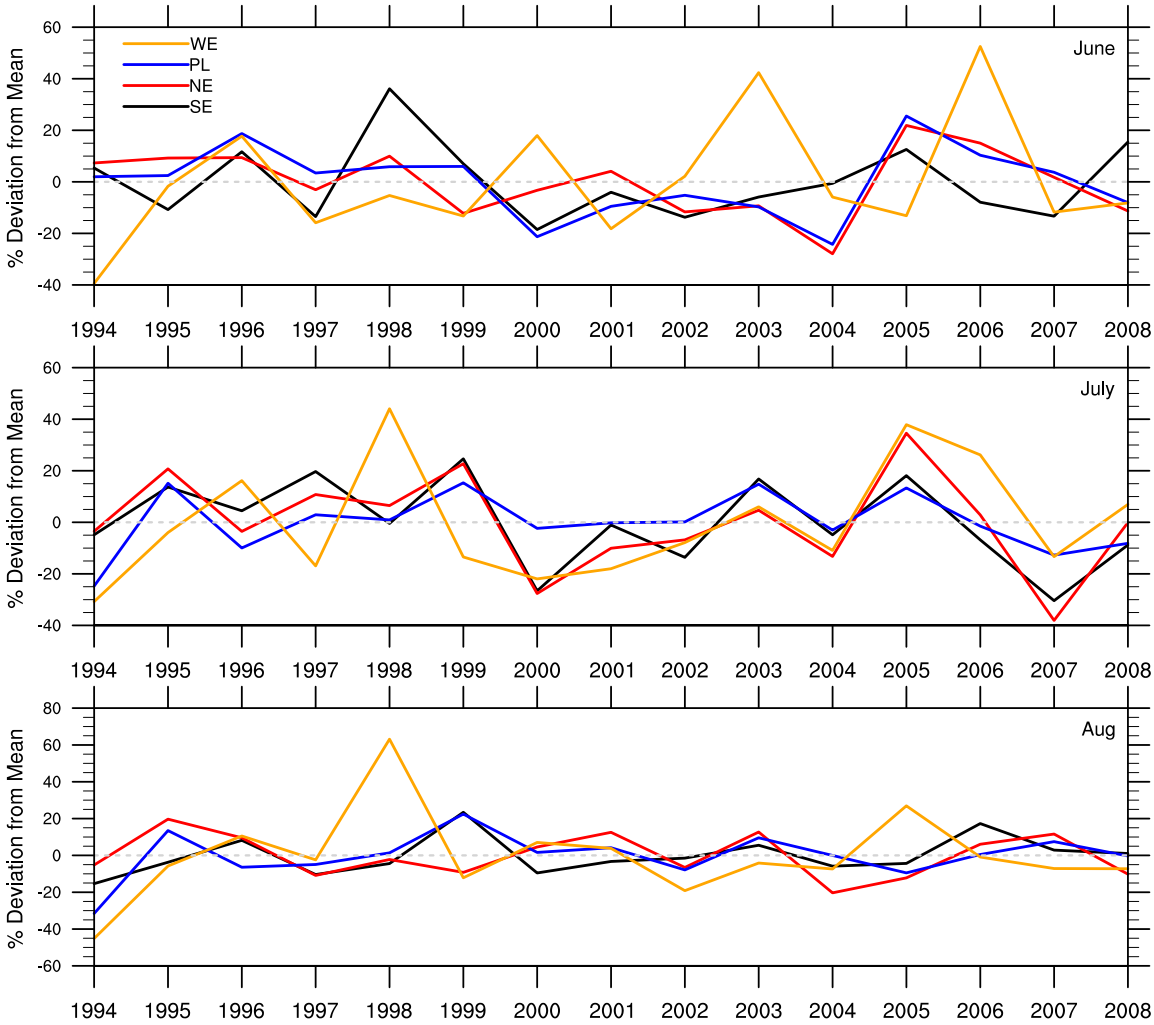

Figure 3.3 Percent departure from mean of normalized isoprene flux (E_N) for June, July, and August over the (black) Southeast, (red) Northeast, (blue) Plains, and (orange) West regions.

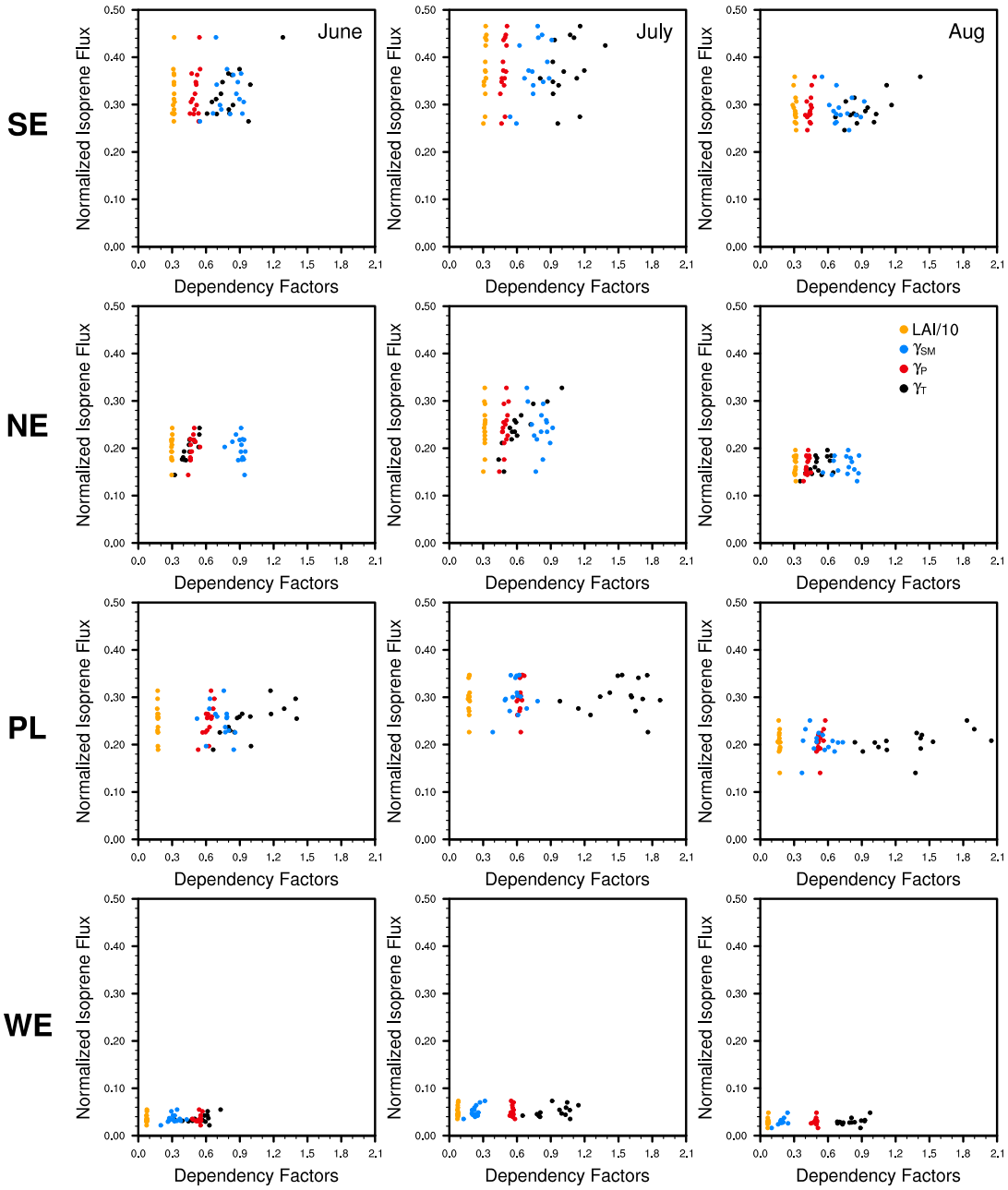

Figure 3.4 Dependency factors, (orange) LAI, (black) γ_T, (blue) γ_{SM}, and (red) γ_P, versus E_N for the Southeast, Northeast, Plains, and West regions (Figure 1). Note that LAI is divided by 10 for illustrative purposes. Each marker represents the monthly average for one simulation year averaged over the specified region.

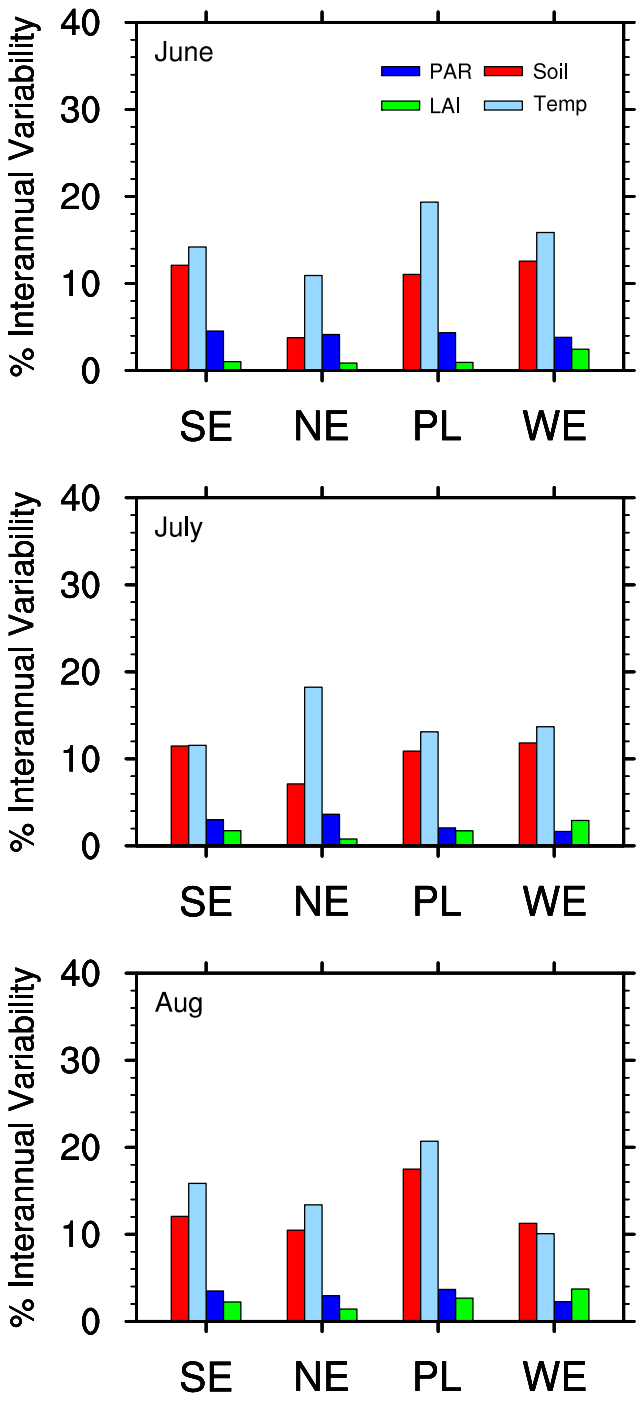

Figure 3.5 Percent interannual variability of temperature, PAR, soil moisture, and LAI dependency factors (Equation 3.1).

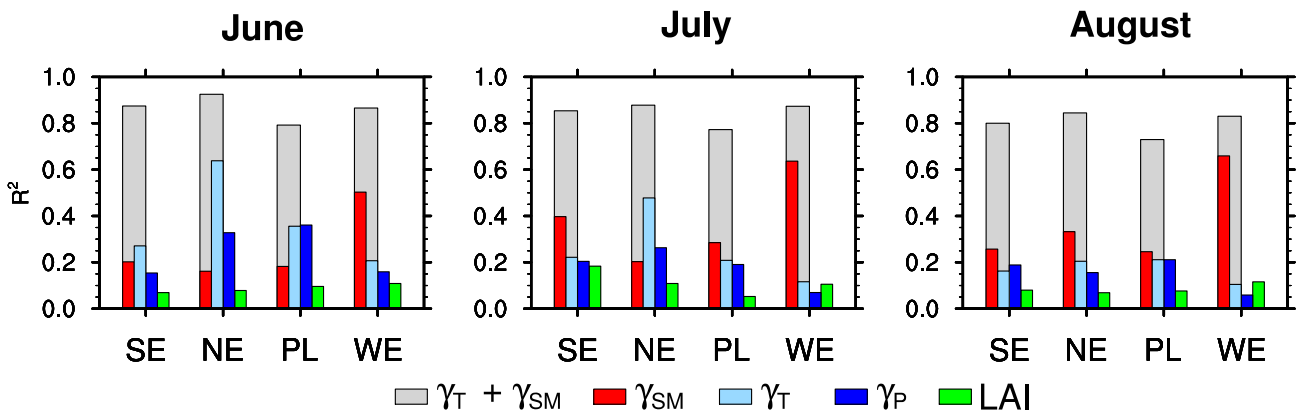

Figure 3.6 Correlation between (cyan) temperature, (blue) PAR, (red) soil moisture, (green) LAI dependency terms, and (gray) the sum of the temperature and soil moisture dependency factors against total isoprene flux interannual variability, *dE*. See Equation 6 for dependency terms.

Table 3.1 Interannual variability (IAV) of isoprene flux by region and month, 1994-2008

Table 1. Interannual variability (IAV) of isoprene flux by region and month, 1994-2008

Region	June	July	August
Southeast	11.8%	13.0%	7.8%
Northeast	10.5%	13.7%	10.2%
Plains	10.4%	8.4%	8.1%
West	17.7%	18.3%	14.9%

Chapter 4

Soil Moisture-Temperature Coupling Regimes provide a mechanistic explanation for ozone-meteorology Correlations

4.1 Introduction

Tropospheric ozone (O_3) is a well recognized secondary air pollutant that presents a hazard to human health (Lippmann, 1989; Bernard and Ebi, 2001; Knowlton et al., 2004; Bell et al., 2007) and agriculture (Heck et al., 1982; Akimoto, 2003; Ashmore et al., 2006). The eastern United States is especially prone to high summer O_3 concentrations caused by the combination of warm, stagnant meteorological conditions and abundant O_3 precursor species, such as biogenic isoprene (Chameides et al., 1988; Fiore et al., 2005; Guenther et al., 2006) and anthropogenic nitrogen oxides (Frost et al., 2006). A variety of modeling and observational studies have found that changes in temperature and humidity are the two primary predictors for O_3 for the Eastern U.S. (Cox and Chu, 1993; Sillman and Samson, 1995; Aw and Kleeman, 2003; Vukovich and Sherwell, 2003; Camalier et al., 2007; Dawson et al., 2007; Zheng et al., 2007; Zeng et al., 2008; Chan, 2009; Weaver et al., 2009; Blanchard et al., 2010a; Davis et al., 2011). The strength of these two variables as predictors varies spatially. However, the physical mechanism describing the

spatial pattern and the strong anti-correlation with humidity in the Southeast has not been explained in the literature.

Using statistical methods, Camalier et al., (2007) demonstrated that the primary O_3-predictor variables have a clear north-south transition, where high latitude O_3 (> 38°N) is strongly correlated to maximum temperature and lower latitude O_3 (<36°N) to humidity. Subsequent studies showed similar north-south gradients in predictor variables with humidity being anti-correlated with O_3 in the Southeast (Davis et al., 2011). Rasmussen et al., (2012) found that a climate-chemistry model (the Geophysical Fluid Dynamics Laboratory Atmospheric Model; GFDL-AM) captures the temperature-ozone relationship north of 37°N yet underestimates this relationship farther south. As noted by Rasmussen et al., (2012) this north-south behavior suggests a latitudinal shift in the regime controlling O_3 concentrations and may reflect inherent weaknesses in model physics.

Although there is agreement that temperature is the dominant controller of ambient O_3 concentrations, warmer temperatures often coincide with other meteorological conditions favorable to O_3 production (Cardelino and Chameides, 1995; Vukovich, 1995), such as stagnant conditions, reduced cloud cover, and drier soils. Early work found that drier soil moisture initialization resulted in increased sensible heat flux and warmer temperatures promoting higher O_3 concentrations throughout the boundary layer (Jacobson, 1999). From the climate perspective, there is increasing evidence that soil moisture can strongly influence sub-seasonal temperature and precipitation (Fennessy and Shukla, 1999; Pal and Eltahir, 2001; Fischer et al., 2007a; Kim and Hong, 2007; Wu et al., 2007b; Koster et al., 2010; Guo et al., 2011). This process of improved predictability is dictated by the ability of soil to retain information of prior precipitation

events long after an event has passed. This leads to changes in surface flux partitioning where drier (wetter) soils have been shown to reduce (promote) subsequent precipitation and increase (decrease) temperatures in some regions (Betts et al., 1996; Findell and Eltahir, 1997; Eltahir, 1998; Koster et al., 2010). Because summer surface air temperatures may ultimately be controlled by soil moisture, interannual changes in O_3 may exhibit signatures of the soil moisture-temperature coupling relationship.

The aims of this study are twofold: 1) to evaluate the relationship between O_3 interannual variations and soil moisture, a climate-scale variable and 2) to describe the physical mechanism that produces commonly observed correlations between O_3, temperature and humidity over the Eastern U.S. We will present a unified framework for explaining the latitudinal characteristics and patterns that are generally observed in the O_3 and humidity relationships.

4.2 Data and Methods

4.2.1 Observational and Data Assimilation Products

Hourly O_3 and isoprene concentration data in August from 1994-2010 are obtained from the Environmental Protection Agency's Air Quality System (EPA-AQS) Photochemical Assessment Monitoring Stations (US EPA). We focus on the hours of peak O_3 production and select EPA-AQS data from each day between 12pm to 4pm. Analysis is confined to stations within the eastern U.S. (25-50°N and 98-68°W). Data are filtered to include those stations and years with at least a half a month of measurements available. August is selected in this study due to peak summer temperatures and the potential for drought.

A suite of atmospheric and land surface data from Phase 2 of the North American Land Data Assimilation System (NLDAS2) is used for the climate data analysis. NLDAS2 provides hourly temperature, incident solar radiation (R), and specific humidity at $1/8^{th}$ degree resolution from 1994-2010 (Mitchell et al., 2004). NLDAS2 atmospheric forcing fields are elevation-adjusted quantities derived from the North American Regional Reanalysis (NARR; 32 km) (Mesinger et al., 2006) and are temporally and spatially disaggregated to the high resolution of the NLDAS2 (Cosgrove et al., 2003). Incident radiation is bias-corrected using 5 years of hourly GOES-8 satellite data (Pinker et al., 2003). The use of adjusted and bias-corrected atmospheric forcing fields allows for confidence when comparing these quantities against EPA-AQS station measurements. Surface variables (soil moisture, net surface radiation (R_n), and latent (λE) and sensible heat (H) fluxes) are acquired from NLDAS2-MOSAIC land surface model (Koster and Suarez, 1992, 1994). NLDAS2-MOSAIC is forced by NLDAS2 atmospheric data, including precipitation, pressure, and wind components in addition to the variables described above. Because NLDAS2 uses daily Climate Prediction Center (CPC) precipitation gauge data (Xie and Arkin, 1997) and Stage II 4 km hourly Doppler radar output, the NLDAS2-MOSAIC soil moisture and surface flux products are more accurate than the same surface variables output from free-running climate model simulations. In this study, we define soil moisture as soil water contained within the first 40 cm to capture a majority of root structure. Soil moisture at 100 and 200 cm depths were also examined and were not found to modify the conclusions reached in the current study. To avoid any single grid cell bias, NLDAS2 data are averaged over a quarter degree region around each EPA-AQS station.

4.2.2 Soil Moisture-Temperature Coupling Parameter

To identify factors limiting surface evapotranspiration, we employ a soil moisture-temperature coupling diagnostic ($\rho(E,T)$) defined as the Pearson correlation between evapotranspiration(E) and temperature (T) (Seneviratne et al., 2006). Negative values of $\rho(E,T)$ are referred to as soil moisture-limited or "coupled" while positive values are energy-limited or "uncoupled". The negative correlation between E and T ($\rho(E,T)<0$) represents an increase in temperature that occurs in soil moisture-limited regimes, where energy shifts away from latent heat flux due to limited soil moisture and towards more sensible heat flux and warmer temperatures . For energy-limited regimes ($\rho(E,T)>0$), soil moisture is plentiful and therefore evapotranspiration is only limited by the amount of surface energy available.

We calculate a modified version of $\rho(E,T)$ that uses midday average E and T for each August (e.g. the correlation between 31 days of E and T for each year) to calculate a monthly $\rho(E,T)$. By using daily correlations instead of annual correlations, interannual variations in the coupling parameter can be calculated and years of soil moisture-temperature coupling can be identified. The physical mechanism behind using $\rho(E,T)$ calculated from daily data is still physically consistent with the underlying connections between temperature and evapotranspiration (Seneviratne et al., 2010). Other soil moisture-atmosphere coupling diagnostics were examined (Dirmeyer, 2011) and returned similar results.

4.3 Results

4.3.1 Spatial Patterns of Ozone Concentrations and Correlations

Average August midday (12-4pm) O_3 over the Eastern U.S. is between 45-65 ppb with the highest concentrations occurring along the eastern seaboard, the Ohio River Valley, and Tennessee River Valley (Figure 4.1a). The lowest concentrations are found in northern New England, Florida, and the Northern Plains. Figure 4.1b shows the correlation between O_3 and temperature ($\rho(T,O_3)$) for August at each of the EPA-AQS stations with at least 10 years of data. Consistent with prior studies (Camalier et al., 2007; Davis et al., 2011; Rasmussen et al., 2012), temperature demonstrates a positive correlation throughout the domain with strongest correlations at higher latitudes ($R > 0.7$) and weakening correlations to the South ($R < 0.5$). The correlation between specific humidity and ozone ($\rho(q,O_3)$; Figure 4.1c) shows a similar north-to-south decrease as temperature, however with a transition from positive correlation coefficients to negative correlation coefficients south of the 37th parallel. Although humidity has been highlighted as a primary driver of O_3 interannual variations in the South (Camalier et al., 2007; Blanchard et al., 2010a; Davis et al., 2011), the physical mechanism explaining this correlation has yet to be described with any detail.

4.3.2 Meteorological and Climate Controls on Ozone

The soil moisture-temperature coupling parameter ($\rho(E,T)$) described in Section 4.2.2 as calculated from NLDAS data at the EPA station locations shows a similar spatial behavior as $\rho(q,O_3)$ (Figure 4.2a). Specifically, stations where soil moisture perturbations exert greater control on near-surface temperatures (e.g. negative values of $\rho(E,T)$) correspond to stations with a weaker $\rho(T,O_3)$ and negative $\rho(q,O_3)$. This suggests that the

ozone-meteorological relationships may be influenced by soil moisture forcing over the Southern U.S., representing a long-term climate forcing on O_3.

Comparing average O_3 concentrations for dry versus wet years highlights this potential soil moisture driven response (Figure 4.2b-c). Dry (wet) years are defined as negative (positive) deviations from the mean August condition of soil moisture from 1994-2010 at each EPA-AQS station (Figure 4.2c). Drier years correspond to increased midday O_3 over much of the Eastern U.S. (Figure 4.2b). There are some locations, however, that exhibit a weak change or decrease in O_3 when soil conditions are drier, such as parts of Central Ohio and the Chicago Metropolitan area. These weak correlations occur in regions when $\rho(E,T)$ is positive, indicating that temperature does not respond to soil moisture perturbations as readily. In the soil moisture limited Southeast ($\rho(E,T < 0)$, O_3 is more than 5 ppb higher during dry years with individual station differences greater than 12 ppb. Here we highlight three regions spanning a range of average coupling strengths, the Atlanta Metropolitan area (33-34.5°N and 83-85.4°W; referred to as ATL), a Mid-Atlantic region (37-39°N and 76-78°W; referred to as MID), and a Northeast region (40-42°N and 73-75°W; referred to as NE) in Figure 4.2c. In general, O_3 interannual variability is highest in ATL spanning a range of almost 40 ppb, while MID and NE vary by 15-20 ppb. Similarly soil moisture anomalies are weaker for NE and greater MID and ATL. All three regions show good correlation between soil moisture anomalies and O_3 concentrations with MID exhibiting the strongest relation (R=-0.66) and ATL the weakest (R=-0.36). The weak correlation for ATL is attributed, in part, to the reduction of NO_x emissions initiated in the early 2000's, which has been shown to reduce O_3 concentrations over the Southeast (Frost et al., 2006; Kim et al., 2006; Gego et al., 2007; Bloomer et al., 2009). Taking the years before (1994-1999) and

after (2000-2010) emissions reductions correlation becomes stronger for ATL, -0.46 and -0.58 respectively.

To better understand these environmental controls on O_3 interannual variability, zonally average anomalies are presented (Figure 4.3), where anomalous conditions are defined as deviations from the mean August conditions from 1994-2010 at EPA-AQS stations. In 1999, O_3 anomalies reach 12 ppb from the 30-36th parallels (Figure 4.3a), and this persists in 2000 with a more limited extent to the south (to 33°N). During the historic 2007 drought in the Southeast (Luo and Wood, 2007), O_3 concentrations were 4-10 ppb higher. The lowest O_3 anomalies occurred in 2009 from 32-38°N and were more than 10 ppb below the 17-year average during a wet year (Figure 4.3d). Typically, the largest absolute interannual variations occur south of 37°N, which is also the location of the transition from the energy-limited to soil moisture-limited regime as defined in Section 4.2.2 (Figure 4.4).

During the years with the largest O_3 anomalies (1999, 2000, and 2007), incident radiation and temperature anomalies are also higher than average (Figures 4.3b and 4.3c). For 1999 and 2000, incident radiation was about 40 W m^{-2} than the 17-year mean. Similarly in 2007 incident radiation was anomalously high (20-50 W m^{-2}) over the southern half of the U.S. The high incident radiation anomalies suggest that there was less cloud cover during these years for the southern half of the U.S. Warm temperature anomalies are concurrent with the incident radiation anomalies, with 2007 as the warmest year in the South (> 3 K), and 1999 and 2000 having weaker positive anomalies (0.5-3 K). Temperature anomalies also correspond to drier than average soil moisture conditions (Figure 4.3d), with 2000 and 2007 as the driest years in the time series. Soil moisture spatial anomalies follow the same pattern as temperature anomalies in the

South. Persistent dry soil moisture anomalies have been shown to lead to warmer temperatures by increased partitioning of radiation to sensible heat (Diffenbaugh et al., 2007; Fischer et al., 2007a; Hirschi et al., 2011; Jaeger and Seneviratne, 2011), and this is consistent with our findings for $\rho(E,T)$. The similar spatial patterns of surface variable anomalies highlight the ability of a climate scale variable such as soil moisture to modulate O_3 concentrations interannually via land-atmosphere interactions.

4.3.3 Soil Moisture-Temperature Coupling and Ozone

To understand the relationships between predictor climate variables (T, q, R) and O_3, we use the land-atmosphere coupling parameter $\rho(E,T)$ (described in Section 4.2.2) to define soil moisture-limited versus energy-limited regimes (Figure 4.4). Zonally averaged interannual changes in $\rho(E,T)$ show negative values south of the 35th parallel, indicating soil moisture-limited control on surface fluxes for all years except 2009. North of 40°N, evapotranspiration tends to be energy limited ($\rho(E,T)>0$). In the Mid-Atlantic region (35-40°N) the limiting factor varies interannually, with some years being soil moisture limited and others strongly energy limited suggesting a transition zone at these latitudes. As this is a zonal average of $\rho(E,T)$, individual stations within each latitudinal band may have larger $\rho(E,T)$ interannual variability (figure not shown).

Zonally averaged correlations between O_3 and certain environmental variables exhibit north-to-south features similar to the coupling parameter (Figure 4.4). Consistent with station data in Figure 4.1, temperature is positively correlated with O_3 throughout the Eastern U.S. with stronger correlations at higher latitudes (Figure 4.4; R=0.2-0.7). In contrast, specific humidity correlations exhibit a latitudinal gradient with a transition

from negative values in the South to positive values in the North. This transition occurs in the same Mid-Atlantic region (35-40°N) as the transition from soil water limited to energy limited (Figure 4.4). Incident radiation is positively correlated with O_3 from 29-35°N (R=0.7) and weakens slightly north of 35°N (R=0.3-0.6) in the Mid-Atlantic transition region.

The normalized latent heat flux ($\lambda E/R_N$) defines the portion of net surface radiation (R_N) partitioned to evapotranspiration and accounts for spatial and temporal variations in radiation, such as from cloud cover. $\lambda E/R_N$ is negatively correlated with O_3 for much of the U.S. and coefficients are often greater than temperature or humidity correlations (R<-0.6). Given the consistently strong interannual correlation between $\lambda E/R_N$ and O_3, $\lambda E/R_N$ may prove to be a better predictor of yearly changes in O_3 than other more commonly used variables. The strong correlation further highlights surface energy partitioning as a possible and necessary component for describing widely observed relationships between O_3, and temperature and humidity (Camalier et al., 2007; Blanchard et al., 2010a; Davis et al., 2011). The mechanism underlying this behavior is discussed in more detail in Section 4.4.

Consistent with the strong negative correlation between O_3 and $\lambda E/R_N$ in the South (Figure 4.4), the Bowen ratio ($H/\lambda E$), is generally higher in soil moisture-limited regimes when $\rho(E,T)$ is strongly negative, reflecting low evapotranspiration (Figure 4.5a). Higher Bowen ratios indicate that more available surface energy is partitioned towards heating the surface rather than the phase change of available water. For energy-limited regions ($\rho(E,T)>0$) in the northern latitudes, Bowen ratios remain relatively low suggesting equal partitioning between H and λE. For the soil moisture-limited regimes ($\rho(E,T)<0$) in the South, lower latitude stations show a tendency for R_N to partition more towards

sensible heat due to the drier surfaces. Because the Bowen ratio is dependent on net surface radiation, we also examine the sensitivity of λE and H to R_N using linear regression slopes (β) of daily variables (Figures 4.5b and 4.5c). Each point in Figure 4.5 refers to a particular year and station over the 1994-2010 time series, with slopes and correlation coefficients calculated using the 31 days of August for that particular year. Points with absolute values of the correlation coefficients ($|R|<0.3$) less than 0.3 are removed. The slopes, $\beta(R_N, H)$ and $\beta(R_N, \lambda E)$, represent the change in the respective surface fluxes given a change in net surface radiation available. Large positive or negative values of β indicate greater sensitivity of surface fluxes to radiation. The most prominent feature in $\beta(R_N, H)$ and $\beta(R_N, \lambda E)$ is the difference in sensitivity between soil-limited ($\rho(E,T)<0$) and energy limited conditions ($\rho(E,T)>0$). Sensible heat flux becomes more sensitive to perturbations in net radiation when evapotranspiration is soil moisture-limited. For latent heat flux, $\beta(R_N, \lambda E)$ shows a clear transition from positive to negative response to changes in net radiation (Figure 4.5c). Physically, latent heat flux decreases with increasing net radiation as soil moisture dries over the course of August. This is consistent with higher Bowen ratios and drier surface conditions.

Focusing on three smaller regions, ATL, MID, and NE defined in Section 4.3.2, higher O_3 concentrations generally occur during years that are soil moisture-limited particularly at lower latitudes (Figure 4.6). Ozone concentrations show a larger response to soil moisture limitations ($\rho(E,T)<0$) in ATL with 10 ppb and 15 ppb increases in the 50th and 75th percentiles, respectively (Figures 4.6a-c). These differences are less pronounced for the MID and NE regions in the median and 75th percentiles (< 5 ppb). The different responses to soil moisture coupling regimes across regions can be attributed to differences in temperature (Figure 4.6d-f). Temperatures in ATL increase by 3 K at the

75th percentile and by 2.1 K at the 50th; whereas for MID the rise in temperatures during coupled years is 1.5 and 2.5 K for the 50th and 75th percentiles. NE exhibited even weaker temperature changes less than 1.5 K. Although $\lambda E/R_N$ reductions during soil moisture-limited conditions in ATL and MID are similar (Figure 4.6g-h), the magnitude of coupling is weaker on average for MID ($\rho(E,T)$=-0.44) compared to ATL ($\rho(E,T)$=-0.58) suggesting a dampened temperature response to soil drying.

The different response across regions (e.g. from North to South) may reflect a shift from synoptic to local controls on O_3 interannual changes. Leibensperger et al., (2008) found that mid-latitude cyclone frequency is a good predictor of O_3 interannual variability north of 40°N but was not as significant farther south. It then follows that for the NE region a change in O_3 due to soil moisture-limitations (Figure 4.6c) would be dampened due to the influence of synoptic scale pollutant ventilation. This dampening may also be the case for MID, which is within the transition from predominantly soil-limited to energy-limited (Figure 4.4) and shows a weaker response to O_3 than the South.

4.4 Discussion

4.4.1 Physical Coupling Mechanism

Here we consider the mechanisms controlling temperatures and specific humidity under the two soil moisture-temperature coupling regimes: 1) when evapotranspiration is energy-limited and 2) when evapotranspiration is soil moisture-limited. In the case of energy limitations, the surface flux magnitude is largely dictated by the amount of energy available at the surface. Therefore, increases in the surface fluxes (sensible and latent heat flux) may occur simultaneously as if radiation increases. When evapotranspiration is

soil moisture-limited, an increase in net radiation produces greater energy partitioning towards sensible heat. As a result, temperature in soil moisture-limited regimes increases due to soil drying and/or higher net radiation, whereas temperature increases in energy-limited regimes are solely controlled by the amount of net radiation. This latitudinal difference in temperature sensitivity is illustrated in Figure 4.5b by the increased sensitivity of sensible heat flux to incoming radiation (e.g. greater $\beta(R_N,H)$ when the station is soil moisture-limited). The change in regime is further exhibited by the sign change in $\beta(R_N,\lambda E)$, with a clear transition from energy-limited conditions at higher latitudes to soil moisture limited conditions in the south (Figure 4.4).

4.4.2 Humidity as a Surrogate for Surface Fluxes

Several studies indicate humidity is a good predictor of O_3 variability in the Southeastern U.S. (Camalier et al., 2007; Zheng et al., 2007; Davis et al., 2011), however, our results suggest that this relationship is likely an artifact of the soil moisture-temperature coupling regimes. This is evident in Figure 4.4b, where the normalized latent heat flux ($\lambda E/R_N$) has stronger correlation with O_3 than specific humidity or temperature over much of the eastern U.S. Because these studies use collocated meteorological and O_3 station data, measured humidity may be reflection of near-surface, local evaporative flux. Although a gridded specific humidity product (NLDAS2) is compared with EPA-AQS station data for this analysis, the widely observed correlation between specific humidity and O_3 is replicated here (Figure 4.1c and Figure 4.4).

It is often remarked that the negative correlation between O_3 and humidity can be explained by cloud cover changes (Camalier et al., 2007; Jacob and Winner, 2009; Davis

et al., 2011). Using $\lambda E/R_n$ removes the effects of radiation changes caused by cloud cover from the evaluation surface flux variations. Therefore, it is unlikely that changes in radiation due to cloud cover would produce the O_3-$\lambda E/R_n$ correlation found here for the Southeast. Additionally, prior studies have found the influence of perturbed radiation produces minimal changes in O_3 (Korsog and Wolff, 1991; Sillman and Samson, 1995; Dawson et al., 2007).

Finally, increased concentrations of atmospheric water vapor can reduce background O_3 concentrations through an increased conversion of $O(^1D)$ to the hydroxyl radical (OH), providing a chemical sink for O_3 (Johnson et al., 1999; Racherla and Adams, 2006). Since soil moisture-limited regimes are drier (Figure 4.6) it is expected that atmospheric water vapor concentrations are lower (e.g., lower humidity) and less chemical loss from the chemical pathway described and consequently higher O_3. However, studies in urban environments, like the EPA-AQS sites, have demonstrated (Aw and Kleeman, 2003; Dawson et al., 2007) that the loss of O_3 through this pathway is weak and in high NO_x environments increased water vapor can lead to additional OH formation (Steiner et al., 2006).

4.4.3 Biogenic Isoprene Emissions

Another potential confounding factor in the ozone-climate relationship is the increase in biogenic isoprene emissions under warmer temperatures (Guenther et al., 1994; Petron et al., 2001). Isoprene emissions are strongly controlled by the same environmental factors that explain O_3 formation. Depending on the photochemical regime and NO_x concentrations, increased isoprene emissions can lead to the formation

of more O_3 for sufficiently high NO_x or isoprene can react directly with O_3 in low NO_x regimes (Atkinson, 2000). The photochemical environment of the southeastern U.S. is typically categorized as NO_x-limited and simulated regional O_3 production has been shown to be unresponsive to changes in isoprene concentrations (Fiore et al., 2005). However, urban, high-NOx regions in the Southeast have been shown to be sensitive to biogenic isoprene (Xu et al., 2002) and isoprene can account for approximately 50% of the regional VOC reactivity (Blanchard et al., 2010b).

We evaluate the response of O_3 to changes in isoprene using available isoprene concentration data from EPA-AQS PAMS (Figure 4.7). O_3 is well correlated with isoprene for all regional station averages (R=0.56 for ATL, 0.38 for MID, and 0.58 for NE). The increase in O_3 in soil moisture-temperature coupled years (Figure 4.7) may reflect the positive influence of warmer temperatures on higher regional isoprene emissions. This combined effect is likely strongest over the Southeast, where isoprene emissions are highest (Guenther et al., 2006) as reflected in the higher isoprene concentrations in ATL (> 1 ppb for all years; Figure 4.7). These results suggest that isoprene plays a role in the O_3 concentration increase, yet we note that the likely driver for the emissions increase is the warmer temperatures and increased solar radiation occurring in soil moisture-limited regimes.

Observational studies have suggested that long-term soil water stress on vegetation could reduce isoprene emissions (Fall and Monson, 1992; Sharkey and Loreto, 1993; Brilli et al., 2007; Pegoraro et al., 2007). Figure 4.7 illustrates that reductions in isoprene emissions due to soil moisture are not evident in these regional scale isoprene concentrations, because isoprene concentrations were among the highest measured during the historic 2007 drought over the Southeastern U.S. (Figures 4.2 and 4.3). The

lack of soil moisture stressed reductions on isoprene flux is consistent with satellite-based inferred fluxes over this region (Duncan et al., 2009). Recent modeling work has shown, however, that year-to-year changes in isoprene emissions are jointly controlled by fluctuations in temperature and soil moisture when models include the influence of soil water stress (Tawfik et al., 2012) and by including the soil moisture stress effect model emissions are in better agreement with observations for mid-latitude isoprene emission regions (Proksch et al., 2008).

4.5 Conclusions

We demonstrate the importance of soil moisture and surface energy partitioning in describing the underlying physical mechanism for O_3 interannual and spatial variability. We show that the distinct north-south gradient exhibited between the temperature-ozone and humidity-ozone relationships (Camalier et al., 2007; Zheng et al., 2007; Davis et al., 2011; Rasmussen et al., 2012) arises from different soil moisture-temperature coupling regimes. Surface fluxes normalized by net surface radiation prove to be better predictors of O_3 interannual variability than temperature, humidity, or radiation for a majority of the Eastern U.S. This highlights the need for better representation of surface energy fluxes in models and calls for collocated chemical, surface, and atmospheric measurements. Because it is anticipated that much of the eastern U.S. will experience more frequent heat waves and droughts under a warming climate (Meehl and Tebaldi, 2004; Christensen and Hewitson, 2007; Dai, 2011; Hirschi et al., 2011), understanding the current and projected types of soil moisture-temperature

coupling regimes will be particularly relevant for prediction of present-day and future O_3 air quality.

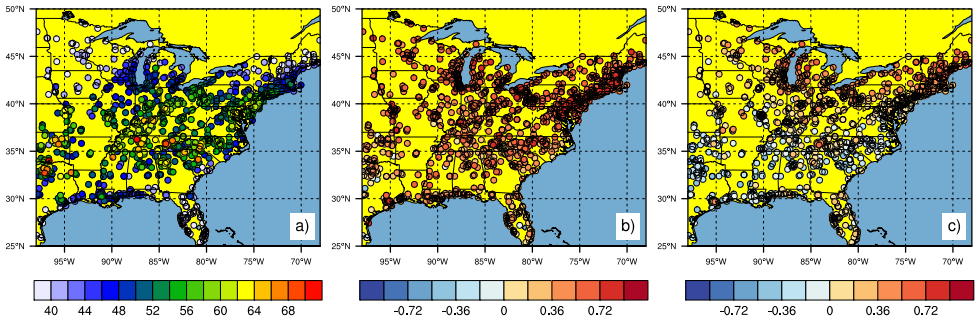

Figure 4.1 a) Midday (12-4pm) average observed ozone concentrations (ppb), and correlation coefficient of midday average ozone concentrations against Phase 2 NLDAS b) temperature and c) specific humidity for August from 1994-2010 at EPA-AQS stations with at least 10 years of data.

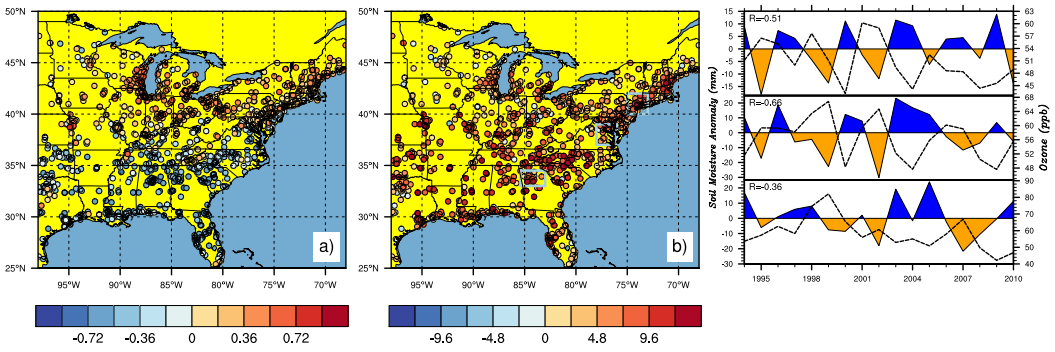

Figure 4.2 a) Correlation between NLDAS evapotranspiration and temperature describing the degree of soil moisture-temperature coupling. Negative values (blue) refer to greater soil moisture influence on temperatures. b) Average midday ozone concentrations (ppb) for anomalously dry soil moisture years minus anomalously wet soil moisture years at each station. c) Interannual change of (black dashed) ozone concentrations and (fill color) soil moisture anomalies defined as the deviation from mean August conditions for 1994-2010 for the (top) Northeast (40-42°N and 73-75°W), (middle) Mid-Atlantic (37-39°N and 76-78°W), and (bottom) Atlanta Metropolitan area (33-34.5°N and 83-85.4°W). Each panel is for August from 1994-2010 at EPA-AQS stations with at least 10 years of data.

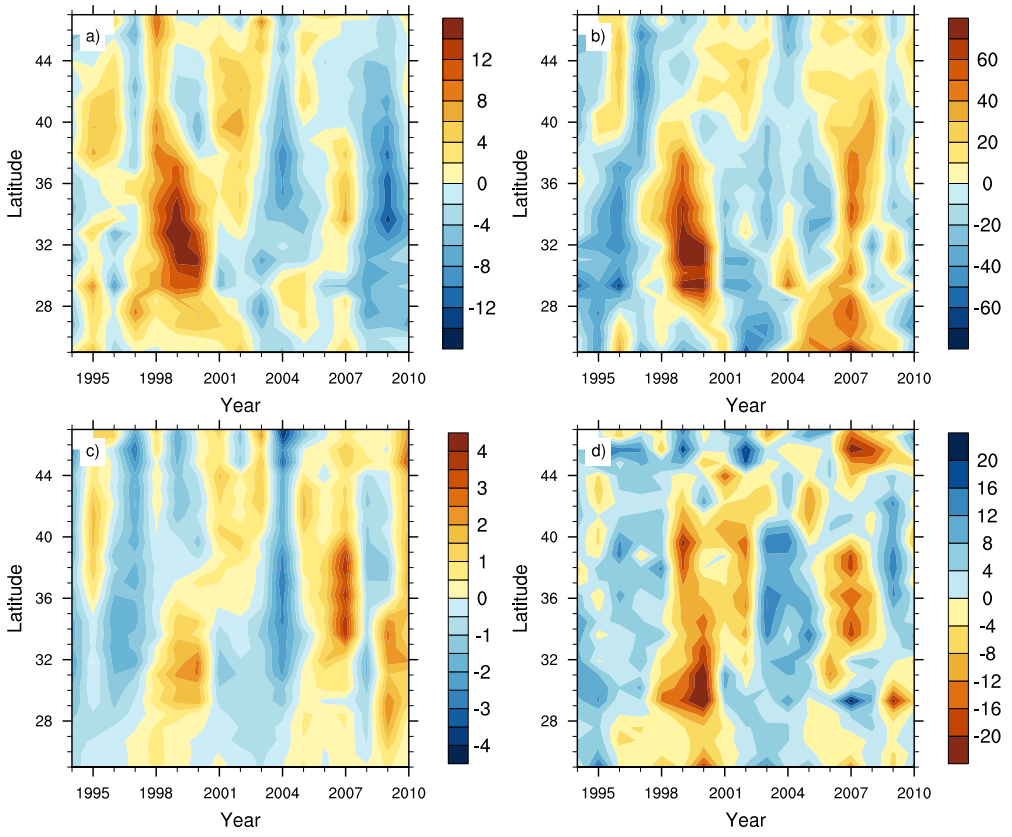

Figure 4.3 August zonally averaged anomalies, defined as the deviation from mean August conditions for 1994-2010, for average midday a) ozone concentrations (ppb), b) incident solar radiation (W m^{-2}), c) near surface temperatures (K), and d) soil moisture from 0-40 cm (mm) at EPA-AQS stations with at least 10 years of data.

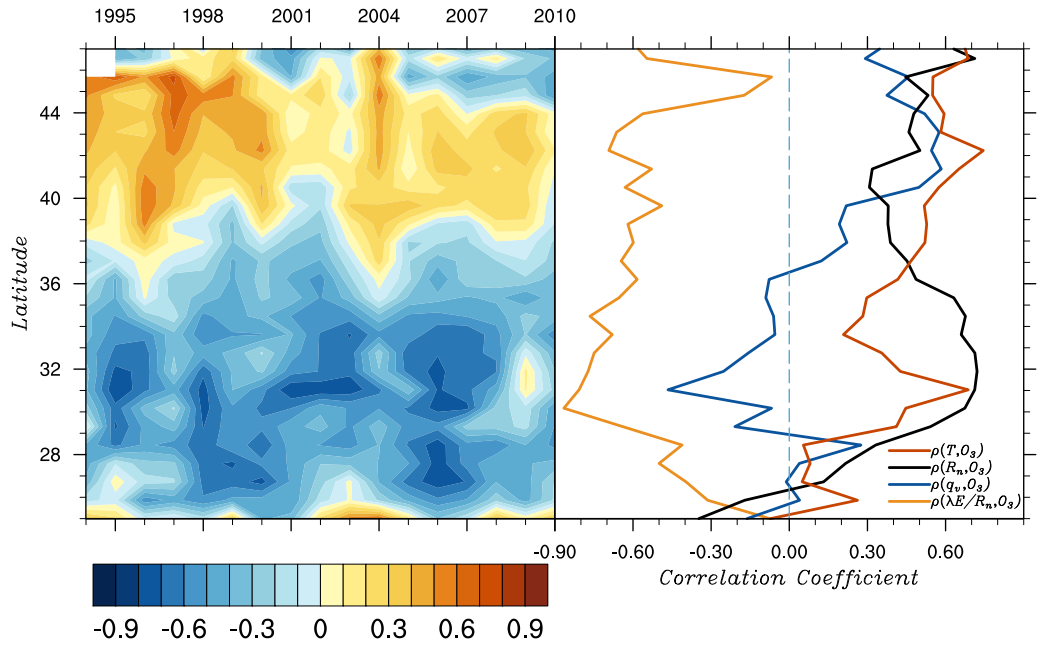

Figure 4.4 Zonally averaged (left) interannual variations in soil moisture-temperature coupling strength ($\rho(E,T)$; see Section 2.2 for more details) and (right) zonally averaged correlation coefficient of midday average ozone concentrations against (red) temperature, (black) incident radiation, (blue) specific humidity, and (orange) latent heat flux normalized by net surface radiation. Both panels are for the month of August.

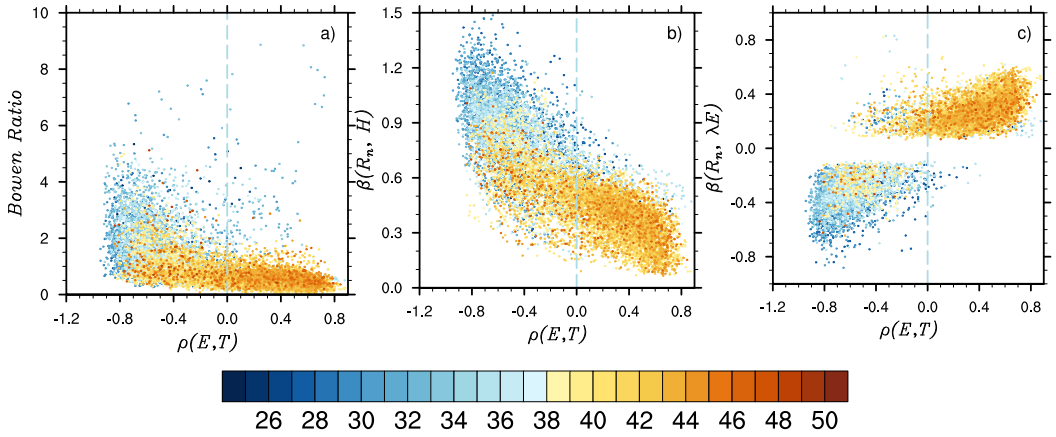

Figure 4.5 a) Bowen ratio, b) slope of daily sensible heat flux (H) against incident radiation, and c) slope of daily latent heat flux (λE) against incident radiation versus the soil moisture-temperature coupling diagnostic (ρ(E,T)). Each point represents a particular year for an EPA-AQS station from 1994-2010 and is colored by latitude.

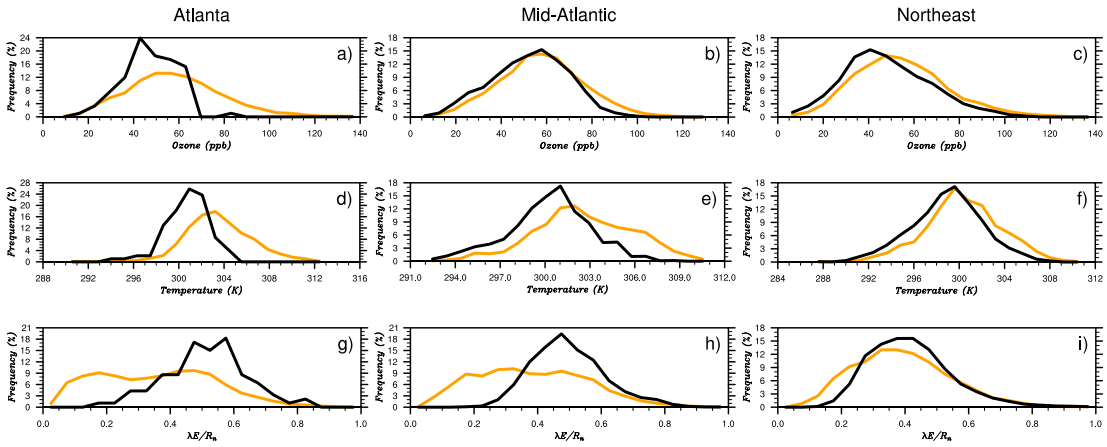

Figure 4.6 Probability distribution functions for midday average (a-c) ozone concentrations, (d-f) temperatures, and (g-i) latent heat flux normalized by net surface radiation, comparing (black) energy limited conditions ($\rho(E,T)>0$; uncoupled) and (orange) soil moisture limited conditions ($\rho(E,T)<0$; coupled) for the Atlanta Metropolitan Area, Mid-Atlantic, and Northeast regions (see Figure 2b for latitude/longitude bounds)

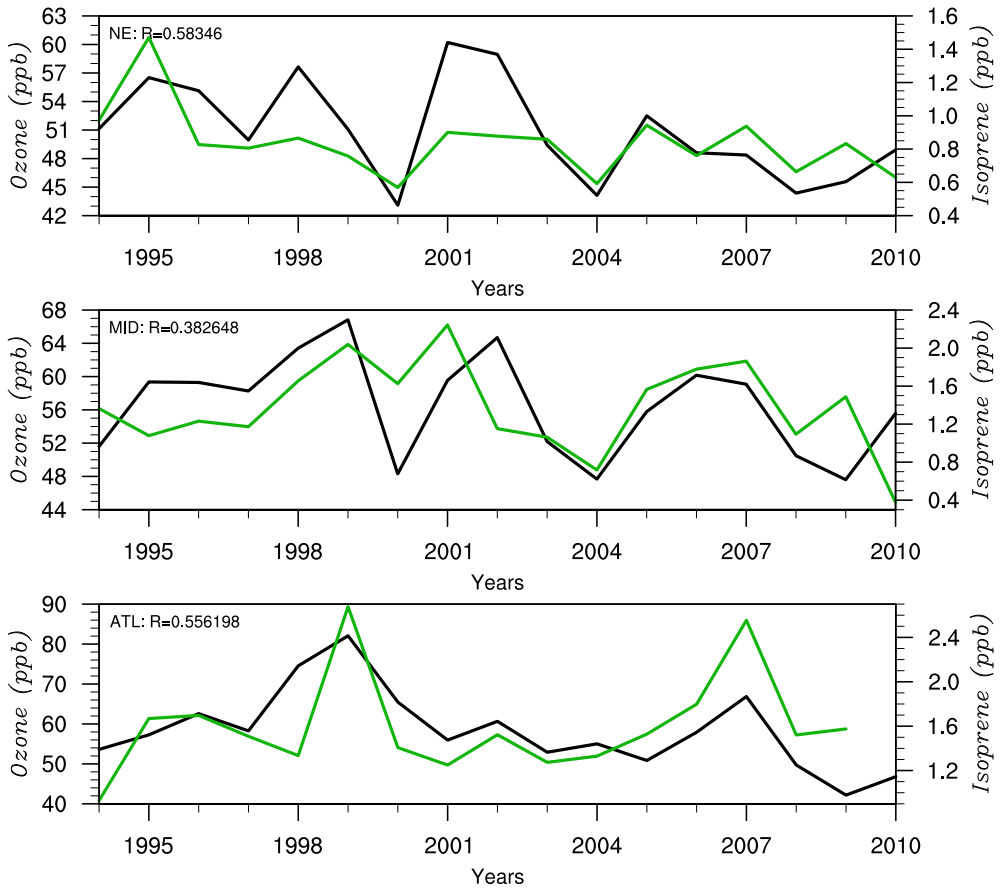

Figure 4.7 Interannual variations of average midday (black) ozone and (green) isoprene concentrations averaged over the (top) Northeast, (middle) Mid-Atlantic, and (bottom) Atlanta Metropolitan Area.

Chapter 5

Capturing observed relationships between the land surface and ozone in chemistry-climate models

5.1 Introduction

Tropospheric ozone (O_3) forms in the atmosphere via a suite of photochemical reactions driven by volatile organic compounds (VOC) and nitrogen dioxides (NO_x = $NO+NO_2$). Due to the adverse effects of O_3 on human health (Lippmann, 1989; Bernard and Ebi, 2001; Knowlton et al., 2004; Bell et al., 2007), many federal regulations to mitigate O_3 concentrations have been implemented. One recent effort by the Environmental Protection Agency's (EPA) was the State Implementation Plan (SIP) (EPA, 2005) to reduce NO_x emissions and consequently reduce O_3. Regional atmospheric chemistry modeling has been conducted to evaluate the success of these regulatory efforts (Frost et al., 2006; Kim et al., 2006; Gego et al., 2007). However, modeling studies suggest that in some locations meteorological variables can have a stronger control on O_3 variability than NO_x emissions reductions (Godowitch et al., 2008). This highlights the

necessity of quantifying an atmospheric chemistry model's ability to reproduce observed O_3 variability and accurately capture O_3-meteorology interactions.

Several recent studies examine the ability of models to simulate observed O_3 interannual variability (Hogrefe et al., 2004; Godowitch et al., 2008; Nolte et al., 2008; Hogrefe et al., 2011; Rasmussen et al., 2012). Comparing observed O_3 to a coupled global climate-chemistry model from 1981-2000, Rasmussen et al., (2012) showed that interannual variations of O_3 are poorly represented in the model for the U.S. Mid-Atlantic and Great Lakes regions. The inability of models to capture yearly O_3 variability over the Eastern U.S. has also been found in regional modeling studies (Hogrefe et al., 2004; Nolte et al., 2008; Hogrefe et al., 2011). Hogrefe et al. (2011) demonstrated that models had a difficulty capturing O_3 variability especially in the lowest O_3 percentiles over the Northeast U.S. Additionally, this study noted that using constant chemical boundary conditions could underestimate the interannual variability by 30-50%. Simulations including time-variant chemical boundary conditions showed improved O_3 interannual variability compared to observations, while exacerbating the underestimated 18-year O_3 trend (Hogrefe et al., 2011).

From a climate change perspective, a multi-model comparison study of regional chemistry models concluded that there were large regional inconsistencies in the response of O_3 to climate change, yet most models projected higher O_3 concentrations under increasing greenhouse gas scenarios (Weaver et al., 2009). However, as noted by Nolte et al., (2008), interannual changes in O_3 are often larger than long-term trends and the increase in O_3 concentrations due to climate change (Weaver et al., 2009). White et al., (2007) also cautioned against using measurements from single-year field campaigns when characterizing regional air quality by highlighting large differences in observed O_3

between anomalously cool and warm years for the Northeast. Many of these studies only briefly discussed year-to-year O_3 variations, and simulations are generally performed for only a few present-day summers with the exception of Rasmussen et al., (2012) who simulated two decades of ozone concentrations with a coupled chemistry-climate model. These limited studies indicate that additional effort is needed to examine if coupled chemistry-climate models can capture interannual changes in O_3 with any fidelity.

Several recent inter-model comparison studies have been conducted to evaluate and synthesize discrepancies of O_3 simulated by coupled climate-chemistry models and/or chemical transport models (Stevenson et al., 2006; Wild, 2007; Fiore et al., 2009; Reidmiller et al., 2009; Weaver et al., 2009; Jonson et al., 2010). Common to all of these studies is the tendency for models to overestimate O_3 concentrations over the Eastern U.S. by more than 10 ppb (Figure 5.1; (Fiore et al., 2009; Reidmiller et al., 2009)). The overestimate is commonly attributed to 1) an incomplete understanding of isoprene-nitrate recycling chemistry (Fiore et al., 2005; Wild, 2007; Wu et al., 2007a; Ito et al., 2009), 2) poor boundary layer ventilation (Castellanos et al., 2011), and 3) model biases in temperature (Godowitch et al., 2008; Nolte et al., 2008; Rasmussen et al., 2012). In the case of isoprene-nitrate recycling, it has been shown that 0% recycling of NO_x (e.g. most efficient NO_x removal) can reduce O_3 by 1-5 ppb (Zhang et al., 2008c; Ito et al., 2009) in regions with high biogenic VOC emissions such as the Southeastern US. However, this reduction in O_3 is not sufficient to alleviate the 10-30 ppb O_3 bias commonly modeled for this region. With regards to temperature biases, Rasmussen et al., (2012) showed that model temperature biases only minimally contributed to the O_3 bias. During a study where North American anthropogenic emissions were reduced by 20%, model O_3 biases were present independent of emissions perturbations, marking a chemical insensitivity to

airmass for the Southeast (Reidmiller et al., 2009). Taken together, it is evident that there is a systematic shortcoming present in current models that may result from a combination of deficiencies in chemistry and climate-chemistry interactions.

This chapter focuses on identifying the behavior of a fully coupled regional climate-chemistry model to evaluate chemical versus meteorological causes of the Southeastern US O_3 bias. More specifically, the goals of the current study are to 1) examine the Eastern U.S. O_3 bias from the perspective of soil moisture-temperature coupling regimes (described in Chapter 4) and its influence on O_3 precursors, and 2) identify drivers of model O_3 variations against observations. The results will be then be placed within the context of model behavior found in prior studies.

5.2 Methods

5.2.1 Description of RegCM-CHEM Climate-Chemistry Model

To evaluate the behavior of O_3 against observed soil moisture-temperature regimes, a gas-phase chemical mechanism (Carbon Bond Mechanism; CBM-Z) (Zaveri and Peters, 1999) is coupled to the RegCM-CLM-MEGAN framework described in Chapter 3. This online coupling allows for the calculation of chemical concentrations of a suite of ozone precursors in each model grid cell within the climate model RegCM. A brief description of the coupled regional climate-chemistry model, referred to as RegCM-CHEM is given here, with a more detailed description in Shalaby et al., (2012). We describe the chemical transport equation and numerical methods employed (Section

5.1.1), the chemical mechanism and solver implemented for this analysis (Section 5.1.2), removal processes (Section 5.1.3), and emissions (Section 5.1.4).

5.2.1.1 Chemical Transport Equation and Numerical Methods

The time-variant solution of chemical tracers in RegCM-CHEM is modified from a simple aerosol transport scheme contained in RegCM4 (Solmon et al., 2006). The basic tendency equation of *j* gas-phase species (*X*) is described as

$$\frac{\partial X^j}{\partial t} = -V \cdot \nabla X^j + F_H^j + F_V^j + T_{cum}^j + S_r^j - R_{w,ls}^j - R_{w,cum}^j - D_{dep}^j + R_{net}^j \quad (5.1)$$

where $\frac{\partial X^j}{\partial t}$ is the rate of change (or tendency) of the tracer *X*, $-V \cdot \nabla X^j$ is the horizontal and vertical advection of X, F_H^j and F_V^j are the vertical and horizontal turbulent diffusion, T_{cum}^j is the cumulus transport, S_r^j is the emissions source term, $R_{w,ls}^j$ and $R_{w,cum}^j$ are the wet removal by large-scale and cumulus precipitation, D_{dep}^j is removal by dry deposition, and R_{net}^j is the net chemical production and loss. Each term is solved above for the individual tracer species and advanced in time using a modified leap-frog numerical scheme. Parameterizations and inputs for some of these terms are described below.

5.2.1.2 Chemical Mechanism and Solver

CBM-Z (Zaveri and Peters, 1999) is a gas-phase chemical mechanism developed as an extension of the Carbon Bond 4 Mechanism (CBM-IV; Gery, 1989 #12631}. CBM-Z includes the additional reaction pathways for several species, including isoprene.

This explicit representation allows CBM-Z to be used for more long-term simulations and for regions with high biogenic isoprene emissions (described in Section 5.2.1.4). CBM-Z uses a lumped species representation for reactive volatile organic compounds (VOC) based on the carbon bond structure making it more computationally efficient. Several studies have shown the ability of CBM-Z to simulate O_3 in urban and rural environments (Zaveri et al., 2003; Jiang and Fast, 2004; Fast and Heilman, 2005; Fast et al., 2006). The current implementation of CBM-Z in RegCM-CHEM solves the stiff system, ordinary differential equations using a computationally efficient radical balance method (RBM) (Sillman, 1991; Schlink et al., 2002). Because much of the chemistry in the troposphere is initiated by the hydroxyl (OH) and peroxy radical (HO_2 and RO_2) reactions, the RBM solves the reverse Euler equations for these short-lived radicals based upon their sources and sinks. Concentrations of other chemical species are then calculated in a reactant-to-product order. Due to its computational efficiency, it is possible to conduct multi-year coupled climate-chemistry simulations with the CBM-Z.

5.2.1.3 Wet and Dry Deposition

Chemical species are removed from the atmosphere via wet and dry deposition. The parameterization schemes for these processes in RegCM-CHEM are based on existing parameterizations as described below. Dry deposition is the primary removal mechanism of gas phase species in RegCM-CHEM. RegCM-CHEM allows 29 CBM-Z species to be dry deposited to the surface from the lowest model layer. This dry deposition scheme is acquired from the Community Land Surface Model version 4 (CLM4) and based on Wesely (1989). More specifically, dry deposition is parameterized

as a series of resistances, which include the aerodynamic resistance, a quasi-laminar near-surface sublayer resistance, stomatal resistance, and non-stomatal resistance. By using the CLM4 implementation, stomatal resistance is linked directly to photosynthetic activity and varies diurnally, consistent with realistic dry deposition behavior. Wet deposition is a minor removal mechanism compared to dry deposition. The current parameterization removes 26 CBM-Z gas phase species and is parameterized following the current implementation in the Model of Ozone and Related Chemical Tracers version 4 (MOZART-4) (Horowitz et al., 2003; Emmons et al., 2010), a global atmospheric chemistry model. Currently, wet deposition is only included for grid-resolved precipitation (Shalaby et al., 2012).

5.2.1.4 Emissions

Anthropogenic, biomass burning, and biogenic emissions are provided to RegCM-CHEM using a suite of inventories and, in the case of biogenic isoprene, an interactive emissions model (MEGAN) (Guenther et al., 2006; Tawfik et al., 2012). These emissions are injected into the lowest model layer and, upon transfer into the RegCM tracer scheme, follow advection, chemistry and removal processes as in Equation 5.1. Anthropogenic and biomass burning emissions are derived from the 0.5° by 0.5° MACCity monthly averaged gridded emissions inventory (Lamarque et al., 2010). This inventory includes yearly emissions reductions from 1990-2010 making it an ideal inventory for exploring model interannual variability. A bimodal diurnal cycle is imposed on the monthly MACCity NO_x emissions to replicate two typically observed rush hour traffic peaks while conserving the total monthly mass flux of NO_x to the atmosphere.

Two different biogenic isoprene emissions are used for this study: 1) an interactive emissions online emissions model (MEGAN) within the RegCM-CHEM framework (Tawfik et al., 2012) that responds directly to model temperature, incident radiation, and soil moisture (described in Chapter 3); and 2) a static 1° by 1° monthly-averaged emissions inventory, POET (Granier et al., 2005) with an imposed diurnal cycle that does not respond to changes in model meteorological conditions. Non-isoprene biogenic emissions (acetone, ethane, ethylene, propane, propene, methanol, carbon monoxide, and NO_x) are also derived from the POET inventory. All emissions inventories (MACCity and POET) are bi-linearly interpolated to the RegCM-CHEM grid from their native grid.

5.2.2 Experiment Design

Four RegCM-CHEM simulations are performed to evaluate possible sources of the Eastern U.S. O_3 model bias and the influence of land-atmosphere coupling on this bias. Simulations are conducted on a 60 by 60 km grid centered at 96°W and 38°N over the continental U.S. (Figure 5.2). The dynamic time step of the model is 200 seconds and land surface fluxes are updated every 600 seconds. Chemical tracer species are processed (Equation 5.1) every dynamic time step, where the chemical tendency (R_{net}^{j}) is updated every 1000 seconds. Initial and 6-hourly lateral physical boundary conditions are provided by the European Centre for Medium Range Weather Forecasts Interim Reanalysis (ERA-Interim) for atmospheric variables (Dee et al., 2011). Weekly prescribe sea surface temperatures are also prescribed using ERA-Interim (Dee et al., 2011). Chemical initial and boundary conditions are provided by an 8-year (2000-2007) monthly

climatological average from the global MOZART model (Horowitz et al., 2003; Emmons et al., 2010). Five summers, starting from June 1st and ending on August 31st, are simulated from 2004-2008, capturing the 2007 drought and the relatively cool 2004 summer. August will be the focus of this model analysis because it coincides with the observed soil moisture-temperature feedback study presented in Chapter 4, and high surface air temperatures and potential for high O_3 concentrations. Soil moisture initialization is provided by Phase 2 of the Global Data Assimilation System (GLDAS2) CLM3.5 model output (Rodell et al., 2004). Initializing summer soil moisture with realistic values has been shown to greatly improve sub-seasonal forecasts of temperature and precipitation (Koster et al., 2010).

Using the model simulation specifications described above, four simulations are performed. The first is a fully interactive simulation allowing land-atmosphere interactions and isoprene emissions to respond to changes in environmental variables (referred to as coupled or COUP). The second simulation prescribes constant monthly climatological soil moisture, effectively decoupling the land surface from the atmosphere (e.g. precipitation does not modify soil moisture), but still allows biogenic isoprene emissions to respond to environmental changes (referred to as uncoupled or UNCOUP). The third (COUP-POET) and fourth (UNCOUP-POET) simulations are the same as the first and second simulations, respectively, however, each use the climatological POET isoprene emissions. POET is a static emissions inventory that does not respond to environmental changes. Differences between the four simulations are summarized in Table 5.1.

Midday (12-4pm) average August isoprene emissions are shown for the four simulations in Figure 5.2. Isoprene emissions are weaker in COUP relative to UNCOUP

and the POET. The isoprene emissions in COUP are reduced by the soil moisture stress factor (γ_{SM}; Equation 3.4) and this effect is stronger in RegCM-CLM-MEGAN than other offline modeling studies (Guenther et al., 2006; Muller et al., 2008). This is attributed to the sensitivity of the soil moisture stress factor to wilting point and the relatively dry CLM soils (Tawfik et al., 2012). Because UNCOUP has constant soil moisture conditions, there is no variability in the soil moisture stress factor and therefore emissions changes are controlled solely by temperature and light. This produces higher emissions overall for UNCOUP (Figure 5.2b). The POET simulations exhibit modest isoprene emissions; however, these emissions do not change from year to year. We use these simulations to explore the factors driving O_3 variability and biases. Specifically, by comparing pairs of simulations we can isolate the effects of land-atmosphere coupling and isoprene flux on O_3. Throughout the remainder of this analysis three different pairings are used:

- COUP-POET versus UNCOUP-POET: Comparison of these two simulations isolates the influence of land-atmosphere coupling on O_3.
- COUP versus COUP-POET: These two simulations use the same interactive treatment of the land surface and therefore have the same meteorology yet different isoprene emissions. Comparison of these two simulations can explain the role of daily and interannual isoprene emissions changes on O_3.
- UNCOUP versus UNCOUP-POET: Comparison of these two simulations highlights the effects of isoprene flux on O_3 in an uncoupled land-atmosphere environment.

All four simulations do not allow O_3 calculated from the chemical mechanism to modify radiative forcing to simplify the analysis (e.g. no O_3 radiative feedbacks).

5.2.3 Chemical Observations and Meteorological Data

Hourly O_3, isoprene, and NO_x data are available from the Environmental Protection Agency's Air Quality System (EPA-AQS) Photochemical Assessment Monitoring Stations (US EPA) for 17 Augusts from 1994-2010. A 5-year subset of observations (2004-2008) corresponding to the simulation period is used to compare against model simulations; however, some statistics are produced for the entire 17 years to provide better information about long-term trends. Concentration data are averaged over peak O_3 production hours (12-4pm) and only stations located in the Eastern half of the U.S. are considered (25-50°N and 98-68°W). Stations must have at least half a month of measurements for each year to be included in the analysis. For direct comparison with the four simulations, model output is sampled at the nearest EPA-AQS station and converted to local station time.

Environmental data are retrieved from the Second Phase of the North American Land Data Assimilation System (NLDAS2) Forcing using the MOSAIC model (Koster and Suarez, 1992, 1994; Mitchell et al., 2004). NLDAS2 is a reanalysis product that assimilates observed precipitation and forecast products into a model system to produce a high temporal and spatial gridded product of land surface variables. To that extent, NLDAS2 is to be regarded as a "quasi-observational" product. Hourly temperature (T), incident (R) and net radiation (R_n), evapotranspiration (E), and latent heat flux (λE) at $1/8^{th}$ degree resolution from 2004-2008 are used for the current analysis. NLDAS2 data

are averaged over a quarter degree region around each EPA-AQS station. Further description of NLDAS2 used can be found in Chapter 4.

5.2.4 Soil Moisture-Temperature Coupling Regimes

To quantify the degree of soil moisture-temperature coupling, we use a diagnostic parameter ($\rho(E,T)$) defined as the Pearson correlation between evapotranspiration (E) and temperature (T) (Seneviratne et al., 2006). Physically, this diagnostic parameter identifies two different land-atmosphere regimes: (1) a soil moisture-limited regime corresponding to negative $\rho(E,T)$ values and (2) an energy-limited regime corresponding to positive values of $\rho(E,T)$. When a regime is soil moisture-limited, temperatures are controlled primarily by changes in evapotranspiration, where more energy is partitioned to sensible heat flux. For energy-limited environments, soil moisture is plentiful and therefore changes in evapotranspiration and sensible heat flux are controlled by the amount of incoming radiation. We use a modified version of $\rho(E,T)$ for this study that uses midday average E and T for each August (e.g. the correlation between 31 days of E and T for each year) to calculate a monthly $\rho(E,T)$. This allows for the evaluation of interannual changes in soil moisture-temperature coupling.

5.3 Results and Discussion

5.3.1 Model Meteorological Bias

Typical meteorological control variables (T and R) and the latent heat flux ratio (Chapter 4; $\lambda E/R_n$) are used to explore if model meteorological biases can explain shortcomings in modeling O_3 (Figure 5.3). To focus on meteorology, the four simulations

will be discussed in terms of coupled (COUP and COUP-POET) and uncoupled (UNCOUP and UNCOUP-POET) land-atmosphere interactions. By not including O_3 radiative feedbacks, the meteorology in the two coupled simulations (COUP and COUP-POET) is identical. Similarly, the meteorology in the two uncoupled simulations is also identical (UNCOUP and UNCOUP-POET).

August midday temperatures in the coupled simulations are generally warmer compared to NLDAS2. The highest model biases occur over the Midwest (>5 K) with a weaker warm bias along the eastern seaboard (0-2 K; Figure 5.3a). The uncoupled simulations (Figure 5.3b) exhibit a cool bias over the Southeast (1-5 K) and otherwise deviate from NLDAS2 by less than 2 K. Although all simulations are initialized with the same GLDAS soil moisture, the coupled simulations are warmer than NLDAS2. This suggests that the coupled simulations dry as the summer progresses resulting in warmer temperatures. In the uncoupled simulations, soil moisture does not change during August, therefore soil drying does not occur and the soil remains at a climatologically constant value. This results in the cooler temperatures for the uncoupled simulations.

Similar to temperature, model incident radiation is 30 W m^{-2} higher than NLDAS2 over most of the U.S. in the coupled simulations (Figure 5.3c-d), reinforcing the notion of drier soils reduced clouds and precipitation in the coupled simulations. The radiation in the uncoupled simulations is also biased high but mainly over the Great Lakes area (> 40 W m^{-2}). The primary difference between the coupled and uncoupled simulations occurs over the South- and Northeast, where the coupled runs have weak biases and the uncoupled runs have 20-60 W m^{-2} less radiation than NLDAS2. In addition to the precipitation feedbacks, the lower radiation found in the model could result in reduced photolysis rates.

To assess the degree of drying between the model and observations, we examine model biases in $\lambda E/R_N$ (Figure 5.3e-f) where negative (positive) values correspond to drier (wetter) surface soil in the model. For much of the Eastern U.S. the surface soil is drier in the coupled simulations, especially in the Midwest and Great Lakes Region. The uncoupled simulations are also drier for these regions but the signal is weaker. Further, the uncoupled simulations are wetter than NLDAS2 throughout the Piedmont region of the Carolinas and parts of the South. Because $\lambda E/R_N$ refers to the fraction of energy partitioned to latent heat flux, drier conditions in the model also correspond to greater energy partitioning to sensible heat flux. This increase in sensible heat flux is likely producing the warm bias illustrated in Figure 5.3a.

To examine the ability of the model to reproduce NLDAS2 meteorological variability, a relative variability bias is calculated and presented in Figure 5.4. The relative variability bias (*RB*) is defined as

$$RB = 1 - \frac{\sigma_X}{\sigma_{OBS}} \qquad (5.2)$$

where σ_X is the standard deviation of a particular model variable, *X*, for the midday average of all days in August from 2004-2008 (e.g. 31 days multiplied by 5 years) and σ_{OBS} is the same as σ_X but for observations. A negative (positive) relative bias means the model has greater (less) variability than observations. The coupled simulations have almost twice the variability of midday average temperatures as the NLDAS2 over the Southeast and the Gulf Coast (Figure 5.4a). The uncoupled simulations have similar temperature variations compared to NLDAS2 (Figure 5.4b), highlighting the role of soil

moisture on surface air temperature calculations. This shows that in coupled simulations land-atmosphere feedbacks amplify initial dry anomalous as the summer progresses. By using GLDAS prescribed climatological soil moisture for the uncoupled simulations, feedbacks do not occur and temperature variability better resembles NLDAS2. For modeled incident radiation (Figure 5.4c-d), the coupled simulations capture NLDAS2 variations well with only slight overestimates. The uncoupled simulations also capture NLDAS2 variations well for much of the U.S. with the exception of stations north of 42°N.

Variations in $\lambda E/R_N$ from NLDAS2 are greater than modeled for much of the Southeast and along the eastern seaboard for the coupled simulations (Figure 5.4e-f). The variability in the uncoupled simulations is reduced even further than the coupled simulations, with only parts of New England showing greater model variability. This result is to be expected in the uncoupled model. As discussed in Chapter 4, observed $\lambda E/R_N$ is a good predictor of year-to-year variability in O_3. If land-atmosphere-chemistry interactions are represented properly in the model we would expect to find the weaker model $\lambda E/R_N$ variability for the South and Northeast translate into weaker model O_3 variability.

5.3.2 Model Soil Moisture-Temperature Coupling

To evaluate if the model can accurately capture the observed land-atmosphere coupling, we compare the coupling parameter for the COUP and UNCOUP simulations against the NLDAS2 product. The model soil moisture-temperature coupling parameter ($\rho(E,T)$), is generally weaker than observed (Figure 5.5). In particular, the model identifies

the Great Lakes and Midwest regions as soil moisture-limited ($\rho(E,T)<0$), whereas observations identify these regions as energy-limited (Figure 5.5). Weaker model $\rho(E,T)$ suggests that model temperatures are less controlled by changes in evapotranspiration than observed. This is consistent with the sunnier, drier, and warmer conditions than observed (Figure 5.4) and describes the Great Lakes and Midwest regions as soil moisture-limited. However, despite this shortcoming in the Midwest, the north-south transition of $\rho(E,T)$ observed in Chapter 4 is captured along the eastern seaboard and can likely represent the north-south transitions and higher degree of coupling in the Southeast.

5.3.3 Model Ozone Bias

The average midday O_3 model bias for the four model sensitivity tests is calculated for five Augusts during the simulation period (2004-2008; Figure 5.6). Model bias is defined as model concentration minus observed (EPA-AQS) concentration. All simulations overestimate O_3 concentrations throughout the eastern U.S. with a few localized exceptions. COUP has the lowest biases of the four simulations, with overestimates ranging from 4-12 ppb in the South and 4-8 ppb in the Mid-Atlantic (Figure 5.6a). To highlight the influence of isoprene emissions on O_3, we compare COUP and COUP-POET (Figure 5.6a and 5.6c). O_3 biases are distinctly lower in COUP than for COUP-POET demonstrating the ability for lower isoprene emissions to reduce O_3 concentrations by more than 8 ppb.

To better isolate the effects of land-atmosphere coupling, simulations that hold isoprene emissions constant from year-to-year and do not respond to changes in environmental conditions are compared (COUP-POET and UNCOUP-POET). Both

POET simulations are biased high with the largest overestimates occurring over large cities (> 10 ppb; Figure 5.6c-d). Despite the warm biases over the Southeast for COUP-POET (>5 K; Figure 5.3), the POET simulations do not differ greatly suggesting that modeled O_3 concentrations are weakly driven by land-atmosphere coupling. This is contrary to the soil moisture-temperature-O_3 relationship discussed in Chapter 4, which implies that the model may not be characterizing certain aspects of the land-atmosphere-chemistry coupled system present in observations. In a strictly decoupled land-atmosphere environment (UNCOUP compared to UNCOUP-POET), model O_3 biases are still larger for UNCOUP-POET even though isoprene emissions are higher on average for UNCOUP (Figure 5.2). This further points towards a low O_3 model sensitivity to land-atmosphere coupling throughout the Eastern U.S.

Focusing on three smaller regions (defined in Figure 5.2), the simulated year-to-year changes in O_3 are compared against observations (Figure 5.7). For the Northeast (NE), all simulations exhibit a high O_3 bias for all years with the highest model departures occurring in 2004 (16-32 ppb). Further, observed O_3 has weak interannual variability (~ 8 ppb range) in the NE (Figure 5.7a). This range of O_3 in the model is well captured; however, none of the simulations reproduce the maximum in 2005 and minimum in 2004.

For the Mid-Atlantic region (MID; Figure 5.6b), observed midday O_3 spans a 12 ppb range with maxima in 2006 and 2007 of about 60 ppb. The uncoupled simulations (UNCOUP and UNCOUP-POET) reproduce the 2007 peak and the subsequent decrease in 2008, while the coupled simulations only capture the 2006 peak. On the whole for MID, the coupled simulations (COUP and COUP-POET) have less O_3 variability than observed (< 8 ppb) and the uncoupled simulations (UNCOUP and

UNCOUP-POET) have high O_3 concentrations but the variability similar to observations.

The Atlanta region has the largest observed variability of all the regions with a range of 17 ppb (Figure 5.7c). The most striking feature in ATL is the lack of interannual variability for any of the model realizations. The COUP simulation only varies by 2 ppb from year-to-year despite the higher than observed temperature variability in the coupled simulations (Figure 5.4), indicating that the muted O_3 variability in COUP is not due to a lack of temperature variability. The observations also show a distinct peak in 2007 corresponding to the historic drought in this year (Luo and Wood, 2007). This peak is only slightly captured by COUP-POET. Although COUP had the lowest absolute bias when compared to observations over the Eastern U.S. (Figure 5.6a), the lack of variability, especially over the ATL, highlights a broader model issue. We find that for MID and NE O_3 interannual variability in the model is largely determined by land-atmosphere coupling. This is illustrated by the strong correlations between UNCOUP and UNCOUP-POET ($R>0.9$) and highlights the importance of land-atmosphere interactions in controlling variability for NE and MID in the model, despite its weak influence on absolute O_3 concentrations (Figure 5.6).

5.3.4 Ozone Response to Meteorological Controls

The modeled response of O_3 to temperature, incident radiation, and $\lambda E/R_N$ for the 5-year period is examined in Figure 5.8. The model has difficulty replicating any of the observed correlations between O_3 and meteorological control variables especially in the Southeast ATL region (Figures 5.8c, 5.8f, 5.8i). In particular, the well-recognized

temperature-O_3 correlation (referred to as $\rho(T, O_3)$) is almost nonexistent for all model simulations for MID and ATL (Figure 5.8a-c). This inability to capture $\rho(T, O_3)$ for MID and ATL is not unique to RegCM-CHEM and has been found in another coupled climate-chemistry model (Rasmussen et al., 2012). The slope and $\rho(T, O_3)$ show improvement with latitude (e.g. the modeled NE shows a similar relationship to observed) but are still poorly represented. All simulations show a lack of sensitivity to temperature in the Mid-Atlantic and Southeast U.S., consistent with the weak response of absolute O_3 concentrations to changes in land-atmosphere coupling. This suggests that model O_3 production and loss is decoupled from meteorological forcing.

Observed O_3 is well correlated with incident radiation for all regions (Figure 5.8d-f). The model, however, very poorly represents the O_3-radiation relationships exhibiting weak correlations (Figure 5.8d-f) that are negative in the NE and MID regions due to a decline in model O_3 above 600 W m^{-2}. At lower radiation values (less than 500 W m^{-2}) the model generally exhibits the largest O_3 bias. Although photolysis is modified by cloud cover in the model, the influence may be insufficient for reducing O_3 photochemistry.

When evaluating the extent of drying and its effects on O_3, the observations are strongly anti-correlated indicating that low λE and dry conditions coincide with higher O_3 (Figure 5.8g-i) as presented in Chapter 4. The model, however, fails to capture the sign of the O_3-$\lambda E/R_N$ correlation, showing higher O_3 concentrations at wetter conditions and the relationship is weaker than observed (R=0.11-0.42 for model; R=0.57-0.73 for observed). This indicates that while RegCM-CHEM can simulate the land-atmosphere coupling conditions reasonably well (Figure 5.5), this does not translate into an accurate O_3-$\lambda E/R_N$ relationship (Figure 5.8g-i). This highlights a fundamental misrepresentation of

land-atmosphere-chemistry interactions in the model and is likely present across other coupled climate-chemistry models which do not accurately characterize $\rho(T, O_3)$.

To diagnose whether systematic biases in meteorological fields are responsible for O_3 biases, we compare O_3 biases (model minus observed) against the biases of several meteorological variables (temperature, radiation, $\lambda E/R_N$, and precipitation; Figure 5.9) for ATL, the region with the weakest O_3-temperature relationship. Here we also focus on the COUP simulation because it is configured to capture biosphere-atmosphere interactions. High model O_3 biases in COUP do not correlate well with biases in temperature and radiation (R=0.07 and 0.15, respectively; Figures 5.9a and 5.9b). This suggests that while high temperature and radiation biases may produce higher than observed O_3 episodically, these biases cannot account for systematic high model O_3. Similar to temperature and radiation biases, model discrepancies in daily average precipitation are poorly related to O_3 biases (Figure 5.9c). O_3 model overestimates greater than 20 ppb correspond to the largest daily precipitation biases. In particular, the large positive biases in precipitation represent instances when a rain event occurs in the model and is not present in the observations. Consistent with the ability of rain events to wet remove ozone precursor species from the atmosphere, misrepresented precipitation events are shown to produce large O_3 biases (> 20 ppb), but do not seem to explain persistent model O_3 overestimates. Instantaneous daily precipitation does not seem to explain persistent model O_3 overestimates; however, the timing of prior hour and day precipitation has been shown to correlate well with the accumulation of midday O_3 over ATL (figure not shown).

Biases in the surface drying parameter, $\lambda E/R_N$, exhibit the best relationship with O_3 biases with R=-0.47 (Figure 5.9d). When the model is drier than NLDAS, O_3

concentrations are 5-50 ppb higher than observed. This O_3-$\lambda E/R_N$ relationship may be due to the ability of $\lambda E/R_N$ to account for changes in air temperature through the relative surface energy being partitioned to sensible heat flux and to respond to changes in precipitation reflected by surface soil moisture modifications. Therefore, $\lambda E/R_N$ serves as a surrogate for these meteorological factors reflecting the effects of instantaneous variables, such as current temperature and radiation, and antecedent events, such as prior day precipitation. Further, the O_3-$\lambda E/R_N$ relationship highlights the importance of surface drying to ozone air quality previously discussed in Chapter 4.

5.3.5 Comparison of Ozone Precursors

Comparing two key O_3 precursors (NO_x and isoprene) to observed precursor concentrations may provide further insight into the O_3 biases (Figure 5.6) and low O_3 variability (Figure 5.7). Midday O_3 model concentrations for five Augusts (2004-2008) show a clear change in variability across regions, with model variability increasing from south to north (e.g. ATL has a modeled range of 40 ppb while NE has a modeled range of 70 ppb; Figure 5.10). Ozone precursors exhibit two distinct departures from observations. The first is low model NO_x concentrations and variability (Figure 5.10d-f). Model NO_x typically range between 1-3 ppb for ATL and MID with slightly higher concentrations in NE, whereas observed NO_x concentrations range from 1-28 ppb. Because NO_x emissions are averaged over a 60 by 60 km grid in the model, this discrepancy in concentration magnitude and range may be more indicative of direct urban point emissions near EPA-AQS stations than deficiencies in RegCM-CHEM. However, by averaging over multiple stations in each region and 5 midday hours, high

episodic bursts should be reduced. The lack of NO_x variability is likely derived from the lack of daily variations in NO_x emissions. The emissions inventory (Section 5.3.1.3) does have interannual variability providing some variation in model NO_x emissions (NE ranges from 14-19 mg m^{-2} day^{-1}; MID ranges from 7.6-9.5 mg m^{-2} day^{-1}; and ATL ranges from 8-10 mg m^{-2} day^{-1}), but the interannual emissions changes are not sufficient to produce variations in model NO_x.

The second distinct model behavior is the high isoprene concentrations, particularly in ATL and MID (Figure 5.10g-i). Observed midday isoprene concentrations do not exceed 5 ppb in any region, whereas modeled ATL isoprene concentrations range from 5-25 ppb except in the COUP simulation (< 5 ppb). Isoprene concentrations for NE are closest to observed values but are still biased high by 1-2 ppb. The low NO_x variability and high isoprene concentrations are most pronounced for ATL. This also corresponds to the region with the lowest O_3 variability and slightly weaker model soil moisture-temperature coupling relative to observations.

Comparing model biases of precursors to O_3 biases for ATL, no clear patterns emerge, however, there are a few noteworthy characteristics (Figure 5.11). Although the model tends to underestimate total nitrogen oxide species, NO_y, by 0-10 ppb and reactive nitrogen oxides, NO_x, by 0-7 ppb, O_3 concentrations are consistently overestimated in COUP by 5-25 ppb (Figures 5.11a and 5.11b). Despite the relatively good agreement between COUP and observed isoprene concentrations, O_3 concentration biases range from -30 to +50 ppb (Figure 5.11c). The overestimated O_3 is unexpected because high NO_x and isoprene concentrations are known to promote higher O_3 production. Therefore, the underestimates of NO_x and well-captured isoprene in the model should tend to produce lower O_3 concentrations than observed, rather than O_3 model over-

prediction present here. This shows that biases in precursor concentrations alone do not explain the systematic O_3 model overestimates.

We use the sample standard deviation to evaluate the model's ability to reproduce O_3 and precursor variability (Table 5.2). Standard deviations are calculated using midday average concentrations for the five simulated Augusts (2004-2008). Standard deviation using 17 years of observed Augusts (1994-2010) is also used to place the five August period in context. Comparing the 5-year to the 17-year observational records, we find O_3 and NO_x variability during the 5-year period is lower than the entire 17-year with little difference in observed isoprene variability (Table 5.2). This lower variability in O_3 and NO_x may be a result of NO_x emissions controls imposed in the early 2000's as part of the EPA's NO_x State Implementation Plan (SIP) Call (EPA, 2005), as past studies have shown that these emissions reductions have translated into reduced O_3 concentrations (Frost et al., 2006; Kim et al., 2006; Gego et al., 2007; Gilliland et al., 2008; Bloomer et al., 2009). Overall, the 5-year record can be regarded as a weaker than average period of variability for O_3 and NO_x.

For all regions and simulations, the model fails to capture the degree of observed O_3 variations, with the exception of UNCOUP-POET for NE (Table 5.2). In the case of isoprene, all the simulations overestimate isoprene concentration variability for ATL. For MID and NE, the interactive MEGAN simulations (COUP and UNCOUP) vastly overestimate emissions while the POET simulations show better agreement with observed variability. Model NO_x variability is unaffected by any model configuration changes and is 6-10 times less than observed (Table 5.2). Because NO_x variations are unaffected by isoprene emission rates and changes to land-atmosphere coupling, the variability of NO_x in the model is likely driven by static inputs, either emissions or boundary conditions.

This weak model variation in NO_x may, in part, explain the lack of O_3 variability seen in RegCM-CHEM.

Holding isoprene emissions constant and isolating the influence of land-atmosphere coupling (e.g. COUP-POET versus UNCOUP-POET) we find that the uncoupled simulations have higher O_3 variability, which suggests that greater model soil moisture-temperature coupling dampens O_3 variations. This is contrary to observations that showed greater O_3 variations occurred in the soil moisture-limited southern half of the U.S. (Chapter 4 and Table 5.1 for the 17-year observations). The effects of land-atmosphere coupling on isoprene concentrations also reduces isoprene variability, especially for ATL and MID where $\rho(E,T)$ shows the largest difference between coupled and uncoupled simulations (figure not shown).

When isolating the effects of isoprene emissions on simulated O_3 variations, the temporally static isoprene emissions inventory (POET) produces more O_3 variability than when using interactive isoprene (MEGAN). This occurs for coupled and uncoupled land-atmosphere simulations, with the exception of UNCOUP-POET for ATL. Further, UNCOUP-POET has the highest O_3 variations of any simulation for NE and MID. This is unexpected because UNCOUP-POET uses static isoprene, NO_x emissions inventories, and a decoupled land surface (e.g. variations in meteorological and emissions forcings are the weakest). Conversely, COUP, the simulation with the greatest potential for meteorological and isoprene emission variations, exhibits the lowest O_3 variability. When considering isoprene variability, as expected, allowing model isoprene emissions to respond interactively to environmental variables (MEGAN) yields greater isoprene concentration variability (Table 5.2). This implies that the ozone formation in the model is relatively insensitive to meteorological and ozone precursor changes that are known to

influence ozone formation, leading us to a discussion of the modeled ozone formation regimes.

5.3.6 The Behavior of Hydroxyl Radical

Based on the set of four simulations, O_3 biases are most sensitive to reductions in isoprene emissions (Figure 5.6) and O_3 variability is most sensitive to land-atmosphere coupling (Figure 5.7). To address these competing issues, the behavior of the hydroxyl radical (OH), the primary oxidant of isoprene in the atmosphere, is analyzed in the model. Because there are few direct measurements of OH, comparison with observations will be limited to citing typical midday values for urban environments of 0.2-0.8 ppt (Ren et al., 2003; Mao et al., 2010). Midday OH concentrations show substantial variability between the four simulations (Figure 5.12). COUP has the highest OH concentrations, with values greater than 0.3 ppt for much of the Eastern U.S. and isolated minima over New England and southern Georgia of 0.1-0.2 ppt (Figure 5.12a). The remaining simulations (UNCOUP and the pair of POET runs) show clear OH depletion corresponding to regions with high isoprene emissions (Figure 5.2). The depletion of OH in these simulations reduces concentrations to midday values of less than 0.08 ppt, well below the limited observed values.

OH concentrations are heavily dependent on isoprene emission rates in MID and ATL (Figure 5.13) where higher isoprene emissions correspond to lower OH concentrations, indicating that the primary oxidant of the atmosphere, OH, is effectively removed and controlled by isoprene emissions. The OH-isoprene relationship in the model produces two different regimes, each of which cause unrealistic chemical

environments. The first regime is the low isoprene emissions case that occurs in COUP with low O_3 interannual variability (Figure 5.7 and Table 5.2). Here isoprene emissions are lower than the other simulations due to restrictions by the g_{SM} factor, and this produces realistic OH concentrations in COUP but consequently removes a major driver of variability. The relatively higher OH concentrations in COUP (Figure 5.12a) lower ozone production rates (Figure 5.13d-f; orange symbols) that limit O_3 variability. The second regime is the high isoprene case of the UNCOUP and POET simulations, where OH is depleted to low concentrations thus producing large amounts of peroxy radicals (RO_2) that accelerate O_3 production (Figure 5.13d-f; orange symbols). This results in a high O_3 bias for these simulations (Figure 5.6). Additionally, photochemistry in the high isoprene case is slowed due to depleted OH making O_3 insensitive to changes in temperature near isoprene source regions such as ATL (Figure 5.8). This explains the poor correlation between O_3 and temperature and the improved correlations in the NE (Figure 5.8)

5.4 Discussion and Conclusions

The current analysis assesses the ability of RegCM-CHEM to capture the magnitude and interannual variability in observed O_3. Modeled O_3 concentrations are not sensitive to high temperature and radiation biases in coupled simulations (Figures 5.3 and 5.6). Additionally, higher soil moisture-temperature coupling results in less O_3 variability (Table 5.2) and has a nearly negligible influence on absolute O_3 concentrations (Figure 5.6). The weak response of O_3 to meteorological variables and land-atmosphere coupling regimes is contrary to observed relationships (Figure 5.8). The most significant

response of model O_3 concentrations is to biogenic isoprene emissions reductions, which reduces O_3 biases by 10 ppb (Figure 5.6) but severely reduces O_3 variability (Figure 5.7 and Table 5.2).

Taking into consideration the sensitivity of model O_3 to isoprene, the primary oxidant of isoprene, OH, is examined. The OH-isoprene relationship produced unrealistic model chemical environments with little O_3 variability when isoprene concentrations are low and high O_3 biases (> 10 ppb) when isoprene concentrations are high (Table 5.2 and Figure 5.11). This lack of balance between OH and isoprene is similar to observed relationships over high isoprene-emitting tropical forests such as the Amazon (Barkley et al., 2011). Comparing several chemical mechanisms, Barkley et al., (2011) found that most mechanisms underestimated OH and over estimated isoprene concentrations over the Amazon. They further observed that model OH concentrations better resemble observations when isoprene emissions are simply reduced. To improve OH concentrations in pristine environments, several studies have suggested including an OH recycling pathway where OH is regenerated after reacting with isoprene (Lelieveld et al., 2008; Paulot et al., 2009; Stavrakou et al., 2010; Taraborrelli et al., 2012). In a more recent study, Taraborrelli et al., (2012) described the chemical mechanism that treats isoprene as an OH buffer, acting as a sink and source. The buffering process was shown to maintain OH concentrations at observed levels in high isoprene source regions, and simultaneously not lead to increased O_3 production. This new OH recycling mechanism would likely improve OH concentrations for the Eastern U.S. and may serve to alleviate some of the O_3 concentration and variability biases found in this study. Therefore, more work will be needed in examining the behavior of other coupled climate-chemistry models and the inclusion of a more recent OH recycling mechanism to help rectify model

issues.

Table 5.1 Description of model sensitivity experiments

Table 1. Description of model sensitivity experiments

Simulation Name	Land-Atmosphere Interaction	Isoprene Emissions
COUP	Fully Coupled	MEGAN interactive
UNCOUP	Uncoupled	MEGAN interactive
COUP-POET	Fully Coupled	POET static
UNCOUP-POET	Uncoupled	POET static

Table 5.2 Standard deviation of ozone, isoprene, and NOx for EPA-AQS (5 and 17 year periods) and model sensitivity test for 5 years. The 5 year period is 2004-2008 and the 17 year period corresponds to the full EPA-AQS dataset from 1994-2010

Table 2. Standard Deviation of ozone, isoprene, and NOx for EPA-AQS (5 and 17 year periods) and model sensitivity tests for 5 years. The 5 year period is 2004-2008 and the 17 year period corresponds to the full EPA-AQS dataset from 1994-2010

	Ozone			Isoprene			NOx		
	NE	MID	ATL	NE	MID	ATL	NE	MID	ATL
Obs 5yr	15.0	15.2	14.1	0.4	0.9	0.9	6.4	3.9	2.4
Obs 17yr	17.4	16.2	18.7	0.4	1.0	0.8	11.1	6.4	2.8
COUP	10.4	7.9	5.3	0.9	1.8	1.7	1.4	0.3	0.4
COUP-POET	13.5	9.8	7.0	0.2	0.7	2.0	1.1	0.3	0.3
UNCOUP	13.6	9.2	7.5	1.0	5.1	6.6	1.2	0.3	0.3
UNCOUP-POET	15.4	10.4	7.4	0.2	0.9	2.5	1.0	0.3	0.3

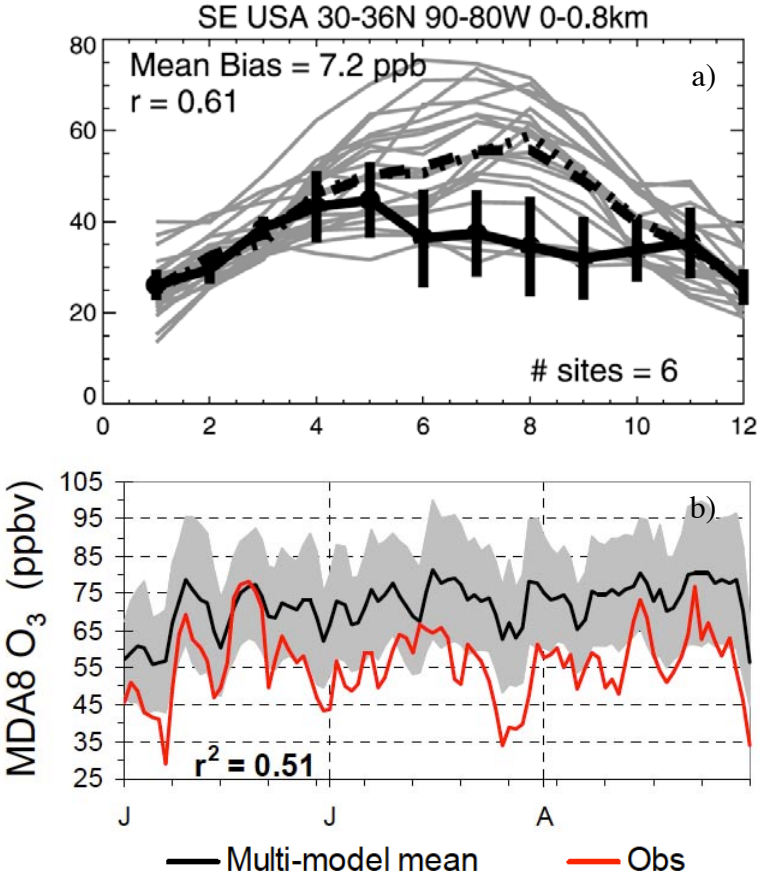

Figure 5.1 a) Monthly model mean O_3 for the year 2001 of (black circles) site averaged observations with (vertical black line) the across site standard deviation, (gray) individual model simulations, and (dashed black) the multi-model mean. b) Maximum daily 8 hour average O_3 for (red) observations, (black) multi-model mean, and (gray shading) the one standard deviation of the model mean for June, July, and August (JJA) over the Southeast. a) figure is Figure 2 from Fiore et al., (2009) and b) is Figure 5 from Reidmiller et al., (2009).

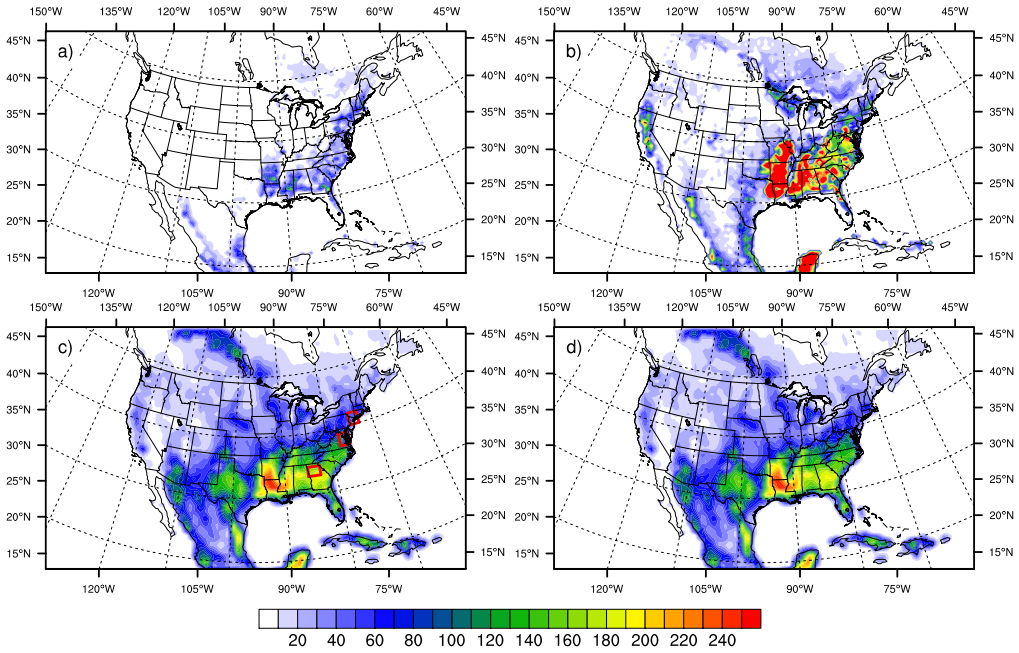

Figure 5.2 August midday (12-4pm) average isoprene emissions from 2004-2008 for a) fully interactive simulation (COUP) using MEGAN, b) decoupled land-atmosphere (UNCOUP) using MEGAN, and c-d) a coupled (COUP-POET) and uncoupled (UNCOUP-POET) simulation using POET isoprene emission inventory. All emissions are in mg m^{-2} day^{-1}. Red boxes in panel c) outline the Northeast (NE; 40-42°N and 73-75°W), Mid-Atlantic (MID; 37-39°N and 76-78°W), and Atlanta Metropolitan (ATL; 33-34.5°N and 83-85.4°W) focus regions.

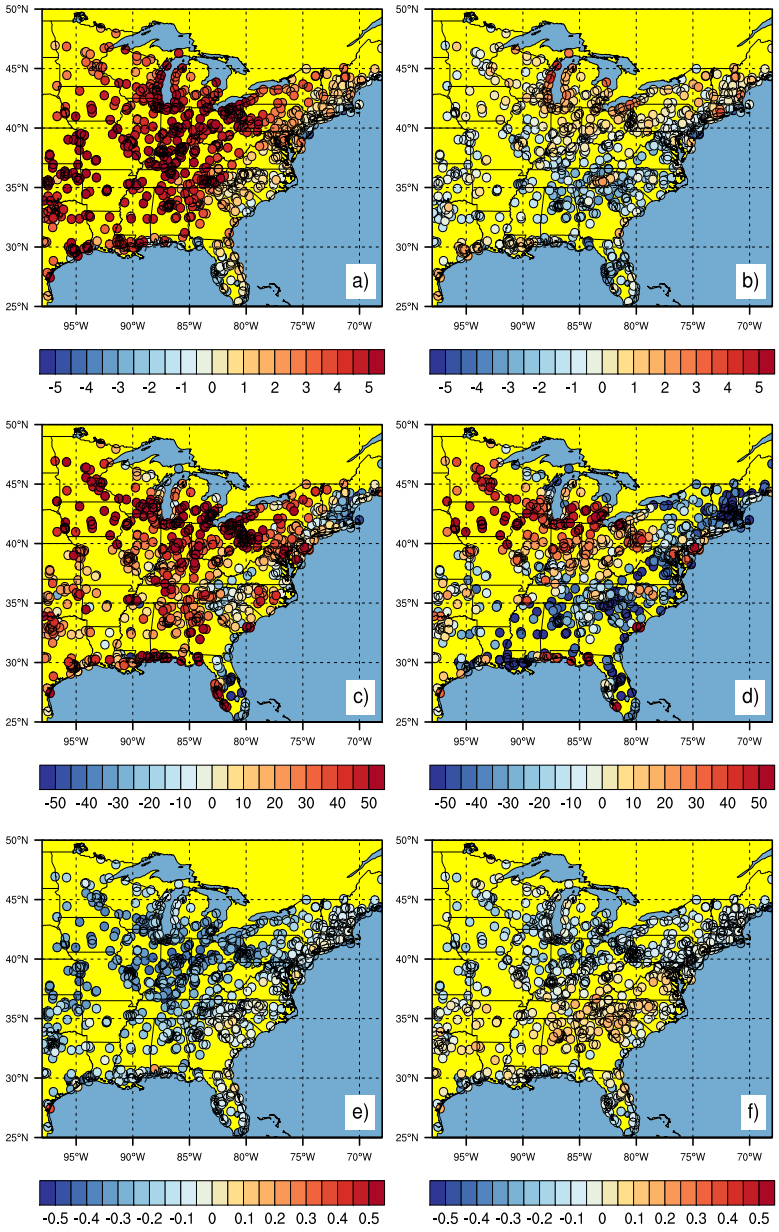

Figure 5.3 Average August midday (12-4pm) model bias from 2004-2008 for a-b) temperature (K), c-d) incident radiation (W m^{-2}), and e-f) latent heat flux ratio ($\lambda E/R_N$) at nearest model grid cell to EPA-AQS stations. The first column shows coupled simulations (COUP and COUP-POET) and the second shows uncoupled simulations (UNCOUP and UNCOUP-POET).

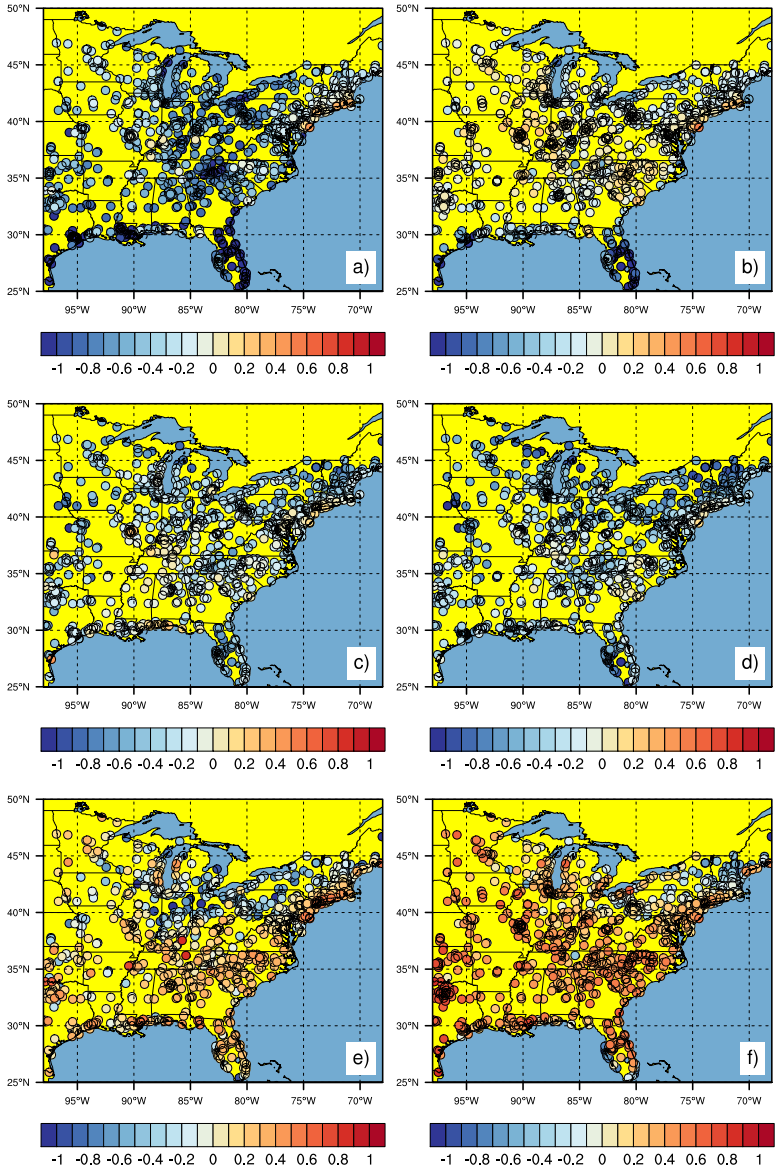

Figure 5.4 Average August midday (12-4pm) relative variation bias from 2004-2008 for a-b) temperature (K), c-d) incident radiation (W m-2), and e-f) latent heat flux ratio ($\lambda E/R_N$) at nearest model grid cell corresponding to the closest EPA-AQS station. The first column is for coupled simulations (COUP and COUP-POET) and the second is for uncoupled simulations (UNCOUP and UNCOUP-POET).

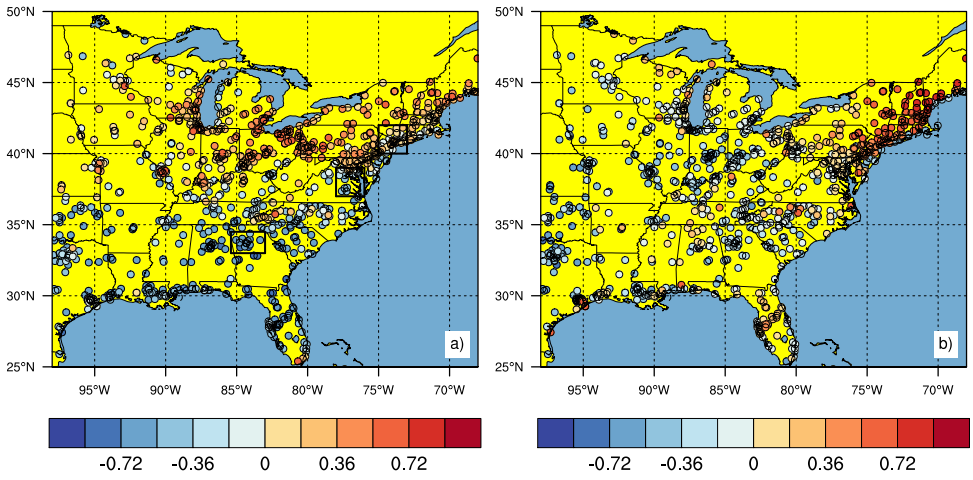

Figure 5.5 Correlation between evapotranspiration (E; mm day^{-1}) and temperature (T; K) describing the degree of soil moisture-temperature coupling, $\rho(E,T)$, for a) NLDAS2 and b) coupled model simulations (COUP and COUP-POET). Negative values (blue) refer to greater soil moisture influence on temperatures.

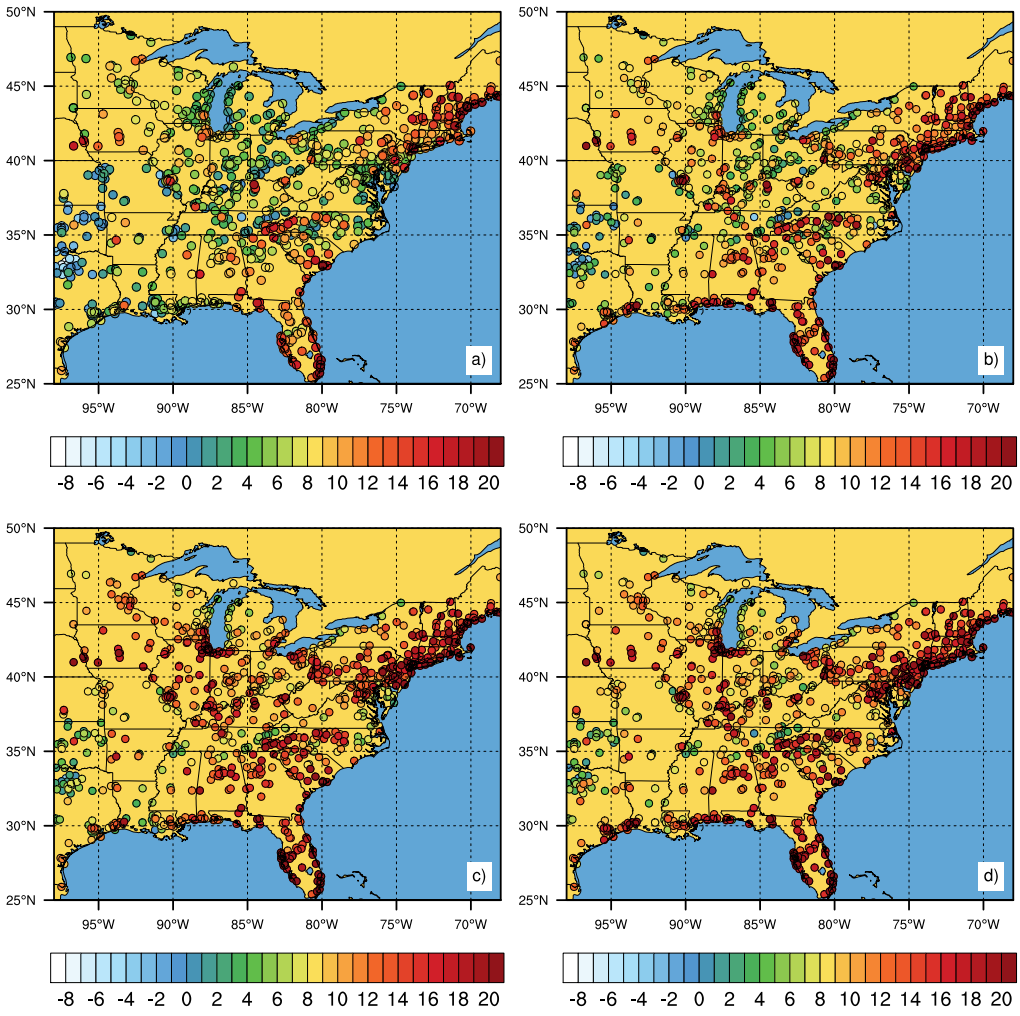

Figure 5.6 Average August midday (12-4pm) O_3 model bias from 2004-2008 for a) COUP, b) UNCOUP, c) COUP-POET, and d) UNCOUP-POET simulation in ppb. Circles refer to the model grid cell corresponding to the closest EPA-AQS station.

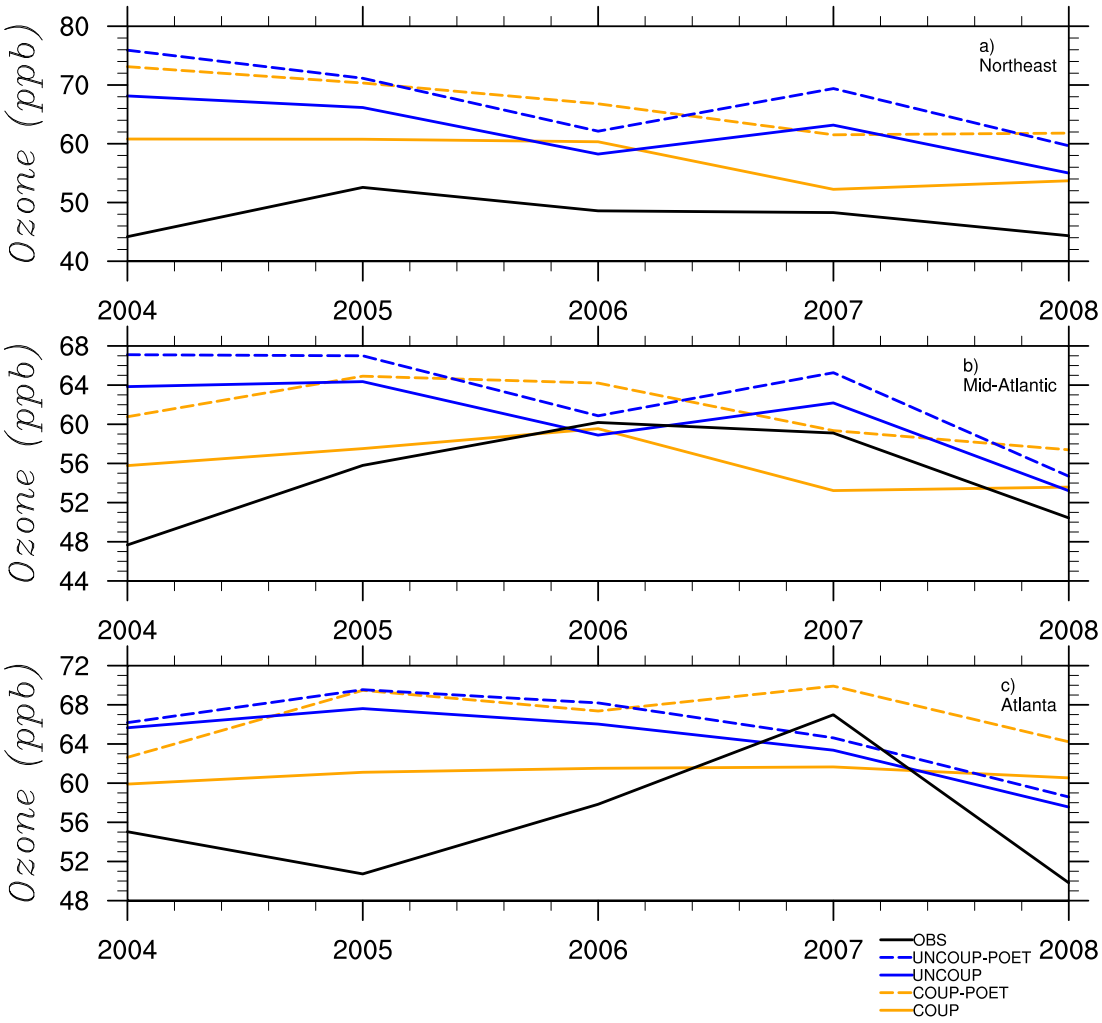

Figure 5.7 Average August midday O_3 concentrations (ppb) for a) the Northeast, b) Mid-Atlantic, and c) Atlanta regions highlighted in Figure 1. Orange lines correspond to coupled simulations (COUP and COUP-POET) and blue lines correspond to uncoupled simulations (UNCOUP and UNCOUP-POET). Simulations using POET isoprene emissions inventory are dashed and solid lines use the interactive MEGAN algorithms.

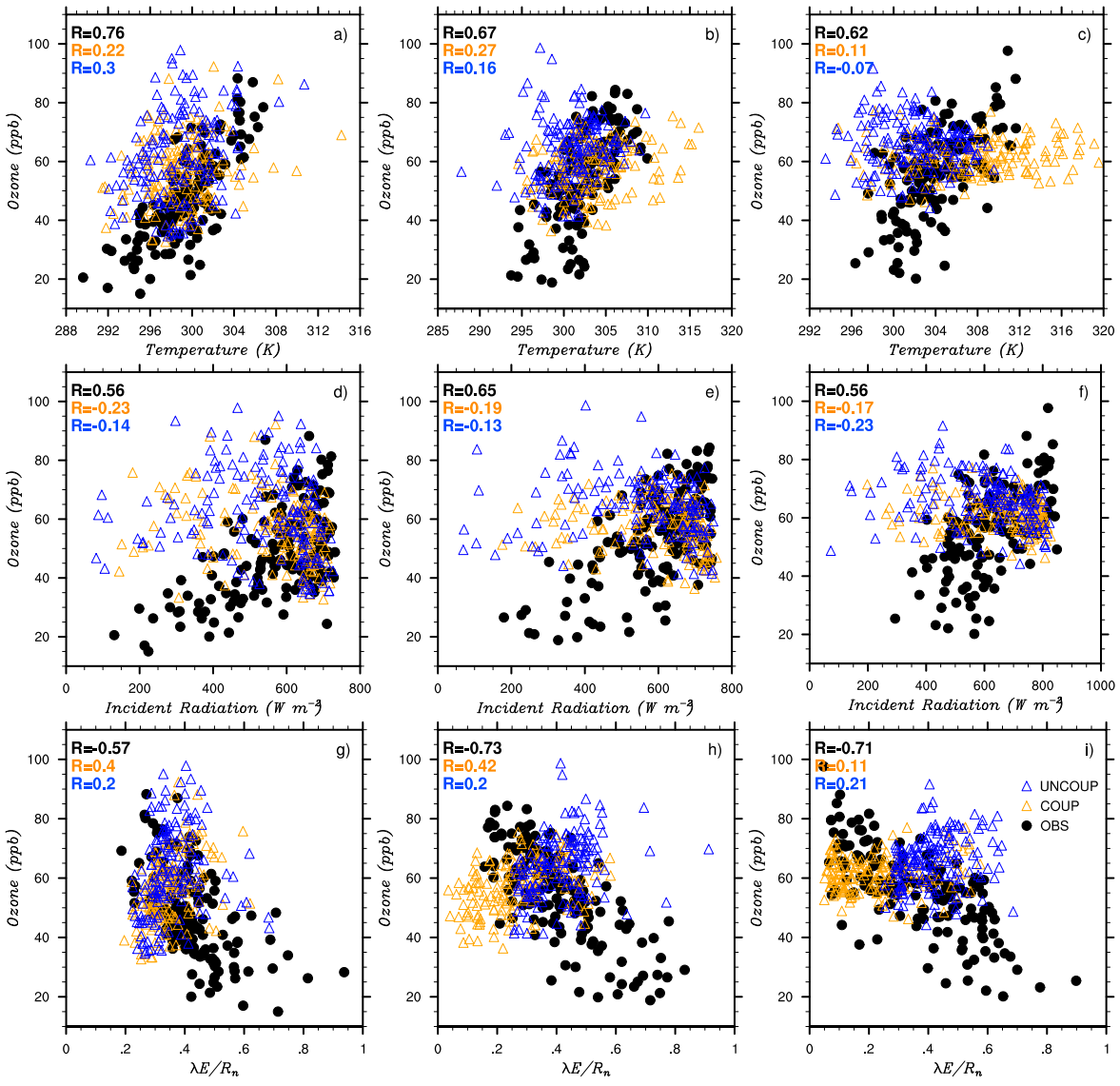

Figure 5.8 Midday average August O_3 concentrations (ppb) versus (a-c) temperature (T; K), (d-f) incident radiation (R_N; W m^{-2}), and (g-i) latent heat flux ratio ($\lambda E/R_N$; unitless) for observations (black dots; EPA-AQS O3 and NLDAS2 T, R_N and $\lambda E/R_N$), COUP (orange triangles), and UNCOUP (blue triangles) model runs from 2004-2008. Color coded correlation coefficients are displayed in the top left corner of each panel. The left column is the Northeast region (NE), the center column is the Mid-Atlantic (MID), and the right column is the Atlanta region (ATL).

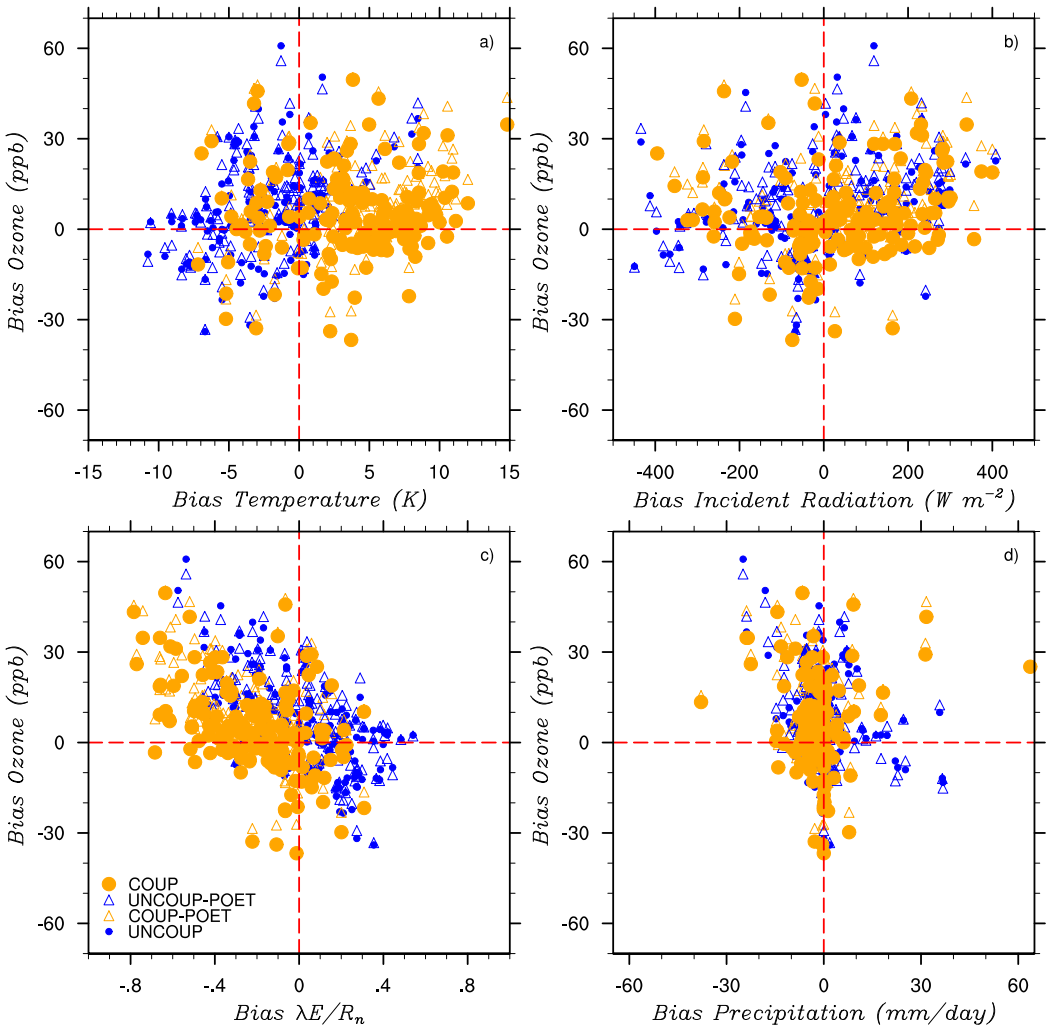

Figure 5.9 Model bias (model minus NLDAS) for midday average August O_3 concentrations (ppb) versus (a) temperature (T; K), (b) incident radiation (R_N; W m^{-2}), (c) latent heat flux ratio ($\lambda E/R_N$; unitless), and (d) daily total precipitation (mm/day) biases for the Atlanta region (ATL) from 2004-2008.

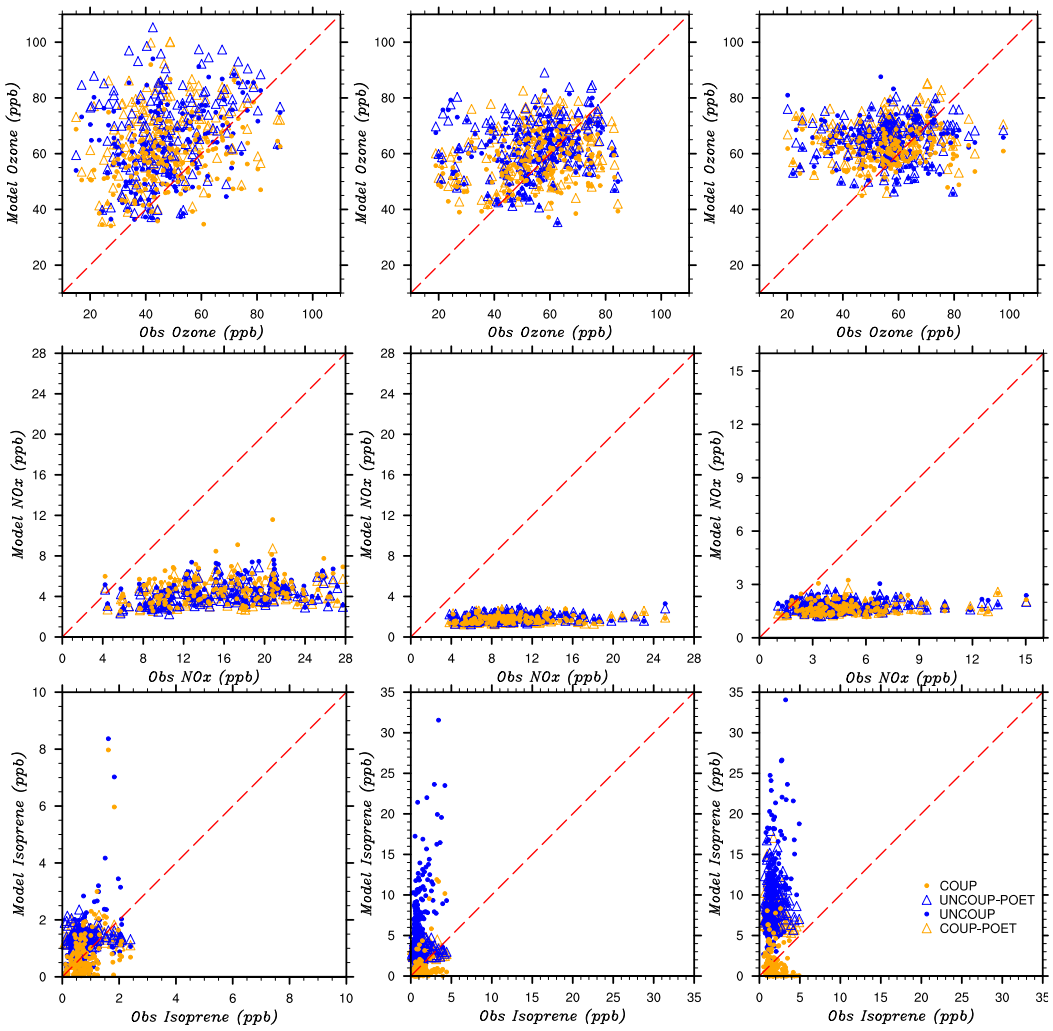

Figure 5.10 Observed versus modeled midday (12-4pm) average August (a-c) O_3, (d-f) NO_x, and (g-i) isoprene concentrations for (orange dots) COUP, (blue dots) UNCOUP, (orange triangles) COUP-POET, and (blue triangles) UNCOUP-POET model runs. Observations based on EPA-AQS concentration measurements from 2004-2008. Each point represents a single midday average concentration in ppb. The red dashed line is the 1:1 perfect correlation line. The left column is the Northeast region (NE), the center column is the Mid-Atlantic (MID), and the right column is the Atlanta region (ATL).

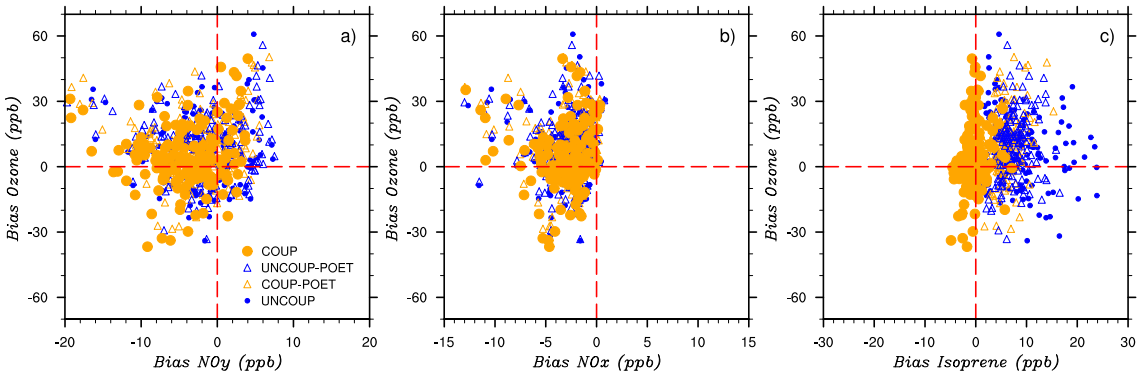

Figure 5.101 Model bias (model minus observed) for midday average August O_3 concentrations (ppb) versus (a) NO_y (ppb), (b) NO_x (ppb), (c) isoprene (ppb) concentration biases for the Atlanta region (ATL) from 2004-2008.

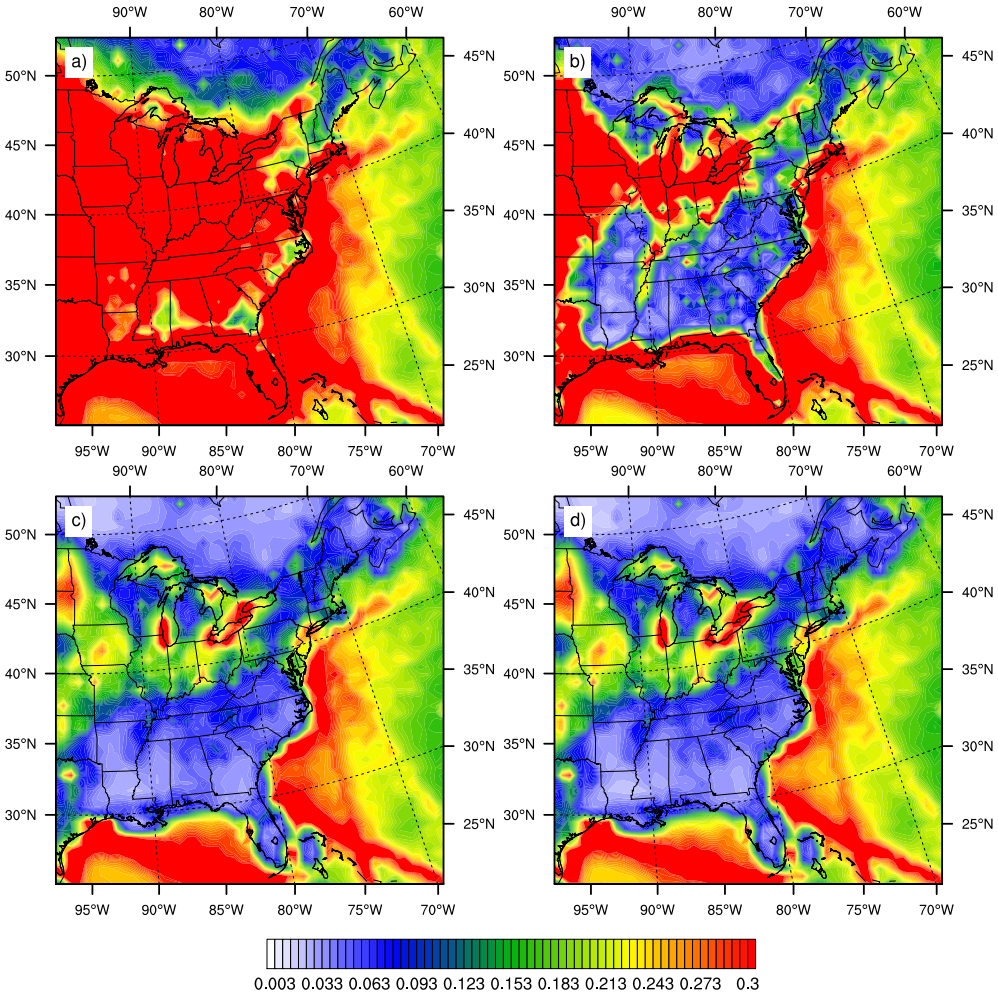

Figure 5.112 Midday average August OH concentrations (ppt) from 2004-2008 for a) COUP, b) UNCOUP, c) COUP-POET, and d) UNCOUP-POET simulation.

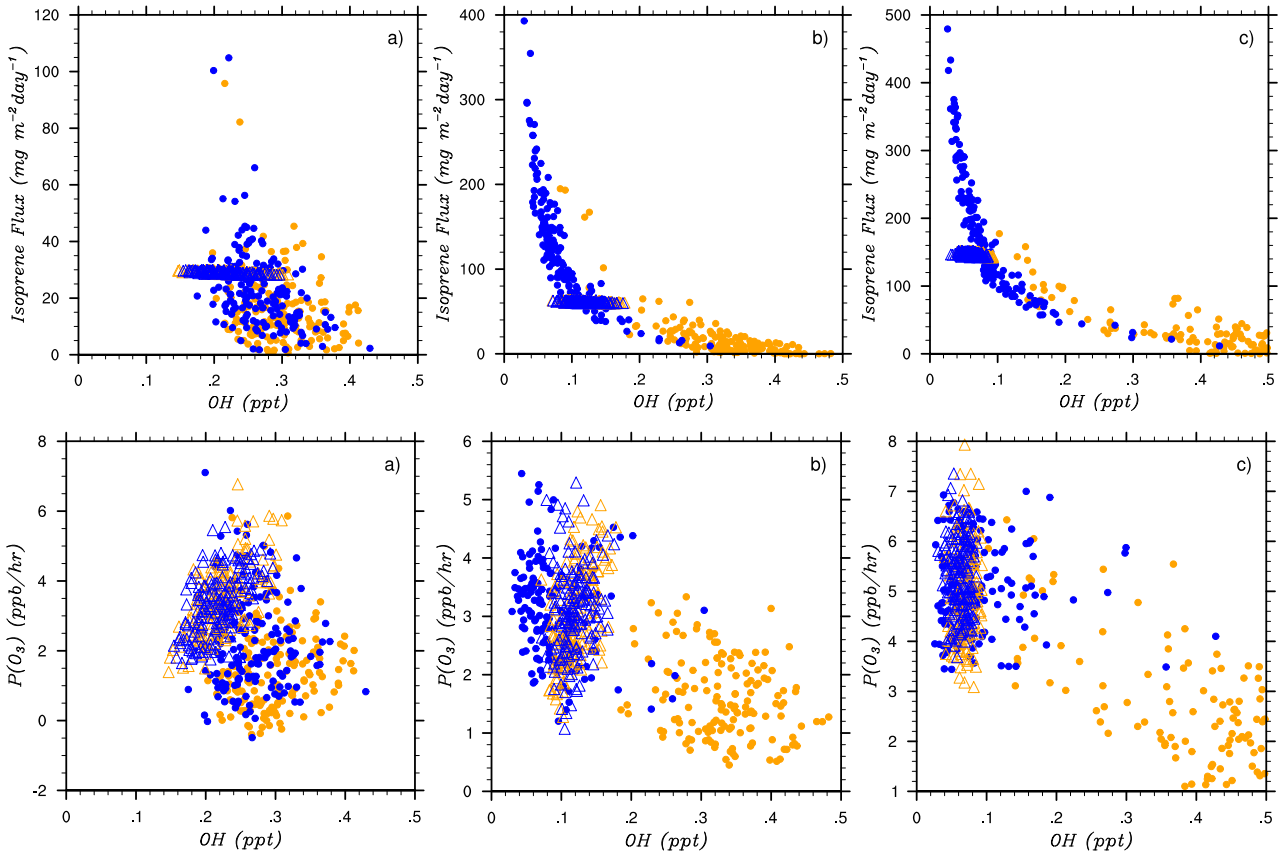

Figure 5.123 Midday average modeled August OH concentrations (ppt) compared with (a-c) isoprene emissions (mg m^{-2} day^{-1}) and (d-f) net O_3 production rates (ppb hr^{-1}) for (orange dots) COUP, (blue dots) UNCOUP, (orange triangles) COUP-POET, and (blue triangles) UNCOUP model runs from 2004-2008. The left column is the Northeast region (NE), the center column is the Mid-Atlantic (MID), and the right column is the Atlanta area (ATL).

Chapter 6

Conclusions

6.1 Summary of Work

Land-atmosphere interactions play an important role in modifying surface air temperatures (Seneviratne et al., 2006; Zhang et al., 2008a; Hirschi et al., 2011) and precipitation (Findell and Eltahir, 1997; Koster and Suarez, 2001; Koster et al., 2004; Ferguson and Wood, 2011) in the climate system. In some regions, these perturbations in either the land or atmosphere component can feedback and potentially amplify the initial signal. Soil moisture, in particular, serves as the slowly varying moisture source to the atmosphere and evolves on climate length time-scales, making it an important component of the land-atmosphere system. The surface climate as defined by the land surface also influences tropospheric chemistry through climatic conditions and natural emissions from the terrestrial biosphere. The overarching goal of this work is to assess the role of soil moisture and land-atmosphere coupling on surface climate (Chapter 2), biogenic volatile organic compound (VOC) emissions (Chapter 3), and tropospheric ozone formation (Chapters 4 and 5). This work bridges the typically distinct fields of regional climate and atmospheric chemistry.

A valuable tool in assessing land-atmosphere feedbacks is coupled chemistry-climate models. In an effort to assess the behavior of coupled models, model components relevant to land-atmosphere-chemistry interactions are systematically included in a regional climate model, RegCM. Each additional component provides a method to examine land-atmosphere interactions in a fully coupled framework, where soil moisture, emissions and the resulting atmospheric chemistry are calculated within a single model at similar dynamical and chemical timesteps.

The first model improvement is an update of the land surface parameterization of RegCM by replacing a second-generation land surface model (the Biosphere-Atmosphere Transfer Scheme; (Sellers et al., 1986; Dickinson et al., 1993)) with a third-generation land model (the Community Land Model version 3.5 (CLM); (Oleson et al., 2008; Tawfik and Steiner, 2011)). This coupled model (RegCM-CLM) was introduced in Chapter 2 and implemented to evaluate soil moisture-atmosphere coupling on decadal scales. Originally soil moisture-atmosphere coupling was thought to be negligible outside of summer due to weak surface fluxes (Zhang et al., 2008a). This study (Tawfik and Steiner, 2011), however, demonstrates the ability of soil water phase to promote subsequent liquid precipitation events near the freezing line in the continental U.S. The more detailed representation of vegetation, explicit soil temperature calculations, and inclusion of multiple snow layers in RegCM-CLM allow for the examination of this new cold season soil moisture-atmosphere coupling mechanism, as described through the following steps:

1) The feedback mechanism is initiated by sufficient soil liquid water giving the land surface a higher thermal inertia.
2) Additional soil liquid water produces more stable and warmer soil temperatures.

3) Higher soil temperatures and more liquid water available for evaporation increases surface fluxes (latent and sensible heat flux).
4) Greater surface fluxes translate to warmer air temperatures and greater moisture static energy.
5) Warmer air temperatures and higher moist static energy promote more liquid phase precipitation.
6) The feedback cycle is complete when the increase in liquid precipitation increases soil water.

This soil phase-precipitation feedback occurs near the freezing line over the continental U.S., where the model is most sensitive to changes in soil water phase. This freezing line transition zone is analogous to dry-to-wet transition zone found during boreal summer (Koster et al., 2004; Guo et al., 2006; Dirmeyer).

The RegCM-CLM is also capable of replicating the widely documented summer soil-temperature coupling over the Great Plains (Koster et al., 2004; Guo et al., 2006; Zhang et al., 2008a; Dirmeyer). In this region, soil moisture can strongly influence surface temperatures and subsequent precipitation, leading to a definition of the region as strongly coupled. The ability of RegCM-CLM to capture this coupling provides confidence that the model is behaving consistently with other models and observations and the RegCM-CLM results may be broadly applicable to other coupled land-atmosphere models.

Moving towards a fully interactive coupled climate-chemistry model, a biogenic emissions model, the Model of Emissions of Gases and Aerosols from Nature (MEGAN; (Guenther et al., 2006)), is coupled to RegCM-CLM (Tawfik et al., 2012). Biogenic VOC emissions are very sensitive to environmental variables and many chemistry-climate

studies use existing climatological inventories that cannot capture the coupled nature of changing climate conditions on emissions. MEGAN uses empirically based relationships to calculate these naturally occurring emissions, where emissions respond directly to changes in temperature, light, leaf area index (LAI), and soil moisture. Here we focus on isoprene due to its photochemical relevance, particularly in the Eastern U.S. In Chapter 3 the interannual response of isoprene to changes in temperature, light, soil moisture, and LAI is examined using a novel approach to account for the variability from each environmental factor. We found that no single variable drives isoprene interannual variability, but rather the combined influence of soil moisture and temperature accounts for greater than 80% of isoprene variability over the U.S. This suggests that the signal of soil moisture and temperature controls on isoprene flux variability may affect ozone (O_3) concentrations in certain chemical environments. However, because temperature itself is a strong driver of O_3, the soil moisture-temperature controls on isoprene variability may be convoluted. A set of simulations using a coupled climate-chemistry model is necessary to isolate these convolved effects on tropospheric O_3.

Observed O_3 relationships are established using O_3 and isoprene concentration measurements from the Environmental Protection Agency's Air Quality System (EPA-AQS) Photochemical Assessment Stations (PAMS) (US EPA) and data assimilated meteorological products from the Second Phase of the North American Land Data Assimilation System (NLDAS2) (Mitchell et al., 2004). Chapter 4 explores the influence of soil moisture-temperature coupling on O_3. It was found that soil moisture-temperature coupling provides a mechanistic explanation for the widely observed correlations between O_3 and temperature, and O_3 and humidity. More specifically, years when evapotranspiration is limited by the amount of soil moisture (referred to as "soil moisture-

limited") correspond to strong negative O_3-humidity correlations. Years with evapotranspiration limited by the amount of net surface radiation (referred to as "energy-limited") have strongly positive O_3-temperature correlations. A clear north-south gradient was observed over the Eastern U.S. where soil moisture-limited (energy-limited) conditions were found primarily south (north) of the 37th parallel. Under soil moisture-limited conditions, O_3 concentrations tend to be higher. The physical mechanism producing high O_3 in soil moisture-limited conditions results from the different partitioning of surface fluxes. When evapotranspiration is limited by soil moisture, less net surface radiation is partitioned towards evaporation and more towards heating the surface (e.g. more sensible heat flux). Greater sensible heat flux then increases near-surface temperatures, which accelerates O_3 photochemistry. Because evapotranspiration is reduced for soil moisture-limited conditions, water vapor flux to the atmosphere is reduced. This causes near-surface humidity to decrease and simultaneously causing warmer surface air temperature. Therefore, the widely observed correlation between humidity and O_3 is a consequence of surface drying. Surface wetness (the latent heat flux ratio; $\lambda E/R_N$) is also shown to be a better predictor of O_3 concentrations than humidity, further accenting the importance of soil moisture conditions on O_3 air quality.

To assess the efficacy of models to replicate the observed land-atmosphere-chemistry interactions, a gas phase chemistry mechanism (Zaveri and Peters, 1999) is coupled to the RegCM-CLM-MEGAN model framework. An extended version of the Carbon Bond Model (Gery et al., 1989) that includes an explicit representation of isoprene chemistry is used (CBM-Z; (Zaveri and Peters, 1999)). A full description of the coupled regional climate-chemistry model (RegCM-CHEM) is provided in Shalaby et al., (2012). RegCM-CHEM allows for isoprene emissions from MEGAN to be passed

directly to CBM-Z, providing temporally evolving emissions that respond to changes in environmental conditions. Using RegCM-CHEM, four simulations were performed to evaluate model sensitivity to isoprene emissions and land-atmosphere coupling against observed relationships. A 10-30 ppb O_3 bias, prevalent across multiple models in the southeastern U.S. (Fiore et al., 2009; Reidmiller et al., 2009), is examined alongside the skill of RegCM-CHEM to capture observed variability. Chapter 5 demonstrates that RegCM-CHEM had difficulty reproducing the observed sensitivity of O_3 to temperature especially over the Southeastern U.S., despite reproducing general pattern of land-atmosphere coupling found in observations. The interannual variability of O_3 is poorly captured by RegCM-CHEM but deficiencies are not unique to our coupled model (Rasmussen et al., 2012). Of the four simulations performed, improvements in the absolute O_3 concentration bias resulted in unrealistically low interannual O_3 variability. Simulations indicate that this behavior is due to the interaction between isoprene and its primary atmospheric oxidant, hydroxyl (OH). As illustrated in Chapter 5, high isoprene emissions deplete OH concentrations producing isoprene oxidation products that increase O_3 production. This yields high model O_3 biases. For low isoprene emissions conditions, OH concentrations are more realistic but these simulations experience a reduction in O_3 variability.

6.2 Broad Implications

This work describes the mechanisms connecting soil moisture, a variable known for influencing climate-scale processes, to O_3 air quality. The policy relevance of tropospheric O_3 stems from its potential hazard to human health (Lippmann, 1989;

Bernard and Ebi, 2001; Knowlton et al., 2004; Bell et al., 2007) and agriculture (Heck et al., 1982; Akimoto, 2003; Ashmore et al., 2006) at high concentrations. Bridging between O_3 air quality and climate serves to link the public health-relevant issue of O_3 air quality to longer-term policy adaptation strategies as outlined by the United Nations Intergovernmental Panel on Climate Change (IPCC) (Confalonieri et al., 2007). Anthropogenic NO_X emissions reductions have been successful in improving O_3 air quality when adopted. In particular, the implementation of the EPA's NO_x State Implementation Plan (SIP) (EPA, 2005) returned lower O_3 concentrations in less than decade for the Southeastern U.S. (Frost et al., 2006; Kim et al., 2006; Gego et al., 2007). Improving O_3 air quality can prove to be difficult, however, due to the contribution of biogenic emissions and climate variability, which are not subject to control strategies. As Godowitch et al., (2008) point out meteorological variability can have a stronger control on O_3 variability than NO_x emissions reductions in some regions. The current work accented this issue by identifying the importance of the soil moisture-temperature on isoprene emission variability (Chapter 3) and suggested a mechanistic explanation for commonly observed correlations between O_3 and meteorological variables. A coupled climate-chemistry model was shown to generally reproduce the soil moisture-temperature relationship, but contrary to observations, O_3 concentrations were insensitive to land-atmosphere feedbacks. The lack of land-atmosphere-chemistry interactions is prevalent in other coupled models as well. By providing a mechanistic explanation of observed O_3 behavior, a first step is taken towards incorporating these relationships in coupled climate-chemistry models. The inclusion into models will provide policy makers with better tool for assessing potential long-term impacts of mitigation measures prior to implementation based on physical processes rather than statistical techniques.

One of the goals of the IPCC is to provide scientific reports regarding the current state of the global climate and project into the future a range of plausible outcomes given a set of emissions scenarios. Future scenarios all identify warmer climates by the year 2050 as induced by the radiative forcing (RF) from long-lived greenhouse gases, such as CO_2. As policy makers look to adopt adaptation and mitigation strategies to curtail warming, measures that provide rapid results become appealing. Particular focus has been given in recent years to reducing short-lived climate forcing (SLCF) species, such as O_3 (Shindell et al., 2008; Chang et al., 2009). A short-lived climate forcing species is defined as compound that directly influences the Earth's energy budget and has an atmospheric lifetime of a few days or weeks. Estimates of the RF for O_3 are derived from coupled global climate-chemistry models and chemical transport models due to the lack of direct global measurements (Forster and Ramaswamy, 2007). Because the measure of success for reducing O_3 as a SLCF is predicated on the RF estimates of models, it becomes necessary to evaluate the ability of models to replicate observed concentrations and variability. While efforts have been dedicated to assessing the influence of future climate change on O_3 (Hogrefe et al., 2004; Murazaki and Hess, 2006; Steiner et al., 2006; Dawson et al., 2008; Kunkel et al., 2008; Zeng et al., 2008; Jacob and Winner, 2009; Liao et al., 2009; Racherla and Adams, 2009; Weaver et al., 2009), understanding and pinpointing model shortcomings has received less attention (Davis et al., 2011; Hogrefe et al., 2011). Furthermore, of the studies that investigated model deficiencies mentioned, neither used coupled climate-chemistry models, the primary tool of IPCC future projections. This current work attempts to fill this much needed gap by, first, providing mechanistic explanations for observed O_3 -meteorology interactions, and

second, evaluating model ability to capture these observed relationships over a region known for poor model performance.

6.3 Recommendations for Future Work

This work highlights the importance of soil moisture in the climate system and its ability to influence precipitation, temperatures, biogenic emissions, and O_3. Although the role of soil moisture on climate has been well-established (Yeh et al., 1984; Karl, 1986; Yang et al., 1994; Findell and Eltahir, 1997; Ferguson and Wood, 2011; Lo and Famiglietti), there have been few direct long-term measurements of soil moisture. Of the measurements that are available, they are often limited to a single station in one larger region (Hollinger and Isard, 1994). There have also been efforts to infer soil moisture content from satellites using microwave remote sensing techniques (Kerr et al., 2001; Entekhabi et al., 2009; Entekhabi et al., 2010); however, these measurements penetrate only a few centimeters into the soil and therefore would not capture root zone soil moisture, which is pertinent to climate applications. Therefore, more extensive long-term soil moisture measurements that extend throughout the root zone and span the regional scale are needed. Ideally these would include coincident measurements of temperature, humidity, surface fluxes, and O_3 concentrations to help examine land-atmosphere-chemistry feedbacks.

Beyond the direct measurements of land and atmospheric parameters, there is also a limited dataset of biogenic isoprene fluxes to the atmosphere. In the US, there are only two or three flux stations with consistent measurements of isoprene fluxes with virtually no measurements over the past two decades in the Southeast, a region known for

high isoprene emissions and poor model performance with regards to simulating O_3. In order to better evaluate model chemical regimes, including correct emissions inputs is vital. Additionally, the network of isoprene concentration measurement is limited, and more observations of isoprene concentrations would greatly improve the ability to assess model chemistry.

Modeling the chemistry-climate interactions, particularly over the Southeast, has shown large positive biases in O_3 estimates. This has been attributed to poor meteorology (Godowitch et al., 2008; Nolte et al., 2008; Rasmussen et al., 2012), weak pollutant ventilation (Castellanos et al., 2011), and the fate of isoprene in the atmosphere (Fiore et al., 2005; Wild, 2007; Wu et al., 2007a; Ito et al., 2009) in models. Further efforts are needed to evaluate the ability of models to capture basic observed relationships, such as the ozone-temperature relationship in the difficult to simulate Southeastern U.S. Additionally, there has been little evaluation of interannual variability of ozone, but limited results suggest that coupled and uncoupled models are unable to capture the observed variability (Hogrefe et al., 2011; Rasmussen et al., 2012). More specifically, it would be advantageous to conduct a multi-model inter-comparison study of these coupled climate-chemistry model behaviors. Each participating model would perform simulations for at least 5 years, and model interannual variability and biases would be examined. Before this type of assessment is performed it is difficult to have confidence in emissions perturbation or climate change studies of O_3 for regions plagued by systematic biases.

The evaluation presented here indicates that reproducing the ozone-temperature relationships in coupled chemistry-climate models is not possible at this time. This must be rectified in order to evaluate the effect of climate change on O_3 formation in the

future, which is needed for both an understanding of air quality and the role of ozone as a climate-forcing agent. A more integrated approach is, therefore, necessary requiring cross-discipline collaboration between the climate modeling and chemistry/air quality communities in order to rectify model shortcomings.

References

Abbot, D.S., et al., 2003. Seasonal and interannual variability of North American isoprene emissions as determined by formaldehyde column measurements from space. Geophysical Research Letters 30, 1999-2002.10.1029/2003gl017336.

Akimoto, H., 2003. Global air quality and pollution. Science 302, 1716-1719

Andreae, M.O., Rosenfeld, D., 2008. Aerosol-cloud-precipitation interactions. Part 1. The nature and sources of cloud-active aerosols. Earth-Science Reviews 89, 13-41.10.1016/j.earscirev.2008.03.001.

Arnason, G., et al., 1968. A Numerical Experiment in Dry and Moist Convection Including Rain Stage. Journal of the Atmospheric Sciences 25, 404-&

Arneth, A., et al., 2008. Why are estimates of global terrestrial isoprene emissions so similar (and why is this not so for monoterpenes)? Atmospheric Chemistry and Physics 8, 4605-4620

Arneth, A., et al., 2011. Global terrestrial isoprene emission models: sensitivity to variability in climate and vegetation. Atmos. Chem. Phys. 11, 8037-8052.10.5194/acp-11-8037-2011.

Arnts, R.R., et al., 1982. ESTIMATES OF ALPHA-PINENE EMISSIONS FROM A LOBLOLLY-PINE FOREST USING AN ATMOSPHERIC DIFFUSION-MODEL. Atmos. Environ. 16, 2127-2137.10.1016/0004-6981(82)90283-9.

Ashmore, M., et al., 2006. Ozone - a significant threat to future world food production? New Phytologist 170, 201-204

Ashworth, K., et al., 2010. Sensitivity of isoprene emissions estimated using MEGAN to the time resolution of input climate data. Atmospheric Chemistry and Physics 10, 1193-1201.10.5194/acp-10-1193-2010.

Atkinson, R., 2000. Atmospheric chemistry of VOCs and NOx. Atmos. Environ. 34, 2063-2101

Atlas, R., et al., 1993. The Effect of Sst and Soil-Moisture Anomalies on Gla Model Simulations of the 1988 United-States Summer Drought. Journal of Climate 6, 2034-2048

Aughey, S., 1880. Sketches of the physical geography and geology of nebraska. 326

Aw, J., Kleeman, M.J., 2003. Evaluating the first-order effect of intraannual temperature variability on urban air pollution. Journal of Geophysical Research-Atmospheres 108.Artn 4365
Doi 10.1029/2002jd002688.

Baldocchi, D., et al., 1995. The Fluxes and Air Chemistry of Isoprene above a Deciduous Hardwood Forest. Philosophical Transactions of the Royal Society of London Series a-Mathematical Physical and Engineering Sciences 351, 279-296

Barkley, M.P., et al., 2011. Can a "state of the art" chemistry transport model simulate Amazonian tropospheric chemistry? Journal of Geophysical Research-Atmospheres 116.Artn D16302
Doi 10.1029/2011jd015893.

Beljaars, A.C.M., et al., 1996. The anomalous rainfall over the United States during July 1993: Sensitivity to land surface parameterization and soil moisture. Monthly Weather Review 124, 362-383

Bell, M.L., et al., 2007. Climate change, ambient ozone, and health in 50 US cities. Climatic Change 82, 61-76.Doi 10.1007/S10584-006-9166-7.

Benjamin, M.T., et al., 1996. Low-emitting urban forests: A taxonomic methodology for assigning isoprene and monoterpene emission rates. Atmos. Environ. 30, 1437-1452.10.1016/1352-2310(95)00439-4.

Bernard, S.M., Ebi, K.L., 2001. Comments on the process and product of the health impacts assessment component of the national assessment of the potential consequences of climate variability and change for the United States. Environ. Health Perspect. 109, 177-184

Betts, A.K., 2004. Understanding hydrometeorology using global models. Bulletin of the American Meteorological Society 85, 1673-+.10.1175/bams-85-11-1673.

Betts, A.K., Ball, J.H., 1995. The FIFE surface diurnal cycle climate. Journal of Geophysical Research-Atmospheres 100, 25679-25693

Betts, A.K., et al., 1996. The land surface-atmosphere interaction: A review based on observational and global modeling perspectives. Journal of Geophysical Research-Atmospheres 101, 7209-7225

Bhumralkar, C.M., 1975. Numerical Experiments on Computation of Ground Surface-Temperature in an Atmospheric General Circulation Model. Journal of Applied Meteorology 14, 1246-1258

Bisselink, B., Dolman, A.J., 2008. Precipitation Recycling: Moisture Sources over Europe using ERA-40 Data. Journal of Hydrometeorology 9, 1073-1083.10.1175/2008jhm962.1.

Blackadar, A.K., 1966. Climate near Ground. J Franklin I 281, 75-&

Blanchard, C.L., et al., 2010a. NMOC, ozone, and organic aerosol in the southeastern United States, 1999-2007 2 Ozone trends and sensitivity to NMOC emissions in Atlanta, Georgia. Atmos. Environ. 44, 4840-4849.10.1016/j.atmosenv.2010.07.030.

Blanchard, C.L., et al., 2010b. NMOC, ozone, and organic aerosol in the southeastern United States, 1999-2007 1 Spatial and temporal variations of NMOC concentrations and composition in Atlanta, Georgia. Atmos. Environ. 44, 4827-4839.10.1016/j.atmosenv.2010.08.036.

Bloomer, B.J., et al., 2009. Observed relationships of ozone air pollution with temperature and emissions. Geophysical Research Letters 36.Artn L09803 Doi 10.1029/2009gl037308.

Bony, S., et al., 2006. How well do we understand and evaluate climate change feedback processes? Journal of Climate 19, 3445-3482

Boone, A., et al., 2000. The influence of the inclusion of soil freezing on simulations by a soil-vegetation-atmosphere transfer scheme. Journal of Applied Meteorology 39, 1544-1569

Brilli, F., et al., 2007. Response of isoprene emission and carbon metabolism to drought in white poplar (Populus alba) saplings. New Phytologist 175, 244-254.10.1111/j.1469-8137.2007.02094.x.

Budyko, M.J., 1956. Heat Balance of the Earth's Surface. Gidrometeoizdat, Leningrad, 255

Budyko, M.J., 1974. Climate and Life. Academic Press, 508

Calfapietra, C., et al., 2008a. Isoprene emission rates under elevated CO2 and O-3 in two field-grown aspen clones differing in their sensitivity to O-3. New Phytologist 179, 55-61.10.1111/j.1469-8137.2008.02493.x.

Calfapietra, C., et al., 2008b. Isoprene emission rates under elevated CO(2) and O(3) in two field-grown aspen clones differing in their sensitivity to O(3). New Phytologist 179, 55-61.Doi 10.1111/J.1469-8137.2008.02493.X.

Camalier, L., et al., 2007. The effects of meteorology on ozone in urban areas and their use in assessing ozone trends. Atmos. Environ. 41, 7127-7137.10.1016/j.atmosenv.2007.04.061.

Cardelino, C.A., Chameides, W.L., 1995. AN OBSERVATION-BASED MODEL FOR ANALYZING OZONE PRECURSOR RELATIONSHIPS IN THE URBAN ATMOSPHERE. J. Air Waste Manag. Assoc. 45, 161-180

Carlslaw, H.S., Jaeger, C.J., 1959. Conduction of Heat in Solids. Oxford Claredon Press 2, 510

Carlton, A.G., Baker, K.R., 2011. Photochemical Modeling of the Ozark Isoprene Volcano: MEGAN, BEIS, and Their Impacts on Air Quality Predictions. Environmental Science & Technology 45, 4438-4445.10.1021/es200050x.

Castellanos, P., et al., 2011. Ozone, oxides of nitrogen, and carbon monoxide during pollution events over the eastern United States: An evaluation of emissions and vertical mixing. Journal of Geophysical Research-Atmospheres 116.Artn D16307 Doi 10.1029/2010jd014540.

Centritto, M., et al., 2011. Different sensitivity of isoprene emission, respiration and photosynthesis to high growth temperature coupled with drought stress in black poplar (Populus nigra) saplings. Tree Physiology 31, 275-286.10.1093/treephys/tpq112.

Chameides, W.L., et al., 1988. THE ROLE OF BIOGENIC HYDROCARBONS IN URBAN PHOTOCHEMICAL SMOG - ATLANTA AS A CASE-STUDY. Science 241, 1473-1475

Chan, E., 2009. Regional ground-level ozone trends in the context of meteorological influences across Canada and the eastern United States from 1997 to 2006. Journal of Geophysical Research-Atmospheres 114.Artn D05301 Doi 10.1029/2008jd010090.

Chang, W.Y., et al., 2009. Climate Responses to Direct Radiative Forcing of Anthropogenic Aerosols, Tropospheric Ozone, and Long-Lived Greenhouse Gases in Eastern China over 1951-2000. Advances in Atmospheric Sciences 26, 748-762.10.1007/s00376-009-9032-4.

Charney, J., Stone, P.H., 1976. Drought in Sahara - Insufficient Biogeophysical Feedback. Science 191, 100-102

Christensen, J.H., Hewitson, B., 2007. Regional Climate Projections. Climate Change 2007: The Physical Science Basis, 847-940

Collins, W.D., et al., 2006. The Community Climate System Model version 3 (CCSM3). Journal of Climate 19, 2122-2143

Confalonieri, U., B. , et al., 2007. Human health. Climate Change 2007: Impacts, Adaptation and Vulnerability. Contribution of Working Group II to the Fourth Assessment Report of the Intergovernmental Panel on Climate Change. Cambridge University Press, Cambridge, 391-431

Corby, G.A., et al., 1972. General Circulation Model of Atmosphere Suitable for Long Period Integrations. Quarterly Journal of the Royal Meteorological Society 98, 809-&

Cosgrove, B.A., et al., 2003. Land surface model spin-up behavior in the North American Land Data Assimilation System (NLDAS). Journal of Geophysical Research-Atmospheres 108, 19.8845
10.1029/2002jd003316.

Cox, W.M., Chu, S.H., 1993. Meteorologically Adjusted Ozone Trends in Urban Areas - a Probabilistic Approach. Atmospheric Environment Part B-Urban Atmosphere 27, 425-434

Dai, A.G., 2011. Drought under global warming: a review. Wires Clim Change 2, 45-65.Doi 10.1002/Wcc.81.

Dallwigk, E., Briner, E., 1950. Sur Lozonation Des Aldehydes Comportant Une Double Liaison Ethylenique .1. Etude De Laldehyde Cinnamique. Helv. Chim. Acta 33, 2186-2195

Davis, J., et al., 2011. A comparison of CMAQ-based and observation-based statistical models relating ozone to meteorological parameters. Atmos. Environ. 45, 3481-3487.Doi 10.1016/J.Atmosenv.2010.12.060.

Dawson, J.P., et al., 2007. Sensitivity of ozone to summertime climate in the eastern USA: A modeling case study. Atmos. Environ. 41, 1494-1511.Doi 10.1016/J.Atmosenv.2006.10.033.

Dawson, J.P., et al., 2008. Simulating present-day and future air quality as climate changes: Model evaluation. Atmos. Environ. 42, 4551-4566.Doi 10.1016/J.Atmosenv.2008.01.058.

de la Torre, L., et al., 2008. A Climatology Based on Reanalysis of Baroclinic Developmental Regions in the Extratropical Northern Hemisphere, in: Gimeno, L., GarciaHerrera, R., Trigo, R.M. (Eds.), Trends and Directions in Climate Research, pp. 235-255.

Deardorff, J.W., 1978. Efficient Prediction of Ground Surface-Temperature and Moisture, with Inclusion of a Layer of Vegetation. J Geophys Res-Oc Atm 83, 1889-1903

Decker, M.R., Zeng, X., 2009. Impact of Modified Richards Equation on Global Soil Moisture Simulation in the Community Land Model (CLM3.5). Journal of Advances in Modeling Earth Systems 1, 22.doi:10.3894/JAMES.2009.1.5.

Dee, D.P., et al., 2011. The ERA-Interim reanalysis: configuration and performance of the data assimilation system. Quarterly Journal of the Royal Meteorological Society 137, 553-597.10.1002/qj.828.

Dentener, F., et al., 2009. Formation of secondary organic aerosol from isoprene oxidation over Europe. Atmospheric Chemistry and Physics 9, 7003-7030

Dickinson, R.E., 1984. Modeling evapotranspiration for three-dimensional global climate models. Climate Processes and Climate Sensitivity 29, 58-72

Dickinson, R.E., et al., 1989. A Regional Climate Model for the Western United-States. Climatic Change 15, 383-422

Dickinson, R.E., et al., 1993. Biosphere-Atmosphere Transfer Scheme (BATS) version 1e as coupled to the NCAR Community Climate Model. Technical Report National Center for Atmospheric Research

Diffenbaugh, N.S., et al., 2007. Heat stress intensification in the Mediterranean climate change hotspot. Geophysical Research Letters 34.10.1029/2007gl030000.

Dirmeyer, P.A., 1994. Vegetation Stress as a Feedback Mechanism in Midlatitude Drought. Journal of Climate 7, 1463-1483

Dirmeyer, P.A., 2001. An evaluation of the strength of land-atmosphere coupling. Journal of Hydrometeorology 2, 329-344

Dirmeyer, P.A., 2006. The hydrologic feedback pathway for land-climate coupling. Journal of Hydrometeorology 7, 857-867

Dirmeyer, P.A., 2011. The terrestrial segment of soil moisture-climate coupling. Geophysical Research Letters 38.Artn L16702
Doi 10.1029/2011gl048268.

Dirmeyer, P.A., et al., 2006. Do global models properly represent the feedback between land and atmosphere? Journal of Hydrometeorology 7, 1177-1198

Dominguez, F., et al., 2006. Impact of atmospheric moisture storage on precipitation recycling. Journal of Climate 19, 1513-1530

Douville, H., Chauvin, F., 2000. Relevance of soil moisture for seasonal climate predictions: a preliminary study. Climate Dynamics 16, 719-736

Duffy, P.B., et al., 2006. Simulations of present and future climates in the western United States with four nested regional climate models. Journal of Climate 19, 873-895

Duncan, B.N., et al., 2009. Temperature dependence of factors controlling isoprene emissions. Geophysical Research Letters 36, L05813.10.1029/2008gl037090.

Eltahir, E.A.B., 1998. A soil moisture rainfall feedback mechanism 1. Theory and observations. Water Resources Research 34, 765-776

Emanuel, K.A., 1995. ON THERMALLY DIRECT CIRCULATIONS IN MOIST ATMOSPHERES. Journal of the Atmospheric Sciences 52, 1529-1534

Emmons, L.K., et al., 2010. Description and evaluation of the Model for Ozone and Related chemical Tracers, version 4 (MOZART-4). Geosci Model Dev 3, 43-67

Entekhabi, D., et al., 2010. The Soil Moisture Active Passive (SMAP) Mission. P Ieee 98, 704-716.Doi 10.1109/Jproc.2010.2043918.

Entekhabi, D., et al., 2009. The Soil Moisture Active and Passive Mission (SMAP): Science and Applications. Ieee Rad Conf, 83-85

EPA, U., 2005. Evaluating O3 control programs in the Eastern United States: Focus on the NOx Budget Trading Program. Environmental Protection Agency /http://www.epa.gov/airtrends/2005/O3nbp.pdfS EPA-454-K-05-001

Fall, R., Monson, R.K., 1992. ISOPRENE EMISSION RATE AND INTERCELLULAR ISOPRENE CONCENTRATION AS INFLUENCED BY STOMATAL DISTRIBUTION AND CONDUCTANCE. Plant Physiol. 100, 987-992

Fast, J.D., et al., 2006. Evolution of ozone, particulates, and aerosol direct radiative forcing in the vicinity of Houston using a fully coupled meteorology-chemistry-aerosol model. Journal of Geophysical Research-Atmospheres 111.Artn D21305 Doi 10.1029/2005jd006721.

Fast, J.D., Heilman, W.E., 2005. Simulated sensitivity of seasonal ozone exposure in the Great Lakes region to changes in anthropogenic emissions in the presence of interannual variability. Atmos. Environ. 39, 5291-5306.Doi 10.1016/J.Atmosenv.2005.05.032.

Fennessy, M.J., Shukla, J., 1999. Impact of initial soil wetness on seasonal atmospheric prediction. Journal of Climate 12, 3167-3180

Ferguson, C.R., Wood, E.F., 2011. Observed Land-Atmosphere Coupling from Satellite Remote Sensing and Reanalysis. Journal of Hydrometeorology 12, 1221-1254.Doi 10.1175/2011jhm1380.1.

Findell, K.L., Eltahir, E.A.B., 1997. An analysis of the soil moisture-rainfall feedback, based on direct observations from Illinois. Water Resources Research 33, 725-735

Findell, K.L., Eltahir, E.A.B., 2003a. Atmospheric controls on soil moisture-boundary layer interactions. Part I: Framework development. Journal of Hydrometeorology 4, 552-569

Findell, K.L., Eltahir, E.A.B., 2003b. Atmospheric controls on soil moisture-boundary layer interactions. Part II: Feedbacks within the continental United States. Journal of Hydrometeorology 4, 570-583

Fiore, A.M., et al., 2009. Multimodel estimates of intercontinental source-receptor relationships for ozone pollution. Journal of Geophysical Research-Atmospheres 114.Artn D04301
Doi 10.1029/2008jd010816.

Fiore, A.M., et al., 2005. Evaluating the contribution of changes in isoprene emissions to surface ozone trends over the eastern United States. Journal of Geophysical Research-Atmospheres 110.10.1029/2004jd005485.

Fischer, E.M., Schar, C., 2009. Future changes in daily summer temperature variability: driving processes and role for temperature extremes. Climate Dynamics 33, 917-935.Doi 10.1007/S00382-008-0473-8.

Fischer, E.M., et al., 2007a. Contribution of land-atmosphere coupling to recent European summer heat waves. Geophysical Research Letters 34.10.1029/2006gl029068.

Fischer, E.M., et al., 2007b. Soil moisture - Atmosphere interactions during the 2003 European summer heat wave. Journal of Climate 20, 5081-5099.Doi 10.1175/Jcli4288.1.

Forster, P., Ramaswamy, V., 2007. Changes in Atmospheric Constituents and in Radiative Forcing. Climate Change 2007: The Physical Science Basis, 129-234

Frost, G.J., et al., 2006. Effects of changing power plant NO(x) emissions on ozone in the eastern United States: Proof of concept. Journal of Geophysical Research-Atmospheres 111.Artn D12306
Doi 10.1029/2005jd006354.

Fu, J.S., et al., 2011. Impacts of future climate change and effects of biogenic emissions on surface ozone and particulate matter concentrations in the United States. Atmospheric Chemistry and Physics 11, 4789-4806.10.5194/acp-11-4789-2011.

Gantt, B., et al., 2010. The effect of marine isoprene emissions on secondary organic aerosol and ozone formation in the coastal United States. Atmos. Environ. 44, 115-121.10.1016/j.atmosenv.2009.08.027.

Gates, W.L., Imbrie, J., 1975. Climatic Change. Rev Geophys 13, 726-&

Gego, E., et al., 2007. Observation-based assessment of the impact of nitrogen oxides emissions reductions on ozone air quality over the eastern United States. Journal of Applied Meteorology and Climatology 46, 994-1008.Doi 10.1175/Jam2523.1.

Geiger, R., 1965. The climate near the ground, rev. ed. (Translated by Scripta Technica, Inc.). The climate near the ground, rev. ed. (Translated by Scripta Technica, Inc.), xiv+611p. Illus.

Geron, C., et al., 2001. Isoprene emission capacity for US tree species. Atmos. Environ. 35, 3341-3352.10.1016/s1352-2310(00)00407-6.

Gery, M.W., et al., 1989. A photochemical kinetic mechanism for urban and regional scale computer modelling. J Geophys Res 94, 12925-12956

Gilliland, A.B., et al., 2008. Dynamic evaluation of regional air quality models: Assessing changes in O-3 stemming from changes in emissions and meteorology. Atmos. Environ. 42, 5110-5123.Doi 10.1016/J.Atmosenv.2008.02.018.

Giorgi, F., 1990. Simulation of Regional Climate Using a Limited Area Model Nested in a General-Circulation Model. Journal of Climate 3, 941-963

Giorgi, F., Bates, G.T., 1989. THE CLIMATOLOGICAL SKILL OF A REGIONAL MODEL OVER COMPLEX TERRAIN. Monthly Weather Review 117, 2325-2347

Giorgi, F., et al., 2012. RegCM4: Model description and preliminary tests over multiple CORDEX domains. Climate Research.10.3354/cr01018.

Giorgi, F., Mearns, L.O., 1999. Introduction to special section: Regional climate modeling revisited. Journal of Geophysical Research-Atmospheres 104, 6335-6352

Godowitch, J.M., et al., 2008. Modeling assessment of point source NO(x) emission reductions on ozone air quality in the eastern United States. Atmos. Environ. 42, 87-100.Doi 10.1016/J.Atmosenv.2007.09.032.

Goldstein, A.H., et al., 1998. Seasonal course of isoprene emissions from a midlatitude deciduous forest. Journal of Geophysical Research-Atmospheres 103, 31045-31056

Granier, C., et al., 2005. POET, a database of surface emissions of ozone precursors. http://www.aero.jussieu.fr/projet/ACCENT/POET.php

Graus, M., et al., 2006. A relaxed-eddy-accumulation method for the measurement of isoprenoid canopy-fluxes using an online gas-chromatographic technique and PTR-MS simultaneously. Atmos. Environ. 40, S43-S54.Doi 10.1016/J.Atmosenv.2005.09.094.

Greenberg, J.P., et al., 1999. Biogenic volatile organic compound emissions in central Africa during the Experiment for the Regional Sources and Sinks of Oxidants (EXPRESSO) biomass burning season. Journal of Geophysical Research-Atmospheres 104, 30659-30671

Grell, G.A., 1993. PROGNOSTIC EVALUATION OF ASSUMPTIONS USED BY CUMULUS PARAMETERIZATIONS. Monthly Weather Review 121, 764-787

Grotch, S.L., 1988. Regional intercomparison of general circulation model prediction and historical data. U.S. Dep. of Energy Tech Note DOE/NBB-008, 291

Guenther, A., et al., 1999. Isoprene emission estimates and uncertainties for the Central African EXPRESSO study domain. Journal of Geophysical Research-Atmospheres 104, 30625-30639

Guenther, A., et al., 1995. A Global-Model of Natural Volatile Oragnic-Compound Emissions. Journal of Geophysical Research-Atmospheres 100, 8873-8892

Guenther, A., et al., 2006. Estimates of global terrestrial isoprene emissions using MEGAN (Model of Emissions of Gases and Aerosols from Nature). Atmospheric Chemistry and Physics 6, 3181-3210

Guenther, A., et al., 1994. Natural Volatile Organic-Compound Emission Rate Estimates for United-States Woodland Landscapes. Atmos. Environ. 28, 1197-1210

Guenther, A.B., Hills, A.J., 1998. Eddy covariance measurement of isoprene fluxes. Journal of Geophysical Research-Atmospheres 103, 13145-13152

Guenther, A.B., et al., 1993. Isoprene and Monoterpene Emission Rate Variability - Model Evaluations and Sensitivity Analyses. Journal of Geophysical Research-Atmospheres 98, 12609-12617

Gulden, L.E., et al., 2007. Interannual variation in biogenic emissions on a regional scale. Journal of Geophysical Research-Atmospheres 112, D14103.10.1029/2006JD008231.

Guo, Z.C., et al., 2011. Land surface impacts on subseasonal and seasonal predictability. Geophysical Research Letters 38.Artn L24812
Doi 10.1029/2011gl049945.

Guo, Z.C., et al., 2006. GLACE: The Global Land-Atmosphere Coupling Experiment. Part II: Analysis. Journal of Hydrometeorology 7, 611-625

Gutowski, W.J., et al., 2010. Regional Extreme Monthly Precipitation Simulated by NARCCAP RCMs. Journal of Hydrometeorology 11, 1373-1379.Doi 10.1175/2010jhm1297.1.

Haagensmit, A.J., 1952. CHEMISTRY AND PHYSIOLOGY OF LOS-ANGELES SMOG. Industrial and Engineering Chemistry 44, 1342-1346.10.1021/ie50510a045.

Heald, C.L., et al., 2009. Response of isoprene emission to ambient CO(2) changes and implications for global budgets. Global Change Biology 15, 1127-1140.10.1111/j.1365-2486.2008.01802.x.

Heck, W.W., et al., 1982. Assessment of Crop Loss from Ozone. J. Air Pollut. Control Assoc. 32, 353-361

Helmig, D., et al., 1994. Emissions and Identification of Individual Organic-Compounds from Vegetation in 3 Ecosystems in the United-States. Abstracts of Papers of the American Chemical Society 207, 162-ENVR

Helmig, D., et al., 2007. Sesquiterpene emissions from pine trees - Identifications, emission rates and flux estimates for the contiguous United States. Environmental Science & Technology 41, 1545-1553.10.1021/es0618907.

Helmig, D., et al., 2006. Sesquiterpene emissions from loblolly pine and their potential contribution to biogenic aerosol formation in the Southeastern US. Atmos. Environ. 40, 4150-4157.10.1016/j.atmosenv.2006.02.035.

Henderson-Sellers, A., et al., 1993. Tropical Deforestation - Modeling Local-Scale to Regional-Scale Climate Change. Journal of Geophysical Research-Atmospheres 98, 7289-7315

Henry, H.A.L., 2008. Climate change and soil freezing dynamics: historical trends and projected changes. Climatic Change 87, 421-434.10.1007/s10584-007-9322-8.

Hirschi, M., et al., 2011. Observational evidence for soil-moisture impact on hot extremes in southeastern Europe. Nature Geoscience 4, 17-21.10.1038/ngeo1032.

Hogrefe, C., et al., 2011. An analysis of long-term regional-scale ozone simulations over the Northeastern United States: variability and trends. Atmospheric Chemistry and Physics 11, 567-582.Doi 10.5194/Acp-11-567-2011.

Hogrefe, C., et al., 2004. Simulating changes in regional air pollution over the eastern United States due to changes in global and regional climate and emissions. Journal of Geophysical Research-Atmospheres 109.Artn D22301
Doi 10.1029/2004jd004690.

Hollinger, S.E., Isard, S.A., 1994. A Soil-Moisture Climatology of Illinois. Journal of Climate 7, 822-833

Holzman, B., 1937. Sources of moisture for precipitation in the United States. U S Dept Agric Tech Bull 589, 1-38

Horowitz, L.W., et al., 2003. A global simulation of tropospheric ozone and related tracers: Description and evaluation of MOZART, version 2. Journal of Geophysical Research-Atmospheres 108.Artn 4784
Doi 10.1029/2002jd002853.

Isard, S.A., Schaetzl, R.J., 1998. Effects of winter weather conditions on soil freezing in southern Michigan. Phys Geogr 19, 71-94

Ito, A., et al., 2009. Global chemical transport model study of ozone response to changes in chemical kinetics and biogenic volatile organic compounds emissions due to increasing temperatures: Sensitivities to isoprene nitrate chemistry and grid resolution. Journal of Geophysical Research-Atmospheres 114.Artn D09301
Doi 10.1029/2008jd011254.

Jacob, D.J., Winner, D.A., 2009. Effect of climate change on air quality. Atmos. Environ. 43, 51-63.Doi 10.1016/J.Atmosenv.2008.09.051.

Jacobson, M.Z., 1999. Effects of soil moisture on temperatures, winds, and pollutant concentrations in Los Angeles. Journal of Applied Meteorology 38, 607-616

Jaeger, E.B., Seneviratne, S.I., 2011. Impact of soil moisture-atmosphere coupling on European climate extremes and trends in a regional climate model. Climate Dynamics 36, 1919-1939.Doi 10.1007/S00382-010-0780-8.

Jarvis, P.G., 1976. INTERPRETATION OF VARIATIONS IN LEAF WATER POTENTIAL AND STOMATAL CONDUCTANCE FOUND IN CANOPIES IN FIELD. Philosophical Transactions of the Royal Society of London Series B-Biological Sciences 273, 593-610.10.1098/rstb.1976.0035.

Jiang, G.F., Fast, J.D., 2004. Modeling the effects of VOC and NOX emission sources on ozone formation in Houston during the TexAQS 2000 field campaign. Atmos. Environ. 38, 5071-5085.Doi 10.1016/J.Atmosenv.2004.06.012.

Johnson, C.E., et al., 1999. Relative roles of climate and emissions changes on future tropospheric oxidant concentrations. Journal of Geophysical Research-Atmospheres 104, 18631-18645

Jonson, J.E., et al., 2010. A multi-model analysis of vertical ozone profiles. Atmospheric Chemistry and Physics 10, 5759-5783.Doi 10.5194/Acp-10-5759-2010.

Kalnay, E., et al., 1996. The NCEP/NCAR 40-year reanalysis project. Bulletin of the American Meteorological Society 77, 437-471

Karl, T.R., 1986. The Relationship of Soil-Moisture Parameterizations to Subsequent Seasonal and Monthly Mean Temperature in the United-States. Monthly Weather Review 114, 675-686

Kerr, Y.H., et al., 2001. Soil moisture retrieval from space: The Soil Moisture and Ocean Salinity (SMOS) mission. Ieee Transactions on Geoscience and Remote Sensing 39, 1729-1735

Kim, J.E., Hong, S.Y., 2007. Impact of soil moisture anomalies on summer rainfall over East Asia: A regional climate model study. Journal of Climate 20, 5732-5743.Doi 10.1175/2006jcli1358.1.

Kim, S.W., et al., 2006. Satellite-observed US power plant NO(x) emission reductions and their impact on air quality. Geophysical Research Letters 33.Artn L22812 Doi 10.1029/2006gl027749.

Kim, Y., Wang, G.L., 2007. Impact of initial soil moisture anomalies on subsequent precipitation over North America in the coupled land-atmosphere model CAM3-CLM3. Journal of Hydrometeorology 8, 513-533.10.1175/jhm611.1.

Kirstine, W., et al., 1998. Emissions of volatile organic compounds (primarily oxygenated species) from pasture. Journal of Geophysical Research-Atmospheres 103, 10605-10619

Knowlton, K., et al., 2004. Assessing ozone-related health impacts under a changing climate. Environ. Health Perspect. 112, 1557-1563.Doi 10.1289/Ehp.7163.

Konig, G., et al., 1995. Relative Contribution of Oxygenated Hydrocarbons to the Total Biogenic Voc Emissions of Selected Mid-European Agricultural and Natural Plant-Species. Atmos. Environ. 29, 861-874

Korsog, P.E., Wolff, G.T., 1991. An Examination of Urban Ozone Trends in the Northeastern United-States (1973-1983) Using a Robust Statistical-Method. Atmospheric Environment Part B-Urban Atmosphere 25, 47-57

Koster, R.D., et al., 2004. Regions of strong coupling between soil moisture and precipitation. Science 305, 1138-1140

Koster, R.D., et al., 2002. Comparing the degree of land-atmosphere interaction in four atmospheric general circulation models. Journal of Hydrometeorology 3, 363-375

Koster, R.D., et al., 2006. GLACE: The Global Land-Atmosphere Coupling Experiment. Part I: Overview. Journal of Hydrometeorology 7, 590-610

Koster, R.D., et al., 2010. Contribution of land surface initialization to subseasonal forecast skill: First results from a multi-model experiment. Geophysical Research Letters 37, 6.L02402
10.1029/2009gl041677.

Koster, R.D., Suarez, M.J., 1992. Modeling the Land Surface Boundary in Climate Models as a Composite of Independent Vegetation Stands. Journal of Geophysical Research-Atmospheres 97, 2697-2715

Koster, R.D., Suarez, M.J., 1994. The Components of a Svat Scheme and Their Effects on a Gcms Hydrological Cycle. Advances in Water Resources 17, 61-78

Koster, R.D., Suarez, M.J., 2001. Soil moisture memory in climate models. Journal of Hydrometeorology 2, 558-570

Kuhn, U., et al., 2004. Strong correlation between isoprene emission and gross photosynthetic capacity during leaf phenology of the tropical tree species Hymenaea courbaril with fundamental changes in volatile organic compounds emission composition during early leaf development. Plant Cell and Environment 27, 1469-1485.10.1111/j.1365-3040.2004.01252.x.

Kunkel, K.E., et al., 2008. Sensitivity of future ozone concentrations in the northeast USA to regional climate change. Mitig Adapt Strat Gl 13, 597-606.Doi 10.1007/S11027-007-9137-Y.

Lamarque, J.F., et al., 2010. Historical (1850-2000) gridded anthropogenic and biomass burning emissions of reactive gases and aerosols: methodology and application. Atmospheric Chemistry and Physics 10, 7017-7039.10.5194/acp-10-7017-2010.

Lamb, B., et al., 1986. ISOPRENE EMISSION FLUXES DETERMINED BY AN ATMOSPHERIC TRACER TECHNIQUE. Atmos. Environ. 20, 1-8.10.1016/0004-6981(86)90201-5.

Lathiere, J., et al., 2005. Past and future changes in biogenic volatile organic compound emissions simulated with a global dynamic vegetation model. Geophysical Research Letters 32.10.1029/2005GL024164.

Lathiere, J., et al., 2006. Impact of climate variability and land use changes on global biogenic volatile organic compound emissions. Atmospheric Chemistry and Physics 6, 2129-2146

Lawrence, P.J., Chase, T.N., 2007. Representing a new MODIS consistent land surface in the Community Land Model (CLM 3.0). Journal of Geophysical Research-Biogeosciences 112.10.1029/2006jg000168.

Lawrimore, J.H., et al., 2001. Climate assessment for 2000. Bulletin of the American Meteorological Society 82, S1-S55

Leibensperger, E.M., et al., 2008. Sensitivity of US air quality to mid-latitude cyclone frequency and implications of 1980-2006 climate change. Atmospheric Chemistry and Physics 8, 7075-7086

Lelieveld, J., et al., 2008. Atmospheric oxidation capacity sustained by a tropical forest. Nature 452, 737-740.Doi 10.1038/Nature06870.

Leung, L.R., et al., 2003. Hydroclimate of the western United States based on observations and regional climate simulation of 1981-2000. part I: Seasonal statistics. Journal of Climate 16, 1892-1911

Liao, K.J., et al., 2009. Quantification of the impact of climate uncertainty on regional air quality. Atmospheric Chemistry and Physics 9, 865-878

Lippmann, M., 1989. Health-Effects of Ozone - a Critical-Review. Japca J Air Waste Ma 39, 672-695

Llusia, J., et al., 2008. Contrasting species-specific, compound-specific, seasonal, and interannual responses of foliar isoprenoid emissions to experimental drought in a mediterranean shrubland. Int J Plant Sci 169, 637-645.10.1086/533603.

Lo, M.H., Famiglietti, J.S., 2011. Precipitation response to land subsurface hydrologic processes in atmospheric general circulation model simulations. Journal of Geophysical Research-Atmospheres 116.Artn D05107
Doi 10.1029/2010jd015134.

Lorenz, R., et al., 2010. Persistence of heat waves and its link to soil moisture memory. Geophysical Research Letters 37.Artn L09703
Doi 10.1029/2010gl042764.

Luo, L.F., Wood, E.F., 2007. Monitoring and predicting the 2007 U.S. drought. Geophysical Research Letters 34, L22702.10.1029/2007GL031673.

Manabe, S., 1969. CLIMATE AND OCEAN CIRCULATION .I. ATMOSPHERIC CIRCULATION AND HYDROLOGY OF EARTHS SURFACE. Monthly Weather Review 97, 739-&.10.1175/1520-0493(1969)097<0739:catoc>2.3.co;2.

Manabe, S., et al., 1974. Seasonal-Variation of Tropical Circulation as Simulated by a Global Model of Atmosphere. Journal of the Atmospheric Sciences 31, 43-83

Manabe, S., Strickler, R.F., 1964. THERMAL EQUILIBRIUM OF THE ATMOSPHERE WITH A CONVECTIVE ADJUSTMENT. Journal of the Atmospheric Sciences 21, 361-385.10.1175/1520-0469(1964)021<0361:teotaw>2.0.co;2.

Mao, J.Q., et al., 2010. Atmospheric oxidation capacity in the summer of Houston 2006: Comparison with summer measurements in other metropolitan studies. Atmos. Environ. 44, 4107-4115.Doi 10.1016/J.Atmosenv.2009.01.013.

Mccuen, R.H., et al., 1981. Statistical-Analysis of the Brooks-Corey and the Green-Ampt Parameters across Soil Textures. Water Resources Research 17, 1005-1013

McDonald, J., 1962. The Evaporation-Precipitation Fallacy. Institute of Atmospheric Physics

McKinney, K.A., et al., 2011. Emissions of isoprenoids and oxygenated biogenic volatile organic compounds from a New England mixed forest. Atmospheric Chemistry and Physics 11, 4807-4831.10.5194/acp-11-4807-2011.

Meehl, G.A., Tebaldi, C., 2004. More intense, more frequent, and longer lasting heat waves in the 21st century. Science 305, 994-997

Mesinger, F., et al., 2006. North American regional reanalysis. Bulletin of the American Meteorological Society 87, 343-+.Doi 10.1175/Bams-87-3-343.

Mihailovic, D.T., et al., 1999. Sensitivity of soil surface temperature in a force-restore equation to heat fluxes and deep soil temperature. International Journal of Climatology 19, 1617-1632.10.1002/(sici)1097-0088(19991130)19:14<1617::aid-joc448>3.3.co;2-2.

Mitchell, K.E., et al., 2004. The multi-institution North American Land Data Assimilation System (NLDAS): Utilizing multiple GCIP products and partners in a continental distributed hydrological modeling system. Journal of Geophysical Research-Atmospheres 109, 32.D07s90
10.1029/2003jd003823.

Monteith, J.L., 1965. Evaporation and environment. Symp. Soc. Exp. Biol. 19, 205-234

Muller, J.F., et al., 2008. Global isoprene emissions estimated using MEGAN, ECMWF analyses and a detailed canopy environment model. Atmospheric Chemistry and Physics 8, 1329-1341

Murazaki, K., Hess, P., 2006. How does climate change contribute to surface ozone change over the United States? Journal of Geophysical Research-Atmospheres 111.Artn D05301
Doi 10.1029/2005jd005873.

Naik, V., et al., 2004. Sensitivity of global biogenic isoprenoid emissions to climate variability and atmospheric CO2. Journal of Geophysical Research-Atmospheres 109, D06301.Artn D06301
Doi 10.1029/2003jd004236.

Niu, G.Y., Yang, Z.L., 2006. Effects of frozen soil on snowmelt runoff and soil water storage at a continental scale. Journal of Hydrometeorology 7, 937-952

Nolte, C.G., et al., 2008. Linking global to regional models to assess future climate impacts on surface ozone levels in the United States. Journal of Geophysical Research-Atmospheres 113.Artn D14307
Doi 10.1029/2007jd008497.

Oleson, K.W., et al., 2008. Improvements to the Community Land Model and their impact on the hydrological cycle. Journal of Geophysical Research-Biogeosciences 113, G01021.10.1029/2007jg000563.

Pal, J.S., Eltahir, E.A.B., 2001. Pathways relating soil moisture conditions to future summer rainfall within a model of the land-atmosphere system. Journal of Climate 14, 1227-1242

Pal, J.S., Eltahir, E.A.B., 2003. A feedback mechanism between soil-moisture distribution and storm tracks. Quarterly Journal of the Royal Meteorological Society 129, 2279-2297.10.1256/qj.01.201.

Pal, J.S., et al., 2007. Regional climate modeling for the developing world - The ICTP RegCM3 and RegCNET. Bulletin of the American Meteorological Society 88, 1395-+.10.1175/bams-88-9-1395.

Pal, J.S., et al., 2000. Simulation of regional-scale water and energy budgets: Representation of subgrid cloud and precipitation processes within RegCM. Journal of Geophysical Research-Atmospheres 105, 29579-29594

Palmer, P.I., et al., 2006. Quantifying the seasonal and interannual variability of North American isoprene emissions using satellite observations of the formaldehyde

column. Journal of Geophysical Research-Atmospheres 111, D12315.10.1029/2005jd006689.

Paulot, F., et al., 2009. Unexpected Epoxide Formation in the Gas-Phase Photooxidation of Isoprene. Science 325, 730-733.10.1126/science.1172910.

Pegoraro, E., et al., 2007. The effect of elevated CO2, soil and atmospheric water deficit and seasonal phenology on leaf and ecosystem isoprene emission. Functional Plant Biology 34, 774-784.10.1071/fp07021.

Pegoraro, E., et al., 2005. The interacting effects of elevated atmospheric CO2 concentration, drought and leaf-to-air vapour pressure deficit on ecosystem isoprene fluxes. Oecologia 146, 120-129.10.1007/s00442-005-0166-5.

Pegoraro, E., et al., 2004. Effect of elevated CO2 concentration and vapour pressure deficit on isoprene emission from leaves of Populus deltoides during drought. Functional Plant Biology 31, 1137-1147.10.1071/fp04142.

Penman, H.L., 1948. NATURAL EVAPORATION FROM OPEN WATER, BARE SOIL AND GRASS. Proceedings of the Royal Society of London Series a-Mathematical and Physical Sciences 193, 120-&.10.1098/rspa.1948.0037.

Petron, G., et al., 2001. Seasonal temperature variations influence isoprene emission. Geophysical Research Letters 28, 1707-1710

Pierce, T.E., Waldruff, P.S., 1991. Pc-Beis - a Personal-Computer Version of the Biogenic Emissions Inventory System. J. Air Waste Manag. Assoc. 41, 937-941

Pinker, R.T., et al., 2003. Surface radiation budgets in support of the GEWEX Continental-Scale International Project (GCIP) and the GEWEX Americas Prediction Project (GAPP), including the North American Land Data Assimilation System (NLDAS) Project. Journal of Geophysical Research-Atmospheres 108.Artn 8844
Doi 10.1029/2002jd003301.

Pressley, S., et al., 2005. Long-term isoprene flux measurements above a northern hardwood forest. Journal of Geophysical Research-Atmospheres 110, D07301.10.1029/2004JD005523.

Priestley, C.H., Taylor, R.J., 1972. ASSESSMENT OF SURFACE HEAT-FLUX AND EVAPORATION USING LARGE-SCALE PARAMETERS. Monthly Weather Review 100, 81-&.10.1175/1520-0493(1972)100<0081:otaosh>2.3.co;2.

Proksch, P., et al., 2008. Sponge-associated fungi and their bioactive compounds: the Suberites case. Bot Mar 51, 209-218.Doi 10.1515/Bot.2008.014.

Racherla, P.N., Adams, P.J., 2006. Sensitivity of global tropospheric ozone and fine particulate matter concentrations to climate change. Journal of Geophysical Research-Atmospheres 111.Artn D24103
Doi 10.1029/2005jd006939.

Racherla, P.N., Adams, P.J., 2009. US Ozone Air Quality under Changing Climate and Anthropogenic Emissions. Environmental Science & Technology 43, 571-577.Doi 10.1021/Es800854f.

Radtke, R., et al., 1963. Lebensm-Untersuch-Forsch. 119, 293-302

Rasmussen, D.J., et al., 2012. Surface ozone-temperature relationships in the eastern US: A monthly climatology for evaluating chemistry-climate models. Atmos. Environ. 47, 142-153.doi: 10.1016/j.atmosenv.2011.11.021.

Rasmussen, R., 1970. Isoprene: Identified as a Forest-Type Emission to the Atmosphere. Environmental Science and Technology 4, 667-671

Rawls, W.J., et al., 1991. ESTIMATING SOIL WATER RETENTION FROM SOIL PHYSICAL PROPERTIES AND CHARACTERISTICS. Stewart, B. a. (Ed.). Advances in Soil Science, Vol. 16. Ix+240p. Springer-Verlag New York, Inc.: New York, New York, USA; Berlin, Germany. Illus, 213-234

Reidmiller, D.R., et al., 2009. The influence of foreign vs. North American emissions on surface ozone in the US. Atmospheric Chemistry and Physics 9, 5027-5042

Ren, X.R., et al., 2003. OH and HO2 chemistry in the urban atmosphere of New York City. Atmos. Environ. 37, 3639-3651.Doi 10.1016/S1352-2310(03)00459-X.

Reynolds, R.W., et al., 2002. An improved in situ and satellite SST analysis for climate. Journal of Climate 15, 1609-1625

Rhoades, J.W., 1960. Analysis of the Volatile Constituents of Coffee. J. Agric. Food Chem. 8, 136-141

Rind, D., et al., 1989. Change in Climate Variability in the 21st-Century. Climatic Change 14, 5-37

Rinne, H.J.I., et al., 2002. Isoprene and monoterpene fluxes measured above Amazonian rainforest and their dependence on light and temperature. Atmos. Environ. 36, 2421-2426

Rodell, M., et al., 2004. The global land data assimilation system. Bulletin of the American Meteorological Society 85, 381-+.10.1175/BAMS-85-3-381.

Santanello, J.A., et al., 2011. Diagnosing the Sensitivity of Local Land-Atmosphere Coupling via the Soil Moisture-Boundary Layer Interaction. Journal of Hydrometeorology 12, 766-786.Doi 10.1175/Jhm-D-10-05014.1.

Schar, C., et al., 1999. The soil-precipitation feedback: A process study with a regional climate model. Journal of Climate 12, 722-741

Schlink, U., et al., 2002. Longitudinal modelling of respiratory symptoms in children. Int. J. Biometeorol. 47, 35-48.Doi 10.1007/S00484-002-0142-2.

Sellers, P.J., et al., 1997. Modeling the exchanges of energy, water, and carbon between continents and the atmosphere. Science 275, 502-509.10.1126/science.275.5299.502.

Sellers, P.J., et al., 1986. A SIMPLE BIOSPHERE MODEL (SIB) FOR USE WITHIN GENERAL-CIRCULATION MODELS. Journal of the Atmospheric Sciences 43, 505-531.10.1175/1520-0469(1986)043<0505:asbmfu>2.0.co;2.

Seneviratne, S.I., et al., 2010. Investigating soil moisture-climate interactions in a changing climate: A review. Earth-Science Reviews 99, 125-161.Doi 10.1016/J.Earscirev.2010.02.004.

Seneviratne, S.I., et al., 2006. Land-atmosphere coupling and climate change in Europe. Nature 443, 205-209.10.1038/nature05095.

Shalaby, A., et al., 2012. Implementation and evaluation of online gas-phase chemistry within a regional climate model (RegCM-CHEM4). Geoscientific Model Development Discuss. 5, 149-188.doi:10.5194/gmdd-5-149-2012.

Sharkey, T.D., Loreto, F., 1993. WATER-STRESS, TEMPERATURE, AND LIGHT EFFECTS ON THE CAPACITY FOR ISOPRENE EMISSION AND PHOTOSYNTHESIS OF KUDZU LEAVES. Oecologia 95, 328-333

Sharkey, T.D., et al., 1996. Field measurements of isoprene emission from trees in response to temperature and light. Tree Physiology 16, 649-654

Shindell, D.T., et al., 2008. Multimodel projections of climate change from short-lived emissions due to human activities. Journal of Geophysical Research-Atmospheres 113.Artn D11109
Doi 10.1029/2007jd009152.

Sickmoller, M., et al., 2000. Observed winter cyclone tracks in the northern hemisphere in re-analysed ECMWF data. Quarterly Journal of the Royal Meteorological Society 126, 591-620

Sillman, S., 1991. A Numerical-Solution for the Equations of Tropospheric Chemistry Based on an Analysis of Sources and Sinks of Odd Hydrogen. Journal of Geophysical Research-Atmospheres 96, 20735-20744

Sillman, S., Samson, F.J., 1995. IMPACT OF TEMPERATURE ON OXIDANT PHOTOCHEMISTRY IN URBAN, POLLUTED RURAL AND REMOTE ENVIRONMENTS. Journal of Geophysical Research-Atmospheres 100, 11497-11508

Solmon, F., et al., 2006. Aerosol modelling for regional climate studies: application to anthropogenic particles and evaluation over a European/African domain. Tellus Series B-Chemical and Physical Meteorology 58, 51-72.Doi 10.1111/J.1600-0889.2005.00155.X.

Stavrakou, T., et al., 2011. First space-based derivation of the global atmospheric methanol emission fluxes. Atmospheric Chemistry and Physics 11, 4873-4898.10.5194/acp-11-4873-2011.

Stavrakou, T., et al., 2009. Global emissions of non-methane hydrocarbons deduced from SCIAMACHY formaldehyde columns through 2003-2006. Atmospheric Chemistry and Physics 9, 3663-3679

Stavrakou, T., et al., 2010. Improved global modelling of HO(x) recycling in isoprene oxidation: evaluation against the GABRIEL and INTEX-A aircraft campaign measurements. Atmospheric Chemistry and Physics 10, 9863-9878.Doi 10.5194/Acp-10-9863-2010.

Steiner, A.L., et al., 2005. The coupling of the Common Land Model (CLM0) to a regional climate model (RegCM). Theoretical and Applied Climatology 82, 225-243.10.1007/s00704-005-0132-5.

Steiner, A.L., et al., 2009. Land surface coupling in regional climate simulations of the West African monsoon. Climate Dynamics 33, 869-892.10.1007/s00382-009-0543-6.

Steiner, A.L., et al., 2006. Influence of future climate and emissions on regional air quality in California. Journal of Geophysical Research-Atmospheres 111.Artn D18303
Doi 10.1029/2005jd006935.

Stevenson, D.S., et al., 2006. Multimodel ensemble simulations of present-day and near-future tropospheric ozone. Journal of Geophysical Research-Atmospheres 111.10.1029/2005JD006338.

Stockli, R., et al., 2011. A global reanalysis of vegetation phenology. Journal of Geophysical Research-Biogeosciences 116, G03020.Artn G03020

Doi 10.1029/2010jg001545.

Taraborrelli, D., et al., 2012. Hydroxyl radical buffered by isoprene oxidation over tropical forests. Nature Geoscience 5, 190-193.Doi 10.1038/Ngeo1405.

Tawfik, A., et al., 2012. Quantifying the contribution of environmental factors to isoprene flux interannual variability. Atmos. Environ. 54, 216-224.doi: 10.1016/j.atmosenv.2012.02.018.

Tawfik, A.B., Steiner, A.L., 2011. The role of soil ice in land-atmosphere coupling over the United States: A soil moisture-precipitation winter feedback mechanism. Journal of Geophysical Research-Atmospheres 116.Doi 10.1029/2010jd014333.

Teuling, A.J., et al., 2006. Observed timescales of evapotranspiration response to soil moisture. Geophysical Research Letters 33.Artn L23403
Doi 10.1029/2006gl028178.

Tie, X., et al., 2003. Biogenic methanol and its impacts on tropospheric oxidants. Geophysical Research Letters 30.10.1029/2003GL017167.

US EPA, 2011. Air Quality System Data Mart: US Environmental Protection Agency. http://www.epa.gov/ttn/airs/aqsdatamart

Velikova, V., et al., 2005. Localized ozone fumigation system for studying ozone effects on photosynthesis, respiration, electron transport rate and isoprene emission in field-grown Mediterranean oak species. Tree Physiology 25, 1523-1532

Viterbo, P., et al., 1999. The representation of soil moisture freezing and its impact on the stable boundary layer. Quarterly Journal of the Royal Meteorological Society 125, 2401-2426

Vukovich, F.M., 1995. Regional-Scale Boundary-Layer Ozone Variations in the Eastern United-States and Their Association with Meteorological Variations. Atmos. Environ. 29, 2259-2273

Vukovich, F.M., Sherwell, J., 2003. An examination of the relationship between certain meteorological parameters and surface ozone variations in the Baltimore-Washington corridor. Atmos. Environ. 37, 971-981.Doi 10.1016/S1352-2310(02)00994-9.

Walker, M.D., Diffenbaugh, N.S., 2009. Evaluation of high-resolution simulations of daily-scale temperature and precipitation over the United States. Climate Dynamics 33, 1131-1147.10.1007/s00382-009-0603-y.

Wang, S.Y., et al., 2009. Evaluation of precipitation in the Intermountain Region as simulated by the NARCCAP regional climate models. Geophysical Research Letters 36.10.1029/2009gl037930.

Warneke, C., et al., 2010. Biogenic emission measurement and inventories determination of biogenic emissions in the eastern United States and Texas and comparison with biogenic emission inventories. Journal of Geophysical Research-Atmospheres 115.10.1029/2009jd012445.

Warneke, C., et al., 1999. Acetone, methanol, and other partially oxidized volatile organic emissions from dead plant matter by abiological processes: Significance for atmospheric HOx chemistry. Global Biogeochemical Cycles 13, 9-17

Weaver, C.P., et al., 2009. A Preliminary Synthesis of Modeled Climate Change Impacts on Us Regional Ozone Concentrations. Bulletin of the American Meteorological Society 90, 1843-1863.Doi 10.1175/2009bams2568.1.

Wesely, M.L., 1989. Parameterization of Surface Resistances to Gaseous Dry Deposition in Regional-Scale Numerical-Models. Atmos. Environ. 23, 1293-1304

White, A.B., et al., 2007. Comparing the impact of meteorological variability on surface ozone during the NEAQS (2002) and ICARTT (2004) field campaigns. Journal of Geophysical Research-Atmospheres 112.Artn D10s14
Doi 10.1029/2006jd007590.

Wild, O., 2007. Modelling the global tropospheric ozone budget: exploring the variability in current models. Atmospheric Chemistry and Physics 7, 2643-2660

Wilkinson, M.J., et al., 2009. Leaf isoprene emission rate as a function of atmospheric CO(2) concentration. Global Change Biology 15, 1189-1200.10.1111/j.1365-2486.2008.01803.x.

Wu, S.L., et al., 2007a. Why are there large differences between models in global budgets of tropospheric ozone? Journal of Geophysical Research-Atmospheres 112.10.1029/2006JD007801.

Wu, W.R., et al., 2007b. Covariabilities of spring soil moisture and summertime United States precipitation in a climate simulation. International Journal of Climatology 27, 429-438.10.1002/joc.1419.

Xie, P.P., Arkin, P.A., 1997. Global precipitation: A 17-year monthly analysis based on gauge observations, satellite estimates, and numerical model outputs. Bulletin of the American Meteorological Society 78, 2539-2558

Xu, Y.W., et al., 2002. Estimates of biogenic emissions using satellite observations and influence of isoprene emission on O-3 formation over the eastern United States. Atmos. Environ. 36, 5819-5829

Yang, F.L., et al., 2001. Snow-albedo feedback and seasonal climate variability over North America. Journal of Climate 14, 4245-4248

Yang, R., et al., 1994. The Influence of Initial Soil Wetness on Medium-Range Surface Weather Forecasts. Monthly Weather Review 122, 471-485

Yeh, T.C., et al., 1984. The Effect of Soil-Moisture on the Short-Term Climate and Hydrology Change - a Numerical Experiment. Monthly Weather Review 112, 474-490

Zaveri, R.A., et al., 2003. Ozone production efficiency and NOx depletion in an urban plume: Interpretation of field observations and implications for evaluating O-3-NOx-VOC sensitivity. Journal of Geophysical Research-Atmospheres 108.Artn 4436
Doi 10.1029/2002jd003144.

Zaveri, R.A., Peters, L.K., 1999. A new lumped structure photochemical mechanism for large-scale applications. Journal of Geophysical Research-Atmospheres 104, 30387-30415

Zeng, G., et al., 2008. Impact of climate change on tropospheric ozone and its global budgets. Atmospheric Chemistry and Physics 8, 369-387

Zhang, H., Frederiksen, C.S., 2003. Local and nonlocal impacts of soil moisture initialization on AGCM seasonal forecasts: A model sensitivity study. Journal of Climate 16, 2117-2137

Zhang, J.Y., et al., 2008a. Contribution of land-atmosphere coupling to summer climate variability over the contiguous United States. Journal of Geophysical Research-Atmospheres 113.10.1029/2008jd010136.

Zhang, J.Y., et al., 2008b. Assessing land-atmosphere coupling using soil moisture from the Global Land Data Assimilation System and observational precipitation. Journal of Geophysical Research-Atmospheres 113.10.1029/2008jd009807.

Zhang, J.Y., Wu, L.Y., 2011. Land-atmosphere coupling amplifies hot extremes over China. Chinese Science Bulletin 56, 3328-3332.Doi 10.1007/S11434-011-4628-3.

Zhang, Y., et al., 2008c. Impacts of regional climate change on biogenic emissions and air quality. Journal of Geophysical Research-Atmospheres 113.Artn D18310
Doi 10.1029/2008jd009965.

Zhao, T.X.P., et al., 2011. Global component aerosol direct radiative effect at the top of atmosphere. International Journal of Remote Sensing 32, 633-655.10.1080/01431161.2010.517790.

Zheng, J., et al., 2007. Interannual variation in meteorologically adjusted ozone levels in the eastern United States: A comparison of two approaches. Atmos. Environ. 41, 705-716.Doi 10.1016/J.Atmosenv.2006.09.010.

Zhuang, X.F., et al., 2012. Dynamic evolution of herbivore-induced sesquiterpene biosynthesis in sorghum and related grass crops. Plant J. 69, 70-80.Doi 10.1111/J.1365-313x.2011.04771.X.